POTENTIAL IMPACT OF CLIMATE CHANGE ON SURFACE RUNOFF AND SEDIMENT YIELD IN A WATERSHED OF LESSER HIMALAYAS

By

SOORYAMOL K. R.

2014-20-115

THESIS

Submitted in partial fulfilment of the

requirements for the degree of

B.Sc. - M.Sc. (Integrated) Climate Change Adaptation

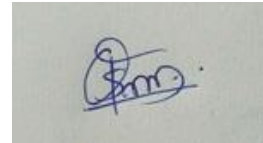**Faculty of Agriculture**

Kerala Agricultural University, Thrissur

ACADEMY OF CLIMATE CHANGE EDUCATION AND RESEARCH

VELLANIKKARA, THRISSUR – 680 656

KERALA, INDIA

2020

DECLARATION

I, hereby declare that this thesis entitled **"POTENTIAL IMPACT OF CLIMATE CHANGE ON SURFACE RUNOFF AND SEDIMENT YIELD IN A WATERSHED OF LESSER HIMALAYAS"** is a bonafide record of research work done by me during the course of research and the thesis has not previously formed the basis for the award to me of any degree, diploma, associateship, fellowship or other similar title, of any other University or Society.

Vellanikkara,   Sooryamol K. R.

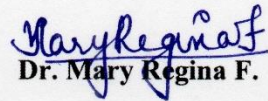Date: (2014-20-115)

CERTIFICATE

Certified that this thesis entitled **"Potential Impact of Climate Change on Surface Runoff and Sediment Yield in a Watershed of Lesser Himalayas"** is a record of research work done independently by Miss Sooryamol K. R. under my guidance and supervision and that it has not previously formed the basis for the award of any degree, diploma, fellowship or associateship to her.
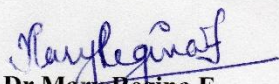
Vellanikkara,

Date:

Dr. Mary Regina F.

(Major Advisor)

Professor (S & WE), College of

Horticulture, KAU, Vellanikkara.

CERTIFICATE

We, the undersigned members of the advisory committee of **Miss Sooryamol K. R.**, a candidate for the degree **B.Sc.- M.Sc. (Integrated) Climate Change Adaptation**, agree that the thesis entitled **"Potential impact of climate change on surface runoff and sediment yield in a watershed of Lesser Himalayas"** may be submitted by **Miss Sooryamol K. R.**, in partial fulfilment of the requirement for the degree.
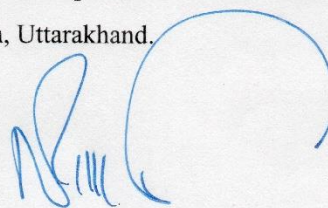
Dr Mary Regina F.
Professor (Soil and Water Engineering)
College of Horticulture
Kerala Agricultural University
Vellanikkara, Thrissur, Kerala.

Dr Suresh Kumar
Scientist/ Engineer- SG & Head,
Agriculture and Soils Department
Indian Institute of Remote Sensing (IIRS)
Indian Space Research Organisation (ISRO)
Department of Space, Government of India
Dehradun, Uttarakhand.

Dr Anitha S.
Professor (Agronomy) and Head
Instructional Farm
Kerala Agricultural University
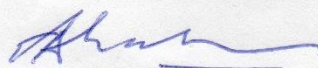Vellanikkara, Thrissur, Kerala.

Dr P. O. Nameer
Special Officer, Academy of Climate
Change Education and Research (ACCER)
Kerala Agricultural University
Vellanikkara, Thrissur, Kerala.

External Examiner
Dr. C. T. ABRAHAM

CONTENTS

LIST OF TABLES

LIST OF FIGURES

LIST OF FIGURES (Contnd.)

LIST OF FIGURES (Contnd.)

LIST ABBREVIATIONS AND EXPANSIONS

Abbreviations	Expansion
AGCM	Atmospheric General Circulation Model
AOGCM	Atmospheric Ocean General Circulation Model
APEX	Agricultural Policy Environmental eXtender
AWC	Available Water Content
AWIFS	Advanced Wide Field Spectrum
AWS	Automatic Weather Station
CHNS	Carbon Hydrogen Nitrogen Sulphur
CN	Curve Number
CNIC	Curve Number Index Coefficient
CNRN	Curve Number Retention
DEM	Digital Elevation Model
DS	Dual Simplex
DTM	Digital Terrain Model
EBM	Energy Balance Model
ENSO	El –Nino in Southern Oscillation
FCC	False Colour Composite
GCM	Global Circulation Model
GHG	Green House Gas Emission
GPS	Global Positioning System
HadCM3	Hadley Centre Model 3
HSG	Hydrologic Soil Group
IMD	India Meteorological Department
IPCC	Intergovernmental Panel on Climate Change
LISS IV	Linear Image Self Scanner
NCEP	National Climate and Environmental Prediction
NDVI	Normalized Difference in Vegetation Index

NSE	Nash- Sutcliffe model Efficiency
OGCM	Ocean General Circulation Model
OLS	Ordinary Least Square
RCM	Regional Climate Model
RCP	Represented Concentration Pathways
RUSLE	Revised Universal Soil Loss Equation
SCM	Single Column Model
SDSM	Statistical Downscaling Model
SPAW	Soil Plant Atmospheric Continuum
USDA	United States Department of Agriculture
USLE	Universal Soil Loss Equation

I. INTRODUCTION

Soil, one of the basic resources which supports the survival of life on earth is degrading and predicted to continue degrading for the next century. The accelerated soil erosion which gradually removes the soil organic matter and thus lowers aggregate stability, reduces the soil depth, soil quality and finally reduces the crop productivity, forest productivity and also reduces the overall soil biodiversity. Eroded topsoil carries away vital plant nutrients from the cropland and makes the farmers to use large quantities of costly fertilizers, for better yield, which can damage human health and contaminate soil, atmosphere and water (Pimental and Burgess, 2013). The rate of land degradation is considerable when compared to the pedogenic processes. This and the exponential population in the world have a significant impact on food security of the future. Unfortunately, India is a country with more than fifty percent of its population depending upon agriculture for their survival. Overdependence and overexploitation of agricultural land makes the soil more vulnerable to erosion, runoff and degradation. When soil is exposed to rainfall, water erosion happens. The impact of hitting raindrops in soil causes splash erosion and they further develop to form sheet, rill and gullies. Apart from rainfall, physical and chemical characteristics of soil, topography, land use, vegetation cover, agricultural practices, and antecedent moisture conditions of a region also influence soil erosion. Since the erosion process depends on the major climatic variables such as rainfall, climate change have a crucial role in soil erosion (Ziadat and Taimeh, 2013). Climate change affects the erosion directly by means of rainfall and indirectly by increased temperature and land use pattern changes. Hence, future projections of the precipitation intensity and frequency for designing conservation measures for protection of soil against the erosion is necessary for the survival of future generation.

In India around 35% of the geographical area is mountainous and out of this approximately 58% is in the Himalayas. In these, the young and fragile northwestern Himalayan mountain ranges are highly eroding regions because of the rugged terrain characteristics, low soil depth, poor water holding capacity and

1

ongoing land use land cover change. Large scale developmental activities like road constructions, mining and increasing population pressure and their dependence on the farming system leads to intense agricultural practices, expansion of cropland by clearing forest land and overgrazing and this contributes to instability and erosion in the Himalayan mountains (Tiwari, 2008). Changes in the precipitation pattern and distribution over Himalayan ranges (Kumar *et al.*, 2011) is gaining more attention of scientists. Since the Himalayas provides food for a vast rural population and contain a unique biological diversity, it is important to assess the erosion risk and adopt conservation practices for the region. However, planning, selection of conservation practices and their implementation for a steep, highly unstable area like Himalaya is difficult. Thus a watershed management approach, which is not only an independent hydrological unit but also acts as a socio-economic and ecological unit, will be suitable for the sustainable development of natural resources. Many scientists have agreed that the unavailability of data from Himalayan ranges is the main roadblock to scientific planning. In this context, Geographical Information System and Remote Sensing can be use efficiently.

Soil conservation and management practices are the only way to save the degrading land. For this soil erosion studies are necessary. Direct measurement of soil erosion from the watershed is impractical and variation of climate necessitates a bulk of data to measure average annual erosion reliably. The scientific community has developed erosion prediction methods such as erosion models and future scenarios of IPCC to make regional assessments of various on-site and off-site impacts of erosion. Modelling and prediction of soil erosion due to climate change can help decision-makers, land managers, small scale farmers and also governments.

A watershed from lesser Himalaya was chosen for the current study. And the objectives were:

- To characterise land use/ land cover and soil hydrological parameters in the watershed.

- To analyze weather parameters and surface runoff of the watershed.

- To study the future climatic scenario and its impact on soil erosion.

- To simulate sediment loss and surface runoff using the Soil and Water Assessment Tool (SWAT) model at the watershed scale.

II. REVIEW OF LITERATURE

A study on the effects of soil erosion by climate change in a lesser Himalayan nano watershed was aimed to predict soil erosion for this century using Representative Concentration Pathways (RCP) scenarios with the help of SWAT model. Observed surface runoff and sediment yield were analysed to calibrate and validate the model for the study area. Relevant studies related to this work are reviewed in this chapter.

2.1 SOIL EROSION PROCESSES

Soil erosion is a process of three stages namely 1) detachment 2) transportation and 3)deposition.The four key sources of erosion are physical (such as wind and water), gravity, chemical reaction, and human induced perturbations (tillage practices). Soil erosion commence with the particles detachment due to the disintegration of their aggregates by the impact, of raindrop, drag force of water and wind or dissolution of binding agent by chemical reaction. These separated particles are carried by water and wind and deposit the particles when the speed of the transporting agent reduces due to the effects of topography or ground cover (Lal, 2001).

2.2 SOIL EROSION IMPACTS

Soil erosion pose a serious risk to the environment by creating onsite issues like the degradation of soil's biological chemical and physical characteristics (Lal *et al*., 2000), nutrient waning (Lal, 2003), loss of organic matter (Langdale *et al*., 1992), loss of soil depth to grow roots and biota (Pimentel *et al*., 1995; Wardle *et al*., 2004) agricultural yield (Lal, 1999), and even farmland decline (Pimentel, 2006). Erosion can also cause number of offsite damages, such as adsorption of chemicals substances on soil particles and subsequent eutrophication in water bodies (Morgan, 2005), fluvial sediment deposition, reservoir sedimentation, and channel silting (Mullan, 2013a).

UNEP (1986) figured that 2 billion ha of biologically productive area has degraded permanently since 1000 AD. Extensively used statistics on soil erosion by Oldeman

(1994) says that the region which is damaged by means of soil erosion amount to 1094 Mha. 751 Mha of this affected severely. There are some regional hotspots of erosion around the world which includes South Asia's Himalayan–Tibetan biome, China's Loess Plateau, sub-humid and semi-arid sub-Saharan Africa, Central America's highlands, the Andean zone, Haiti, and the Caribbean (Scherr and Yadav, 1996). The estimate of global soil erosion rates by Pimentel *et al*. (1995) is 75 billion Mg / year, the study considered an average erosion rate of 100 Mg/ ha for 751 Mha of area affected by extreme soil erosion. Lal and Stewart (1990) and Wen (1993) reported annual soil loss in India is around 6.6 billion tons. Research carried out by the Central Soil Water Conservation Research and Training Institute (2010) estimated average soil loss rate in India induced by erosion is 16.4 tonnes per ha per year, with a loss of 5.334 billion tons per year. Approximately 10% of these total soils removed yearly is left in reservoirs, and reduce about 1–2% of storage capacity, annually, in India (Mandal and Sharda 2011). Milliman and Syvitski (1992) reported that about 20 billion Mg sediment is transported to the ocean annually. Available records on the sediment carriage into the ocean by the rivers around the world is 15–20 billion Mg yearly (Walling and Webb, 1996). The average soil erosion rates of India have been estimated as 0.5 -5 t/ha/yr for areas under natural vegetation, 0.3-40 t/ha/yr for cultivated lands and range of 10-185 t/ha/yr in case of bare soil regions (Singh *et al*., 1981; Morgan, 2005).

As a result of the decline in efficient rooting depth, depletion of plant nutrients, loss of plant (soil) available water, harm to seedlings, reduction of cultivated area due to gully formation and progression, and reduced efficiency of external inputs that harm productivity and environmental regulatory capacity, the effects of erosion on crop yields emerge (Letey 1985; Lal, 1999). About 90% of land productivity fatalities can be attributable to the loss of soil nutrients and water (Pimentel *et al*. 1995). 1-6 kg N, 1-3 kg P, and 2-30 kg K may be a tonne of fertile topsoil, while critically eroded soil may have significantly less of these nutrients (Troeh *et al*., 1991).

Garde and Kothyari (1987) reported that the soil erosion in the northern Himalayas is at a rate of 20 to 25 t ha $^{-1}$yr^{-1}. Thus in Northern Himalayan region management practices to stabilize soil erosion and soil conservation is compulsory. A study conducted by Kalambukattu and Kumar (2017) in Maniyar watershed of mid-Himalayas reported high soil erosion rates from the study area with a value of 65.84 t ha $^{-1}$yr^{-1}. They observed that nearly 63% of watershed generates erosion greater than 10 t ha $^{-1}$yr^{-1} and most of the agricultural area which are mainly rainfed have a major role in soil erosion from the study area. The study concluded with a recommendation of soil and water conservation measures for the watershed on a high risk priority basis. Mondal *et al*. (2018) used three different models (MMF, USLE, and RUSLE) in the Narmada river basin, India and proved that the soil erosion depends on elevation, slope (LS factor in the models) soil type and land use. They found that areas with a high elevation and slope (higher than 20°), areas having a higher content of sandy loam soil and open fallow land are experiencing more erosion than areas with less steep slope, clay soil and settlements respectively.

2.3 REMOTE SENSING AND GIS IN SOIL EROSION STUDIES

In mapping and evaluating landscape features that influence soil erosion, like topography, soils, land use /land cover, relief, and erosion patterns, the implementation of remotely sensed data in the form of aerial photographs and satellite sensor data has been well accepted (Pande *et al.*, 1992). And they also perform a distinctive role in the development of parameters for modelling sediment yield and watershed management from remote locations of watersheds / river basins (Patil *et al.,* 2017). The Geographic Information System (GIS) is a potent tool for managing geo-referenced spatial and non-spatial data for input and output preparation and visualisation, and interaction with models. Data about seasonal land use changes is provided by multi-temporal satellite images. In addition, satellite data could be used to understand erosion characteristics, such as gullies, vegetation rainfall interception, and the cover factor. Assessment of stereoscopic optical and microwave (SAR) remote sensing data (Saha, 2003) can create DEM (Digital Elevation Model), one of the major inputs required for soil erosion modelling.

Sharma and Singh (1995) conducted soil erosion modelling of an agricultural watershed in Bandi river basin using ANSWERS model. Preparation of model inputs like landform, drainage, soil, LULC and delineation and mapping of natural resources were done successfully using Landsat TM false colour composites (FCC) and limited ground truthing. A study by Agriculture and soils Department (ASD) (2001) at Bhogabati watershed Maharashtra, India as part of soil erosion inventory used IRS- 1D : LISS III satellite data for soil and land use/land cover maps preparation and topographic factor (LS) was derived from DEM prepared by GIS analysis. Yuksel *et al*. (2008) used COoRdination of INformation on the Environment (CORINE) model integrated with RS and GIS technology for erosion risk mapping a for watershed in Turkey. To make land use / cover classification in ERDAS imagine, ASTER imagery was chosen. Maps of other factors, such as topography, soil types and climate, were created using ArcGIS v9.2. And they concluded that effective and precise calculation of soil erosion in considerable short time and low charge for big watersheds can be achieved using RS and GIS technology. A study by Fernandez *et al*. (2016) in a mountain range of south Portugal assessed the susceptibility of the study area to rainfall induced erosion. GIS integrated DEM was used to represent topographical characteristics, NDVI for vegetation cover map and other GIS tools for combining maps and classifying vulnerability to rainfall induced soil erosion. Patil *et al*. (2017) estimated annual soil erosion rate using USLE of Shakkar river basin, India. Thematic maps for all the factors in the equation are prepared in GIS environment. The combination of USLE with ArcGIS 9.3 helped them to compute soil erosion potential of the entire watershed, and identified areas of high soil erosion.

2.4 CHANGES IN RAINFALL

Precipitation patterns have also changed significantly, showing intensified rainfall since 1901 over the northern hemisphere's mid-latitude land areas. Increased frequency of extreme storm events in North America and Europe are also reported (IPCC, 2013). Studies have shown that the magnitude and frequency of extreme storm events between 1951 and 2010 are increasing trend in India (Krishnamurthy,

2012). In addition to that, increasing frequency of flash floods in hilly regions, was observed recently due to erratic rain (CSE 2014). In recent years, attention has been paid to spatial variability in rainfall to study interactions between climate, erosion, and tectonics (Anders *et al*., 2006; Barros *et al*., 2006; Bookhagen, 2010).

Impacts of mountainous environments are strong on the spatial and temporal distribution of rainfall in comparison with the impact of plain areas because of the relationship between the amount of rainfall and altitude. Information of rainfall changes with altitude will aid in accurate evaluation of water resources, maximum rainfall assessment, and hydrological modelling of hilly areas (Barros *et al*., 2006). Precipitation is primarily induced by the Indian summer monsoon in the Himalayan foreland and at low to moderate altitudes (Bookhagen *et al*., 2005a; Anders *et al*., 2006; Bookhagen and Burbank, 2006), but the winter rain over the Himalayan regions of north - west India and Pakistan is due to the weather system of Western disturbance (Lang and Barros, 2004; Hatwar *et al*., 2005; Barros *et al*., 2006; Dimri, 2006).

A study conducted by Singh *et al*. (1995) to determine the seasonal and annual distribution of rainfall and snowfall with altitude for the outer, middle and greater Himalayan ranges of the Chenab basin in the western Himalayas showed that the amount of rainfall received at the same altitude in the different ranges of the Himalayas differs, as well as the climatology of precipitation of the Himalayas. Bhutiyani *et al*. (2009) performed an analysis of the Northwestern Himalayan (NWH) area using 140-year (1866-2006) long-term precipitation and temperature data. In the winter precipitation in the NWH, temperature shows a growing but statistically insignificant trend (at 95 percent confidence level) and statistically significant (95 percent confidence level) decreasing monsoon trend and total annual precipitation during the study period. In the post-monsoon rainfall of Dehradun, Pithoragarh and other western Himalayan stations, Pant *et al*. (1999) found a growing trend, compared with a decrease in winter. The significant external factor that induces soil erosion is precipitation (SWCS, 2003). Studies have shown that,

in terms of quantity, frequency , intensity, length and spatiotemporal distribution, changes in rainfall are expected to influence soil erosion.

Maeda *et al*. (2010) proposed that the highlands will be the areas that require more soil conservation consideration because rainfall in the highlands is likely to increase dramatically and thus cause higher rates of soil erosion. Higher rainfall levels are generally correlated with greater runoff and loss of soil (Zabaleta *et al*., 2014), and elevated precipitation will increase soil moisture, soil sealing, crusting, and eventually decline the capacity of infiltration.

Soil erosion is not dependent on the amount of rainfall only. It is not necessary to have an increase in soil erosion by increased rainfall. Storm strength (Nearing *et al*., 2004) and even snowmelt are also significantly reported as influencing soil erosion. Soil erosion is caused by precipitation fluctuations (Zhang and Nearing, 2005). Increased variability of precipitation and extreme events of storms often increase soil loss. When soil conservation approaches are planned, Klik and Eitzinger (2010) and Nunes (2007) specify that extreme storm events should not be ignored. In a few case studies, increased soil loss was expected due to the increased frequency of severe storm events, despite the estimated reduction in rainfall.

The predicted increase in the intensity of precipitation and rainfall energy would alter the erosivity of precipitation and establish a significant gap in spatial patterns between the amount of precipitation and the erosivity of rainfall (Zhang *et al*., 2010). By producing runoff and precipitation erosivity, it will cause the process of soil loss generation. Increases in the quantity of storms will increase the likelihood of producing more rainfall, which in turn will increase soil erosion under bare soil scenarios. Rainfall intensity and frequency are other factors that increase soil loss, as a few daily erosive events of greater intensity cause more than 50 percent of the annual soil loss (Edward and Owen, 1991; Hidalgo *et al*., 2007) Since the degree of soil erosion depends mainly on rainfall energy, soil surface protection during the rainfall event **(**Wischmeier, 1962**)** and precipitation characteristics (such as the intensity, duration, frequency, and total rainfall), it is important to model the trend

of rainfall happening in more extreme events for soil erosion assessment (Edwards and Owens, 1991).

2.5 CLIMATE CHANGE IMPACTS

The consensus of atmospheric scientist community is that climate change is happening, both in terms of precipitation and temperature. Warmer atmospheric temperature due to greenhouse warming is predicted to aim a more vigorous hydrological cycle accompanying with extreme rainfall events (IPCC, 1995). Later they specified again that the global surface warming has happened at a rate of 0.74 ± 0.18° between1906 – 2005 and the increased warming related to atmospheric moisture content can be expected to trigger increased global mean precipitation (IPCC, 2007).

The Himalayas are extremely vulnerable to plentiful rainfall and flooding events mostly during summer monsoon, particularly over south-facing slopes and in the Gangetic Plains of India (Bhatt and Nakamura, 2005). Therefore, we need more studies on precipitation processes in the Himalayas and the consequences of climate change. But because of its extreme, complex topography and lack of adequate rain-gauge data, most studies have ignored the Himalayan region (Shrestha *et al*., 2000).

Variations in the erosive characteristics of rainfall are the direct consequences of climate change (Favis-Mortlock and Savabi, 1996; Williams *et al*., 1996; Favis-Mortlock and Guerra, 1999; Nearing, 2001; Pruski and Nearing, 2002a;). Other consequences are the changes in plant biomass (Nearing *et al*., 2005), and shifting agricultural practice and hence land uses to accommodate the new climatic regime (Williams *et al*., 1996).

Kumar *et al*. (2014) conducted a study over six locations (5 locations of Himachal Pradesh and one from Uttarakhand) which are the part of the Himalayan region. In the western and central part and near the foothills of the Himalayas (Uttaranchal state) and in north-eastern India, the number of rainy days may increase by 5 to 10 days in the western and central part.

The projected climate change is expected to increase soil erosion risks, which can intensify soil degradation and desertification (O'Neal *et al*., 2005), because it is well known that the most erosive power is the high intensity and volume of rainfall. The variation in rainfall pattern due to climate change, contribute to the enhanced rate of soil erosion by the detachment power and the motion of soil particles. The forecast shows that by 2090, soil erosion will increase by 9 percent because of climate change (Yang *et al*., 2003). In terrestrial ecosystems, since there is a correlation between rainfall change and soil erosion processes, rainfall change affects erosion by altering soil characteristics, vegetation, cultivation systems, plant litter and landform (Wei, 2009). The soil properties and soil carbon dynamics are also affected by rainfall-induced soil erosion. Model studies show an increase of 1-20 percent in annual rainfall and an increase in soil erosion in the 21st century of 1.7-241 percent (Blanco and Lal, 2008).

Michael *et al*. (2005) found an increase in precipitation in Germany due to climate change and in the next three decades this will cause a significant increase in erosion rates. A study conducted by Routschek *et al*. (2014) on the basis of the A1B IPCC scenario and four models, namely ECHAM5-OPYC3 (general circulation model), WETTREG2010 (statistical climate downscaling model), METVER (agricultural daily initial soil moisture calculation model) and EROSION 3D, a process-based soil erosion model for the three small catchments of the region of Saxony/Germany, predicted an increased soil erosion rate by 2050. But the study projected a decreased soil erosion rate for the second half of the century because of the lower initial soil moisture as a result of higher temperatures, radiation and a decline of total precipitation amount.

Pruski and Nearing (2002b) found that reduced rainfall and temperature rise created water stress and temperature stress on the production of biomass and crop yield, respectively. In two Mediterranean watersheds, Nunes *et al*. (2013) predicted soil erosion under future climate change scenarios. Results showed reduced soil losses in one watershed even though predicted frequency of severe events was greater. In a warmer climate, this can be due to increased plant cover over an extended growing

season. A study conducted by Zhang and Nearing (2005) projected that in the watershed of El Reno, US, increased evaporation and better crop growth are expected to decrease runoff and soil erosion due to future climate change due to the rise in air temperature.

Modelling is the proper way to predict soil erosion (Li *et al*., 2011; Salazar *et al*., 2012) by including effects of future climate change. Climate models with different future climate scenarios are combined with erosion models. But the main problem with this process is the coarse resolution of global climate models. (Rivington *et al*., 2008; Samaras and Koutitas, 2014). As a result, downscaling techniques have been developed to change climate data resolution from coarse to finer spatial scales, including statistical and dynamic downscaling (Fowler *et al*., 2007). And climate scenarios have also been progressively advanced to more realistic ones, such as the Intergovernmental Panel on Climate Change (IPCC) Special Report on Emission Scenarios (SRES) (Nakicenovic and Swart, 2000) and Representative Concentration Pathways (RCPs). A study conducted by Nearing *et al*. (2005) in Lucky hills and Ganspoel watershed using seven different soil erosion models prove that erosion models are absolutely suitable to study the impact of climate change on erosion and runoff. However, the scientific community is not sure about which kind of model is more suitable for simulation purposes in a definite ecological condition (Tamene, 2005).

2.6 SOIL EROSION MODELS

There are numerous soil erosion models with different levels of difficulty and precision (Francipane *et al*., 2015) such as the Universal Soil Loss Equation (USLE; Wischmeier and Smith, 1978), Revised Universal Soil Loss Equation (RUSLE; Renard *et al*., 1997), Modified Universal Soil Loss Equation (MUSLE), Water Erosion Prediction Project (WEPP) (Nearing *et al*., 1989), and Soil and Water Assessment Tools (SWAT) (Neitsch *et al*., 2011) This chapter describes briefly the models currently used to assess the impacts on soil erosion due to climate change.

Universal Soil Loss Equation (USLE) (Wischmeier and Smith, 1978) is a simple spatially distributed model which uses limited data for the computation of valuable results. It is mainly concentrated for conservation planning technology purposes through predicting soil erosion namely sheet and rill erosion (Lal, 1999).

Universal Soil Loss Equation (USLE) was revised and upgraded in 1985 to design a new Revised Universal Soil Loss Equation (RUSLE) (Morgan, 2005). It was established as a conservation planning and assessment tool by the USDA-Agricultural Research Service (ARS) to predict long-term, annual soil losses. However, its implementation is limited to small areas, as sediment routing across channels cannot be carried out. Main improvements developed in RUSLE are the new R factor distributions; time variance erodibility in the K factor in concern with freeze-thaw processes; new equations for calculating L factor and steepness in the S factor; additional sub-factors for the calculation of C factor; and new P factors for cropland and rangeland (Jones *et al*., 1996).

Modified Universal Soil Loss Equation (MUSLE) was developed as same as RUSLE, but applicable to single storm events. Since the USLE application for each storm event and large areas results in huge calculation errors (Hann *et al*. 1994, Sadeghi, 2004; Sadeghi and Mahdavi 2004; Kinnell, 2005; Chang, 2006; Sadeghi *et al*. 2007a), The R factor used in the USLE/RUSLE equation is replaced by a new runoff factor.

Morgan *et al* . (1984) developed the Morgan – Morgan – Finney (MMF) model to estimate losses of soil in field size on hill slopes. This model is flexible, simple and requires only fewer data compared to the other process-based erosion models (Shrestha, 1997). This physical empirical model predicts the erosion of the soil by subdividing the process into the sediment and water phases. Later, in the revised MMF (Morgan, 2001), the rate of separation of soil particles by precipitation and river runoff is determined together with the capacity for river transport.

A process based model developed by the USDA Agricultural Research Service is the Water Erosion Prediction project (WEPP). It predicts that soil erosion and

sediment development from single slopes would be spatially and temporally dividing, (Flanagan and Nearing, 1995). The effect of CO_2 on soil erosion can be measured using WEPP-CO_2 which is a modified version of the WEPP model.

Soil and Water Assessment Tool (SWAT), developed by the USDA-Agricultural Research Service, is a river-basin scale, continuous time and spatially distributed physically dependent model (Setegn *et al*., 2009) that integrates a system to incorporate land use and field scale management operations in a watershed and determine the effects that can be anticipated from their long-term application (Arnold *et al*., 199). It also incorporates some other models' features (Neitsch *et al*., 2005). To simulate sediment yield at the watershed scale, this model is commonly used (Serpa *et al*., 2015; Azari *et al*., 2016; Parajuli *et al*., 2016). SWAT2009 SWAT98.1 (Neitsch *et al*., 1999a), SWAT99.2 (Neitsch et al., 1999b), and SWAT2000 (Di Luzio *et al*., 2002; Neitsch *et al*., 2002) and SWAT2005 (Neitsch *et al*., 2004, 2005) are now being produced in five variants of the SWAT model.

Borah and Bera (2003) compared three watershed-scale models, including SWAT, and found that all three models have hydrology, sediment, and chemical routine components that are suitable for watershed-scale catchments, and concluded that SWAT is mainly capable of continuous simulations in agricultural watersheds. In order to test the P loss in lowland English captures, Shepherd *et al*. (1999) investigated 14 models, and reported SWAT to be the most applicable model. Van Liew *et al*. (2003a) performed a comparative analysis of SWAT and HSPF streamflow predictions on eight agricultural watersheds within the Washita River Basin in southwest Oklahoma and stated that SWAT gave more accurate results than HSPF under different climatic conditions.

The SWAT applications studied by Gassman *et al*. (2007) demonstrate that the model is a flexible and robust method that can be used to simulate various problems in the watershed. And numerous studies have confirmed that SWAT can, on an annual or monthly basis, reflect hydrologic and/or pollutant loads at different spatial scales. For 10 years, Bingner (1996) simulated runoff of a watershed in northern

Mississippi using SWAT and the model generated acceptable results from multiple sub-basins, except a wooded subbasin, on a daily and annual basis.

Several studies have shown the reliability of SWAT in forecasting sediment loads on various watershed scales. Arnold *et al*. (1999b) compared estimated sediment yields derived from rating curves and simulated average annual sediment loads at five Texas river basins (20,593 to 569,000 km^2) with SWAT simulating average annual sediment loads at five Texas river basins (20,593 to 569,000 km^2) and showing that sediment yields were reasonably well simulated at all river basins compared to estimated sediment yields. Kaur *et al*. (2004) conducted a study at a watershed in Damodar-Barakar, India, the second most extreme eroded area in the world and SWAT projected annual sediment yields moderately well. Later Tripathi *et al*. (2005) directed a comparative study with SWAT and observed daily sediment yield for the same watershed and reported a close agreement with r^2 of 0.89 and NSE of 0.89. Behera and Panda (2006) studied an agricultural watershed located in eastern India using SWAT and got acceptable results of sediment yield during the whole rainy season based on assessments with daily observed data. SWAT also used to project climate change impacts on the various hydrological processes in different regions on watershed -scale.

In order to research the climate change impacts on the hydrology of a watershed in the U.S. southeast region, Ritschard *et al*. (1999) used SWAT and downscaled HadCM2 GCM data and recorded a decrease in potential water supply of up to 10 percent within 20 to 40 years during important agricultural growing seasons on the Gulf Coast (Rahman *et al*. 2010). Using SWAT2005 and a weather generator to apply global climate model projections to stochastic distributions of historical weather data observed and regular future weather data produced,) studied the climate change scenario of low-flow response to A2 (high economic growth, low technology development , high population growth) For the period 2041-2070, projected results showed increased low-flow rates in winter and spring and decreased low-flow rates in the fall.

Mukundan *et al*. (2013) projected potential impacts of climate change on soil erosion and suspended sediment yield in the Cannonsville watershed in New York City for the period 2081-2100 using the SWAT-water balance (SWAT-WB) model and A1B scenario from SRES. Seasonal change research found that , due to a deviation in snowmelt timing and also due to a decrease in the ratio of rainfall collected as snow, expected climate-related changes in soil erosion and sediment yield were more important in the winter.

Using future climate data from GCMs (CCCMA CGCM3.1, CNRM-CM3, MPI ECHAM5, NCAR CCSM3) and SWAT, Shrestha *et al*. (2013) assessed the effect of climate change on the sediment yield in the Nam Ou basin in northern Laos. The results of the study showed that increases in annual stream discharges are likely to vary in the future from 7.4 percent to 66.2 percent, except CNRM-CM3 model which project decrease in rainfall. And some of the results showed very high increases of erosion yields (up to 200 %).

The curve number initial abstraction concept was updated by Bryant *et al*. (2006) and a more detailed simulation of severe (low and high) runoff cases was reported. Borah *et. al.,* (2006) used coupled curve number kinematic wave method of the DWSM (Dynamic Watershed Simulation Model) in SWAT, resulting in better simulation of day-to-day runoff for the Little Wabash River Watershed in Illinois. Kumar *et al*. (2016) conducted a comparative study on the performance of SWAT and SWAT-VSA in a Himalayan watershed of Uttarakhand state and reported more reasonable results from SWAT-VSA than SWAT and revealed the potential of the model to predict spatial distribution of surface runoff without changing the SWAT model structure.

II. MATERIALS AND METHODS

The current study was conducted to understand the impacts of climate change in soil erosion in a watershed that represents the lesser Himalayan landscape by analysing surface runoff and sediment yield and to predict the future soil erosion scenarios for this century. The research carried out in collaboration with Indian Institute of Remote Sensing (IIRS) Dehradun.

3.1 STUDY AREA

The Sitla Rao watershed from the lesser Himalayan landscape which extends between 30° 25'to 30° 30' North latitude and 77° 45' E to 78° 0' East longitude, covering an area of 805 ha (8 sq. km) is the major watershed which contain the study area Pasta (nano watershed). The watershed is located (Fig. 1) in Dehradun district, Uttarakhand state, India. Elevation of the study area ranges from 610 to 1374. East side of the district is bordered by Tehri Garhwal and Pauri Garhwal, its Western boundary share with the Sirmur (Nahan) district of Himachal Pradesh and North-West by the district of Uttarkashi.
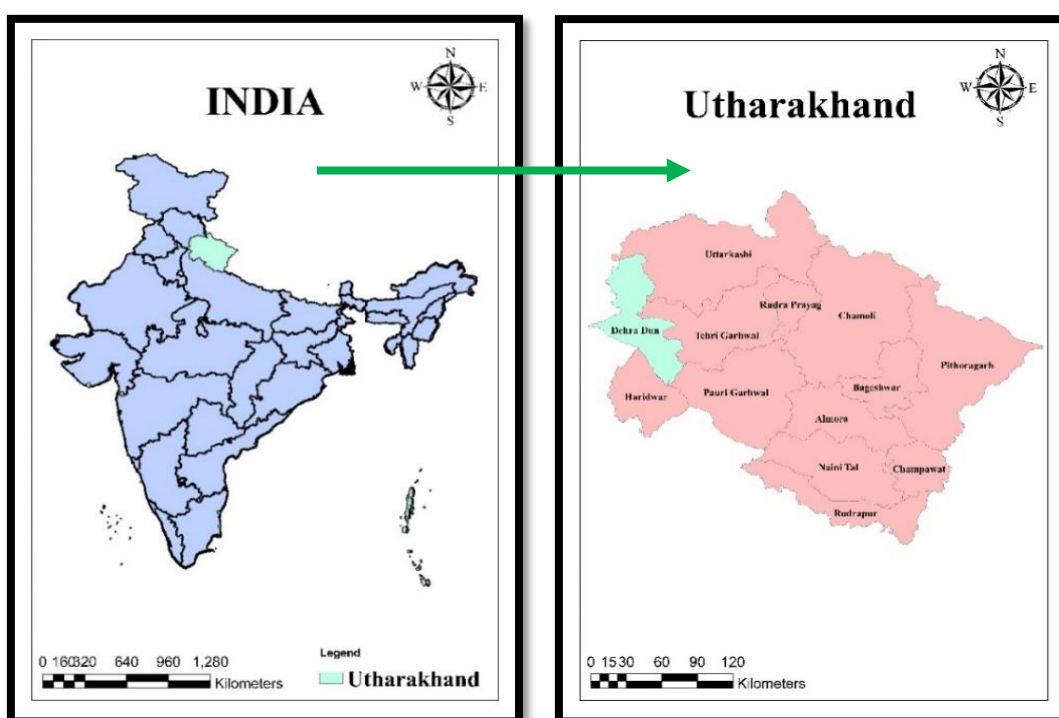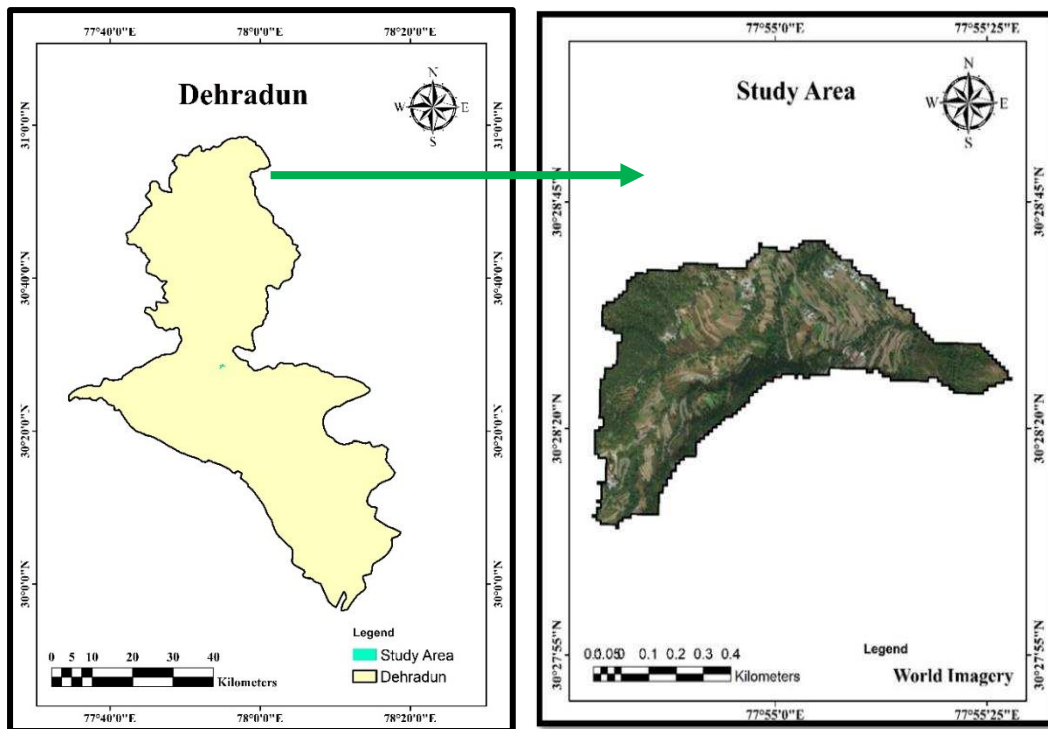
Figure 1. Study area
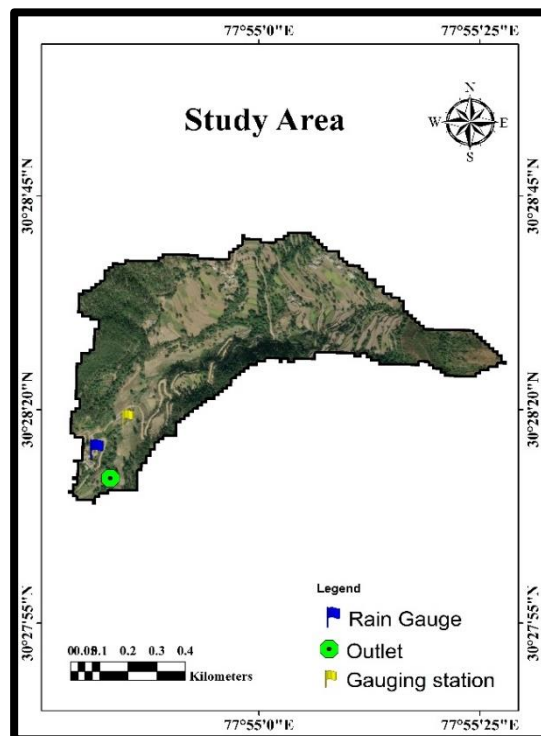
Figure 2. Locations of Rain gauge, outlet and gauging stations in the watershed

The south side is the district of Saharanpur in Uthar Pradesh and at the southern slope touches the boundary of Haridwar. The watershed is a true representation of the lesser Himalayas.

3.1.1 Geology and Physiography

The study area is located in the western part of the Dehradun district which belongs to the Garhwal Himalayas. They contain low to medium grade metamorphic rocks. The Main Boundary Thrust (MBT) divides the Siwalik and lesser Himalayas in Dehradun and the lesser Himalayas further divide into inner and outer lesser Himalayas. Alluvial fans, hillocks, river terraces, and floodplains are the main geomorphic divisions in Dehradun. Fan deposits mainly contain boulders, cobbles, and pebbles with a sandy and silty matrix. And fragments of shale, slate, phyllite, limestone, and sandstone are also found. The watershed is composed of a chain of hills in the upper part, wide-range of piedmonts and river terraces in the middle and the lower parts. The area shows common Himalayan topography that is upper Piedmont, middle piedmont, and lower Piedmont, rugged and high mountain landscape with deep confined valleys, ridges along with erosional planes, river terraces, and hillside slope. The terrain slope ranges from gentle slope <15% in the downstream, to steep slopes >45% in the upper part (Saran *et al*., 2009). River terraces are formed by the lateral shifting of rivers (Bhaware, 2006). Watershed contains pre-Cambrian rocks of lesser Himalaya in the north and thickly bedded multi-storeyed sandstone characterized by mudstone/siltstone of early Palaeozoic to lower Palaeozoic age in the south (Bartarya, 1995).

3.1.2 Soils

Soils of the study area is found to be derived from alluvium parent material. Alfisols, Entisols, and Inceptisols are the major types of soils found in the watershed with textures varying from sandy loam to loam (Saran *et al*., 2010) and low to medium productivity (Singh, 2009). These soils of the study area belong to Ustic class of soil moisture regime and the depth of soil varies from shallow to deep

(Singh, 2009), drainage varies from well to excessive and permeability varies from low to medium (Bhaware, 2006).

3.1.3 Land use / Land cover

The major land units occupying the study area are forests, agricultural lands, scrubland, and settlements. The western part of the study area contains moderately dense to dense Sal (*Shorea robusta*) forest due to the favourable elevation, slope, and climate conditions. Agriculture constitutes a considerable area in the watershed. *Lantana camara* and *Ipomoea fistulosa* are the major shrubs found in the area. Settlement occupation is very less. Langha, Surna, Dobri, Barwa, Pasta, and Pasoli are some of the villages located in the watershed.

3.1.4 Climate

According to Koppen climate classification, the study area comes under the humid subtropical climate (Cwa) (Singh, 2009). The watershed goes through three major seasons. Hot summer season from March to June, the wet monsoon season from July to September and cold winter season from October to February. The mean annual temperature ranges from 15.8°C to 33.30°C. Table 1 shows that the hottest month May experience a maximum temperature of 35.3°C and the coldest month January go has a minimum temperature of 3.6°C. The average annual rainfall for 25 years is 2051.4 mm. Most of the rain falls in the months of July, August, and September (monsoon season). Among these July and August receive maximum rainfall.

3.1.5 Drainage

Sitla Rao is an ephemeral stream which flows south-west and joins the axial Asan River. It is a sixth-order stream according to Strahler (1964) stream ordering method. It flows North-West and joints to the Yamuna River at Dhalipur. Out of the six geomorphological units of Asan river watershed, Sitla Rao belongs to the flood plain. The runoff water from the rivulets such as Gauna, mauti and Koti nadi and other streams of the subwatershed flow into the main river, Sitla Rao. Most of

the numerous small channels are seasonal. Channel belts of the river occupy the lowest elevations in the Dehradun. River terrace of Sitla Rao is gentle to flat in nature. In the downstream reaches, gravels and pebbles constitute a major part of channel sediments. The drainage pattern is dense and is structurally controlled by bedrock geology (Ansari *et al*., 2013).

Table 1. Statistical summary of past climate during 25 years (1983- 2008)

Month	Rainfall (mm)	Relative Humidity (%)	Temperature(^{O}C)		
			Maximum	Minimum	Average
January	46.9	91	19.3	3.6	10.9
February	54.9	83	22.4	5.6	13.3
March	52.4	69	26.2	9.1	17.5
April	21.2	53	32	13.3	22.7
May	54.2	49	35.3	16.8	25.4
June	230.2	65	34.4	29.4	27.1
July	630.7	86	30.5	22.6	25.1
August	627.4	89	29.7	22.3	25.3
September	261.4	83	29.8	19.7	24.2
October	32.0	74	28.5	13.3	20.5
November	10.9	82	24.8	7.6	15.7
December	2.8	89	21.9	4.0	12.0
Average Annual	2051.4	76	27.8	13.3	20.0

3.1.6 Socio-economic conditions

People who live in the watershed are economically very poor. 75% of the population depends mainly on agriculture, forestry, and livestock farming for livelihood. They adopt mixed farming with animal husbandry and crop. Forest serves fuel, wood, and fodder to the rural people and this led to the degradation of forest area. On the steeper slopes, farmers suffer predominantly from erosion problems. Thus they have adopted terrace farming practice for their major crops to avoid erosion risks. Apart from this other soil and water conservation measures are less.

3.1.7 Satellite / remote sensing and topographical data

3.1.7.1 CartoSat-1 DEM

CartoSat-1 is a polar sun-synchronous Indian Remote Sensing satellite used for the cartography and topographical mapping applications. It has two panchromatic cameras with a resolution of 2.5m which helps to take two black-and-white stereoscopic images of an area simultaneously in the visible region of the electromagnetic spectrum.

Cartosat DEM (Fig. 3) with a resolution of 10 meters obtained from IIRS database was used in this study for drainage network analysis, to find slope and aspect, and quantitative analysis of run-off and soil erosion. The study area then extracted from the DEM.

3.1.7.2 IRS Resoursesat-1 LISS IV

The main mission of IRS-P6 Resourcesat-1 (Fig. 4) is the agricultural applications in India. LISS-IV, LISS-III and an Advanced Wide Field Sensor (AWiFS) are the three cameras of the Resourcesat-1. Among this LISS-IV is the high-resolution (5.8m) camera which can operate in three spectral bands (B2, B3, and B4) in the Visible and Near-Infrared Region (VNIR). It has a 10-bit radiometric resolution. The False Colour Composite (FCC) image of IRS Resoursesat-1 LISS IV of the study area obtained from the IIRS database was used as another way to characterise the land use and land cover.
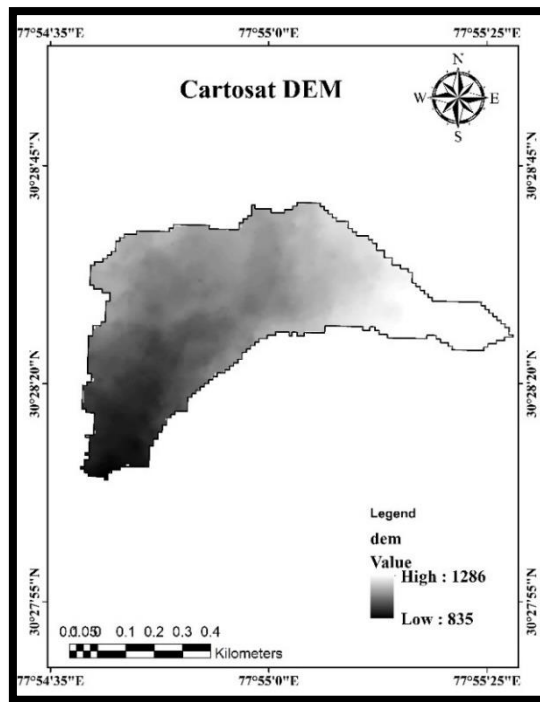
Figure 3. Extracted Cartosat DEM imagery of watershed
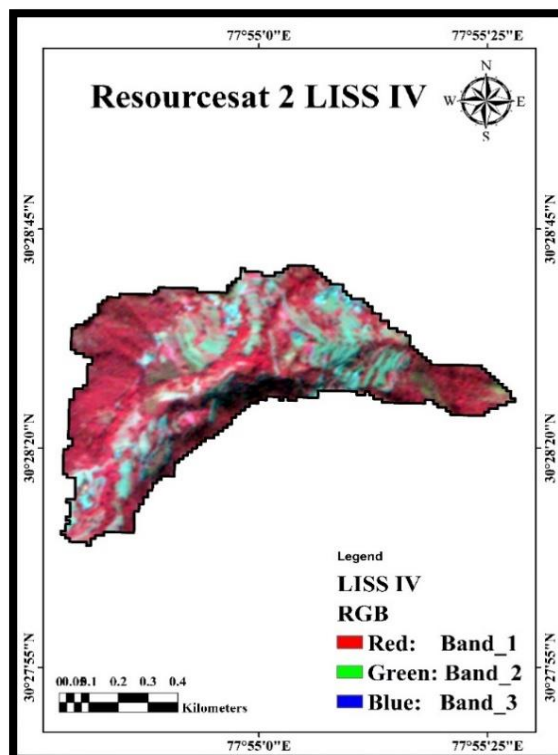
Figure 4. Extracted LISS IV FCC image of the study area

3.1.7.3 Toposheet

Topographic Sheet number 53 F /15 which contain the area Sitla Rao watershed was collected from SOI (Survey of India) and it helped for better sample collection, field surveys, terrain details, and watershed delineation.

3.1.7.4 Google Image (IKONOS)

IKONOS satellite imagery of Google Earth was used to study the watershed in detail and for preparing field plans. It also helped at the time of soil sample collection, visual interpretation of land use and to understand the distribution of collected samples.

3.1.8 Software used

3.1.8.1 ArcGIS

ArcGIS is a geographic information system (GIS) which works using maps and geographic information and has intensive applications in different fields. It was developed by ESRI (Environmental System Research Institute). In this study, ArcGIS version 10.3 was used to generate different types of map, assembling geographical data, DEM analysis and also, the model SWAT interfaced with ArcGIS software which is the Arc SWAT was used for soil erosion prediction. All the analysis in ArcGIS was carried out at Computer lab of Agriculture and Soils Department, IIRS.

3.1.8.2 Statistical software

Statistical Package for Social Science (SPSS) developed by International Business Machines Corporation (IBM) and STATISTICA developed by StatSoft were used for the statistical analysis of the results.

3.1.8.3 Instruments and materials used

The field instruments and lab equipments were used in the study for soil collection, processing and analysis are given in Table 2. All the Samples Were analysed in Central Analytical Laboratory, Agriculture and Soils Department, IIRS.

3.1.8.4 Research framework

A gauged micro watershed named Pasta which is part of Sitla Rao watershed of lesser Himalayas was selected for this study.
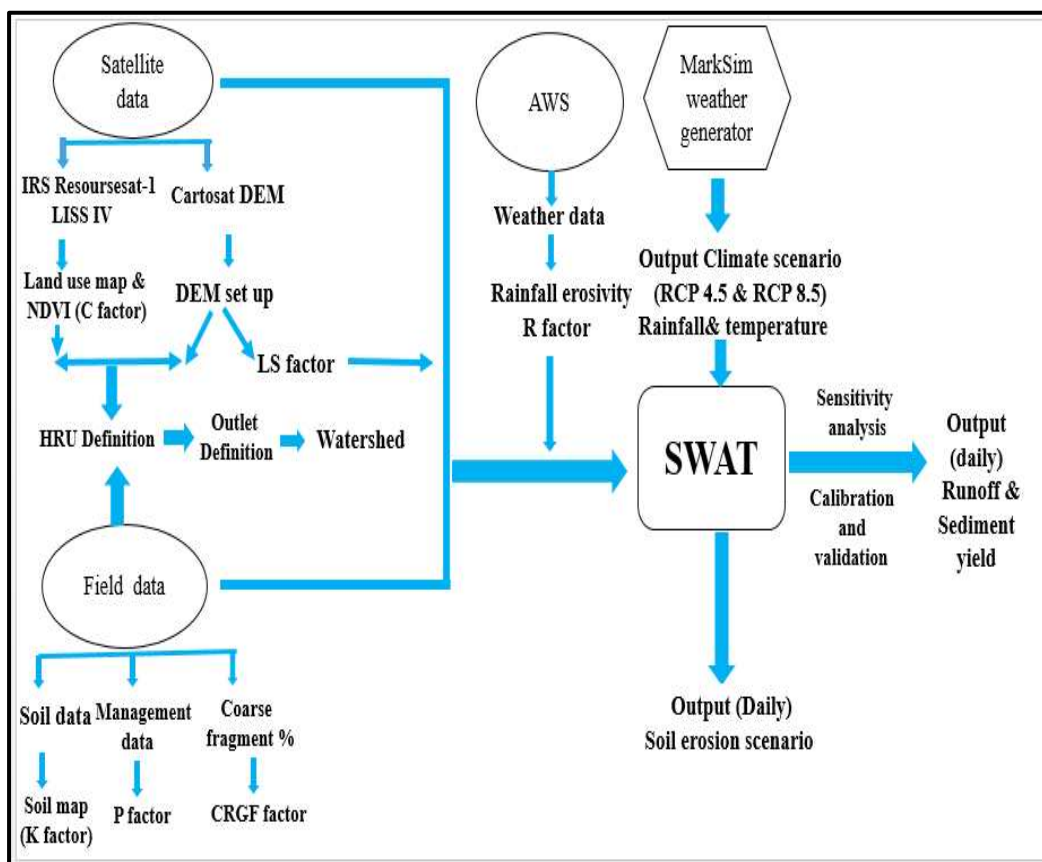
Figure 5. The framework of the study

The Soil and Water Assessment Tool (SWAT) with ArcGIS interface was used to simulate surface runoff and sediment yield. The downscaled future climate of RCP 4.5 and RCP 8.5 obtained for the study area from the Marksim weather Generator

was used. Future soil erosion scenarios under both RCPs were predicted for the 2020s, 2050s, and 2080s after proper calibration and validation.

Table 2. Field instruments and lab equipment used for the study

Field instruments		
Sl. NO.	Instruments	Purpose
1.	GPS (GARMIN)	Geospatial location (Latitude and Longitude)
2.	Soil Auger, Spade, Khurpi	To collect soil samples
3.	Laptop/PC, USB	Downloading data from Automatic Rain gauge, runoff recorder, and AWS
4.	Mini disc infiltrometer	To measure soil hydraulic parameters
5.	Digital camera	To capture field photographs
Lab equipment		
1.	Sieve	To remove roots, plant residues, coarse fragments etc.
2.	pH and EC meter	To analyse pH and EC
3.	Soil Hydrometer	To analyse soil texture
4.	Hot air oven	To dry the samples

3.2 THEMATIC MAP PREPARATIONS

Several thematic maps such as slope, aspect, stream order, land use/land cover, soil and drainage density were generated using ArcGIS 10.3 for this study. Slope, aspect, stream order and drainage density maps were prepared using the extracted DEM of the study area. Land use map, soil map and slope maps were the major input for the model.

3.2.1 Slope and Aspect map

Aspect map was used to find the direction of the slope faces and the flow direction of the streams in the watershed. Various slope classes and elevation ranges in the watershed were analysed with the slope map. The same DEM generated slope map was used as a major input to the SWAT model for erosion prediction.

3.2.2 Stream order and drainage density map

Stream order map prepared according to Strahler method (Strahler, 1957) in ArcGIS software was used to identify the orders of the streams in the study area. Drainage density map created was used to identify the range of drainage density of the streams in the watershed.

3.3 FIELD DATA COLLECTION

Several transect field surveys were carried out during the study period mainly for soil sample collection, land use/land cover identification, observations of erosion, and runoff processes in the watershed. All these field studies were conducted with the help of a GPS receiver (Garmin with an accuracy of ±5 m) to locate areas and for georeferencing. Interview with the villagers was conducted to collect the sowing and harvesting dates. Conservation practices like terracing and stone bund were observed in the cultivated area.

3.3.1 Land use/Land cover (LU/LC) observations.

LISS IV data obtained from IIRS database, IKONOS Google earth satellite imagery and the toposheet 53 F /15 which was collected from SOI played a major role in identifying land use/land cover of the study area. The first two field surveys were conducted in the month of September. Maize, rice, wheat, mustard, sugarcane, gram etc. are the major crops. Maize and rice are mainly cultivated in the Kharif season (rainy season, June and July). Wheat and mustard are grown in the Rabi (winter) season. Moderately dense Sal forest is coming under forest classification. It is observed that higher elevation forest is a mixed type and lower elevation forest is dominated by Sal. The higher elevation regions of steeper slopes are scrubland. The

river terraces are highly populated and extensively used for cultivation. While doing erosion survey and land use/land cover observation, validation of computer-generated slope map in ArcGIS using Digital Elevation Model (DEM) was done using Inclinometer and their georeferencing was conducted with the help of GPS. Height, sowing and harvesting dates of the major crops were collected during the land use/ land cover observations.

Figure 6. Maize and paddy cultivation in the watershed

Figure 7. Soil erosion survey

3.3.2 Erosion survey

Erosion survey (Fig. 7) was conducted in the months of September, January, and the first week of February. Erosion features from different land use, various conservation practices and their maintenance, slope features, farming practices, and coarse fragment percentage were observed and the details were collected according to the soil erosion proforma.

3.3.3 Runoff and sediment data collection

Observed data of runoff and sediment for the year 2016-2018 was required to calibrate and validate the model to generate daily runoff and sediment yield and previous year data was also obtained from IIRS database.

3.3.3.1 Runoff

A rectangular weir structure and a Digital Water Level Recorder (Pressure type) (Fig. 9) at the outlet of Pasta watershed is used to record surface runoff. This pressure-based Digital Water Level Recorder measures daily runoff with an interval of 15 minutes. Surface runoff for each event on a daily basis was calculated using a rating table.

Figure 8. Weir structure at the outlet   Figure 9. Digital Water Level Recorder

3.3.3.2 Sediment

Sediment yield data for 22 rain events were collected (July, August, and September) from the sediment tank at the site of automatic runoff recorder. Sediment filtration was done for all collected samples in the Central Analytical Laboratory (CAL) of IIRS. The filters which contain the filtered sediments were oven-dried and weighed for further calculation. The sediment weight was calculated from the oven dried samples and compared with the volume of water to find the sediment concentration in mg/l.

| Figure 10. Sediment tank | Figure 11. Sediment collection |

3.4 SOIL SAMPLE COLLECTION AND ANALYSIS

A transect soil sample collection (Fig. 12) was conducted in January and February. Google Earth imagery and toposheet were used to plan sample collection from the entire study area. Samples were collected from two different depths; surface (0-15 cm) and subsurface (15-30 cm) and all the locations were marked and georeferenced using GPS. A total of 66 samples were obtained during the sample collection period. All collected soil samples were air-dried and plant residues, gravel, stones etc were removed. Since model requires various physical and chemical properties of soil, for better results the entire samples were sieved through a 2 mm stainless steel sieve and kept in the central analytical laboratory to analyse

soil properties like pH, EC, Texture, Soil moisture, Bulk density, organic carbon and CHNS.
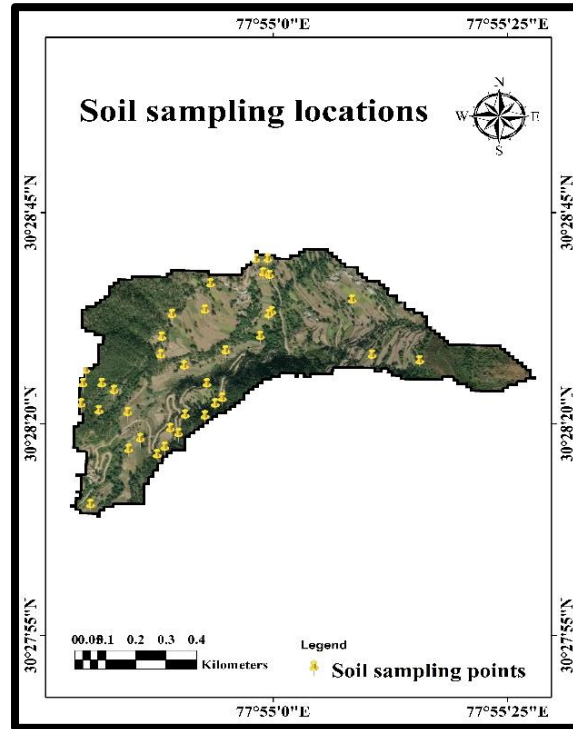
Figure 12. Soil sampling locations
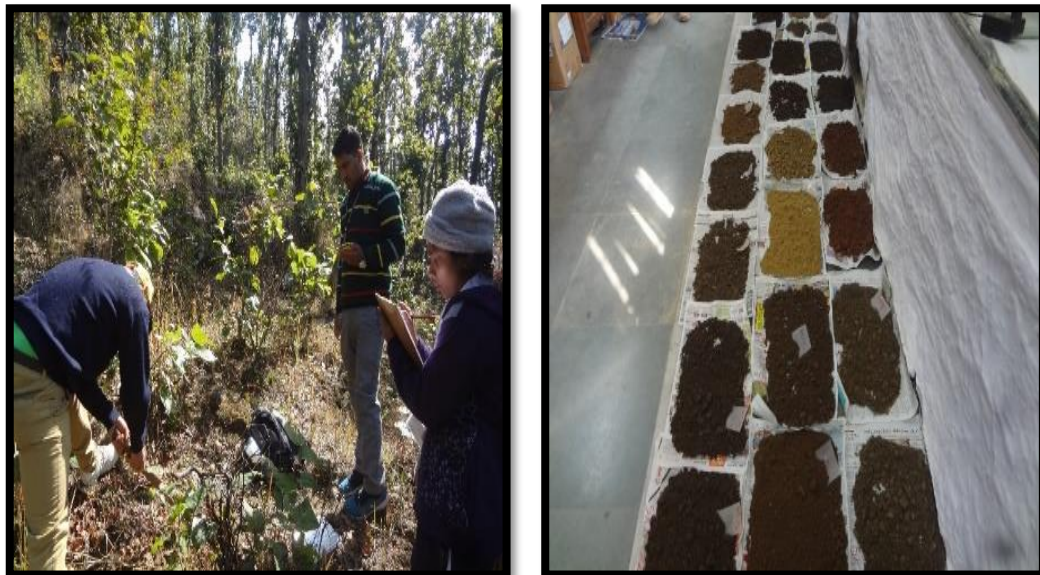
Figure 13. Soil sample collection and air drying

3.4.1 Soil pH and electrical conductivity

Soil pH and electrical conductivity (Fig. 14) are the major soil characteristics which measure the acidity or alkalinity of soil and amount of salts in the soil respectively. SYSTRONICS μ pH System which is calibrated with 3 different buffers (pH 4, 7, and 9.2) was used to measure the pH of the soil sample. EC is a measurement of the dissolved material in a solution. Electrical conductivity analysis was done with SYSTRONICS Conductivity TDS Meter 308 from CAL. Conductivity meter was calibrated prior to analysis.

Figure 14. PH and electrical conductivity analysis

Figure 15. Soil texture analysis

3.4.2 Soil texture

The texture of the collected samples was determined using the Bouyoucos Hydrometer Method (Fig. 15). Organic matter content in the soil was removed by adding hydrogen peroxide and the soil particles dispersed by applying sodium hexametaphosphate solution. Samples were stirred well with an electrical stirrer and transferred into the 1000 ml settling cylinder. After shaking the suspension vigorously, hydrometer readings were taken at the end of 40 seconds. The second reading was taken after 2 hours. Percentage of sand, silt and clay was calculated using the observations and the textural classes were identified using triangular texture diagram.

3.4.3 Bulk density (BD)

For bulk density, the modified wax method was used (Fig. 16). Soil clods collected from the field during the sample collection were dried in the oven at a temperature of 105°C for 2-3 days to remove all the moisture and weighed. These dried clods were dipped in melted wax and dried again. Wax applied clods were dipped into a water-filled cylinder of 500 ml capacity which have an outlet at the upper side having slope directed downward and the water coming through the outlet was collected in the measuring cylinder for further calculation of volume and BD.

Figure 16. Bulk density analysis using modified wax method

$$\text{Bulk density = mass of clod (gm)/volume of clod (ml)}$$

3.4.4 Organic carbon

Organic matter and organic carbon were estimated using Rapid Titration method (Fig. 17) (Walkley and Black, 1934). The reaction between potassium dichromate ($K_2Cr_2O_7$) and concentrated sulphuric acid helped to oxidize the soil samples and they were slowly digested at low temperature. Excess $K_2Cr_2O_7$ was titrated back against standard solution of Mohr salt in presence of sodium fluoride (NaF) and orthophosphoric acid (H_3PO_4) was used as flocculating agents; diphenylamine was used as an indicator and the endpoint of titration was recorded based on the visual colour change from violet to green. Subsequently, organic carbon was calculated as;

$$\text{Percentage of organic matter = Total Organic Carbon} \times 1.72$$

Figure 17. Rapid titration method

3.5 SOIL HYDROLOGICAL PROPERTIES

Unsaturated hydraulic conductivity and infiltration rate were measured using Mini Disk Infiltrometer in different land uses/ land covers. It measures the unsaturated hydraulic conductivity of the medium at different applied tensions. It has suction heads of 0.5 – 7 cm.

$$k = C_1/A$$

Where, k = hydraulic conductivity; C_1 = slope of the curve of the cumulative infiltration versus the square root of time; A = Van Genuchten parameters for a given soil type to the suction rate and radius of the Infiltrometer disk.

3.5.1 Soil Plant Atmosphere Water (SPAW) Model

The SPAW model (Fig. 18) developed by USDA was used to estimate the Available Water Content (AWC) which is a major input in the model. AWC can be estimated by giving soil textural class, organic matter and EC as inputs. It is easy to obtain other parameters like saturated hydraulic conductivity, wilting point, field capacity, matric bulk density etc. from this model.
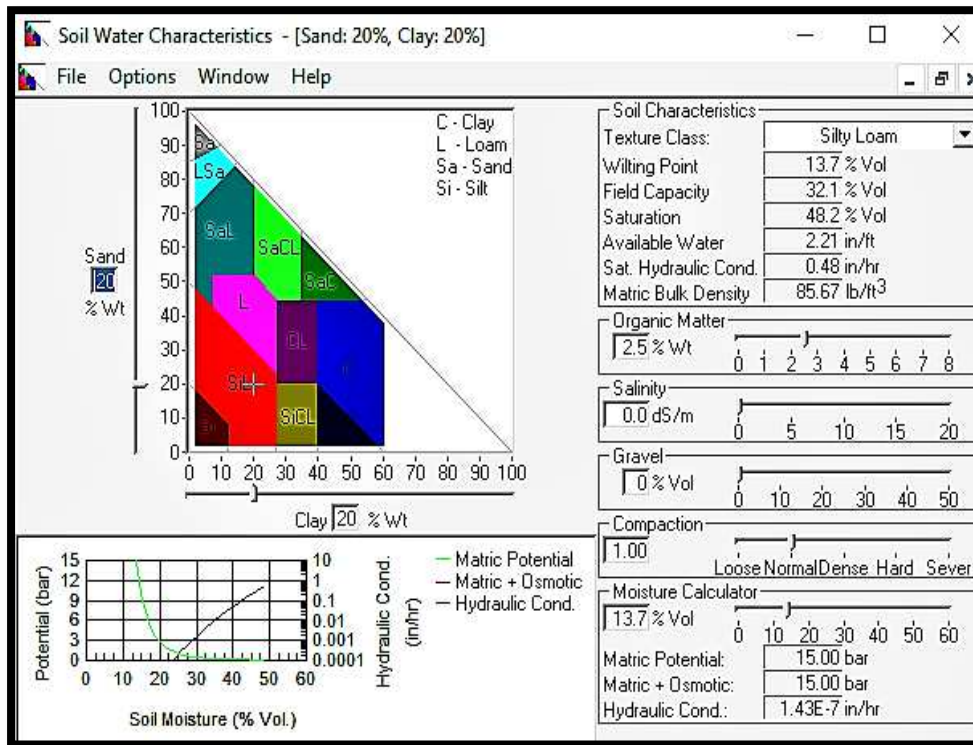
Figure 18. SPAW Model interface

3.6 WEATHER DATA

An Automatic Weather Station (AWS) (Fig. 19) (which measures maximum and minimum temperature, precipitation, solar radiation, maximum and minimum relative humidity, wind speed and direction, and dew point temperature) and a rain gauge (Fig. 20) (to record daily rainfall) was installed by IIRS in the Pasta

watershed was used to collect daily precipitation, maximum and minimum temperature required to model for the year 2016, 2017 and 2018.

Figure 19. Automatic weather station in the study area

Figure 20. Tipping bucket rain gauge in the study area

3.8 SOIL AND WATER ASSESSMENT TOOL (SWAT) MODEL DESCRIPTION

SWAT was developed by Dr. Jeff Arnold (Neitsch *et al.*, 2011) as a part of approximately 30 years modelling experience of USDA Agricultural Research Service (ARS) (Gassman *et al.*, 2007). SWAT is a physically-based (Neitsch *et al.*, 2011) continuous basin-scale model runs on a daily time step. The model is computationally efficient and capable of using readily available inputs to simulate the impact of management on water, sediment, and agricultural chemical yields (Neitsch *et al.*, 2011). In addition to that, the SWAT can be used to model a watershed without gauge data (Gassman *et al.*, 2007; Neitsch *et al.*, 2011). The model is a derivative of the Simulator for Water Resources in Rural Basins (SWRRB) model (Williams *et al.*, 1985; Arnold and Williams, 1987).

SWAT divides the watershed into a number of sub watershed or sub basin and further partitioned to Hydrologic Response Units (HRU) which have unique land use, soil, and management characteristics. The model required observed or generated climatic data of daily precipitation, maximum and minimum temperature, solar radiation, relative humidity, and wind speed data. If the Penman-Monteith method is used, only wind speed is required. If the Penman-Monteith (Monteith, 1965) or Priestly-Taylor (Priestly and Taylor, 1972) method is used to estimate potential evapotranspiration and transpiration, relative humidity is needed by the model. SWAT estimates surface runoff in two ways. SCS Curve Number procedure (SCS, 1972) and the Green and Ampt infiltration method (1911).

3.8.1 SWAT model equations

3.8.1.1 Calculation of surface runoff (Q_{surf})
In this study, surface runoff was calculated using the SCS Curve Number procedure. It is an empirical model developed to estimate runoff from different land use and soil types (Rallison and Miller, 1981) and it is a function of soil's permeability, land use and antecedent soil water conditions (Neitsch *et al.*, 2011).

$$Q_{surf} = (R_{day} - I_a)^2 / (R_{day} - I_a) + S$$

Where Q_{surf} is the rainfall excess (mm H2O), R_{day} is the rainfall depth of the day (mm H2O),

I_a is the initial abstractions which contain surface storage, interception and infiltration before runoff (mmH2O), and S is the retention parameter (mm H2O). S differs spatially because of the variations in soils, land use, management, and slope and temporally as a result of variations in soil water content. The retention parameter can be calculated as:

$$S = 25.4 \ (1000/CN - 10)$$

Where CN is the curve number for the day. I_a is generally assumed as $0.2S$ and thus the equation come to be

$$Q_{surf} = (R_{day} - 0.2S)^2 / (R_{day} - 0.8S) + S \qquad \text{Runoff occurs when } R_{day} > I_a$$

3.8.1.2 **Calculation of peak runoff rate (q_{peak})**

The peak runoff rate of the given rainfall event is the maximum runoff flow rate of that event and it is used to estimate sediment loss. It is an indicator of the erosive power of rainfall. SWAT uses the Modified rational method to estimate the peak runoff rate.

$$q_{peak} = C.i.Area / 3.6$$

Where, q_{peak} is the peak runoff rate ($m^2 \ s^{-1}$), C is the runoff coefficient, i is the rainfall intensity (mm/hr), Area is the HRU area (km^2), and 3.6 is a unit conversion factor. Sediment yield for each HRU was calculated and summed to estimate total sub basin fluxes (Arnold *et al*., 1998).

The erodability of soil (K) happens due to the variation in the soil properties itself. Some soil may erode easier while the other may not (Neitsch et al., 2011). Wischmeier and Smith (1978) noticed a reduced erodability for the soil type which has a decreased silt fraction and increased clay and sand fraction. Erodibility factor

(K) was calculated from the regression equation given by Wischmeier *et al.*, (1971) stated below.

$$K = 2.8 \times 10^{-7} M^{1.14} (12 - \alpha) + 4.3 \times 10^{-3} (b - 2) + 3.3 \times 10^{-3} (c - 3)$$

Where M is the particle size parameter; α is the percent organic matter; b is the soil structure code; c is the profile permeability class.

3.8.1.3 Calculation of soil loss

SWAT uses the MUSLE (Modified Universal Soil Loss Equation) to estimate the erosion by rainfall and runoff which is an upgrade of the USLE (Universal Soil Loss Equation). USLE predicts erosion as a function of rainfall energy. In MUSLE erosion is predicted as a function of runoff factor.

$$Sed = 11.8 \cdot (Q_{surf} \cdot q_{peak} \cdot Area_{hru})^{0.56} K_{usle} \cdot C_{usle} \cdot P_{usle} \cdot LS_{usle} \cdot CFRG$$

where sed is the sediment loss (metric ton), Q_{surf} is the surface runoff (mm), q_{peak} is the peak runoff rate (m^3/s), area$_{hru}$ is the HRU area (ha), K_{usle} is the USLE soil erodibility factor, C_{usle} is the USLE cover and management factor, P_{usle} is the USLE support practice factor, LS_{usle} is the USLE topographic factor, and CFRG is the coarse fragment factor.

3.8.1.4 Cover and Management Factor (C_{usle})

Cover and Management Factor (C_{usle}), is the ratio of soil loss from land cultivated under specified environments to corresponding loss from clean-tilled, continuous fallow (Neitsch *et al.*, 2005). The SWAT model updates C_{usle} daily as the plant cover varies during the growth cycle of the plant. The minimum C factor for the land cover can be calculated from the equation below (Arnold and Williams, 1995)

$$C_{USLE\ mn} = 1.463 \ln[C_{USLE\ aa}] + 0.1034$$

Where, $C_{USLE, mn}$ is the minimum C factor for the land cover and $C_{USLE, aa}$ is the average annual C factor for the land cover.

3.8.1.5 Support practice factor (P usle)

Support practice factor, (P usle) contain soil and water conservation measures like contour tillage, strip-cropping on the contour, and terrace systems. Each support practices have different values, which are further influenced by the slope factor. The P_{usle} is calculated for each land use/cover type and for each sub basin in the management information file.

3.8.1.6 Topographic factor (LS_{usle})

Topographic factor, LS_{usle} is the anticipated ratio of soil loss per unit area from a field slope to that from a 22.1m length of uniform 9 percent slope under otherwise equal conditions (Neitsch et al., 2005). The calculation of LS_{usle} factor can be obtained easily from the input DEM

3.8.1.7 Coarse fragment factor (CFRG)

The coarse fragment factor is the percentage of rock in the soil layer. The value for the *CFRG* factor is provided in the soil database. It can be estimated by

$$CFRG = exp (-0.053.rock)$$

Where rock is the percent rock in the first layer (%)

3.8.2 Model set up

The SWAT model was applied to the pasta micro watershed which has an area of 57 ha for the detailed study. The model implementation was started by creating a new project set up in the Arc SWAT to activate the automatic watershed delineation menu. The watershed delineation part contains five sections

3.8.3 DEM set up

The CartoSat DEM with 10 m resolution obtained from the IIRS database was loaded to the Arc SWAT raster geodatabase. The DEM was projected to the Universal Transverse Mercator (UTM) 43N coordinate system and the Z units were defined in meters. The mask option is useful when the DEM covers a much larger

area than the study area itself. Only the portion of the DEM covered by the mask will be processed and saves time.

3.8.4 Stream Definition

For stream definition, DEM based method which assigns flow path based on the elevation was selected. Flow direction and accumulation option process the DEM map to remove all the non-draining sinks. The Area option in this section suggests an optimal threshold area for the initial stream network definition. In this case, the suggested minimum was 39 ha after the DEM processing and it was adjusted to 2 ha. The smaller the area the more detailed the drainage network. After all these steps the last option stream network was allowed to create streams and outlets to begin the actual process.

3.8.5 Outlet and Inlet Definition

This section gives the options of adding outlets to refine the stream network. The location of the Automatic runoff recorder situated in the micro-watershed was loaded to the interface by dbase table and the outlet of the whole watershed was edited manually.

3.8.6 Watershed Outlet(s) selection and Definition

This option helps to delineate the watershed by manually selecting the whole watershed outlet(s). The entire watershed was partitioned into sub-basins of threshold value of 2 ha.

3.8.7 Calculation of Sub basin Parameters

It is the last section of the Automatic watershed delineation process. Once the watershed is delineated calculation of sub basin parameters option become available.

3.8.8 HRU analysis

To make the simulation easy and accurate SWAT divides the sub-basins into HRUs which are the areas of similar land use, soil and slope. This section of the model helped to reclassify the land use, soils and slope of the study area.

3.8.9 Land use

The land use map prepared from ResourceSat LISS IV data with the help of Google earth and visual interpretation methods is clipped into the watershed area. Later the SWAT's land use database and land use map were linked by a Look Up table.

3.8.10 Soil

Soil physical parameters were stored to the SWAT's soil database through the interface initially, and significant information needed for soil erosion modelling was provided to the model. The prepared soil map was clipped and the database was linked to the map with the help of lookup table.

3.8.11 Slope

Like the land use map and soil map, slope map prepared from the DEM was also clipped into the watershed area. The maximum slope of the study area generated was 167. So the slope was classified into five classes.

The last step was to overlay the reclassified land use, soil and slope map which bring a new layer

3.8.12 HRU definition

Since the model partitioned the study area into a number of HRU for the accurate results, HRU definition is an important step. Here the dominant land use, soils, and slope option was selected for the creation of HRU.

3.8.13 Input table writing

The Write input table option helps to define the Weather Database. Important daily data required by SWAT are precipitation, maximum and minimum temperature,

solar radiation, wind speed, and relative humidity. Monthly average climatic data for weather generator data file (.WGN) was calculated as mentioned in the user manual of the model. And also daily maximum and minimum temperature and precipitation data were prepared. All these inputs are given to the model in ASCII format.
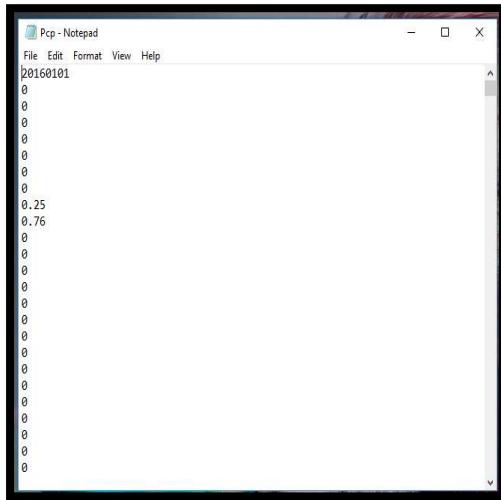
Figure 21. Rainfall input file
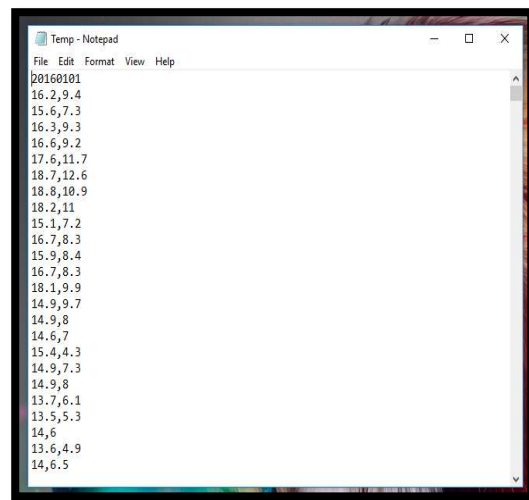
Figure 22. Temperature input file

3.8.14 Editing SWAT Inputs

Analysed soil parameters and crop data were entered by editing the databases of user soil and land cover/plant growth files respectively.
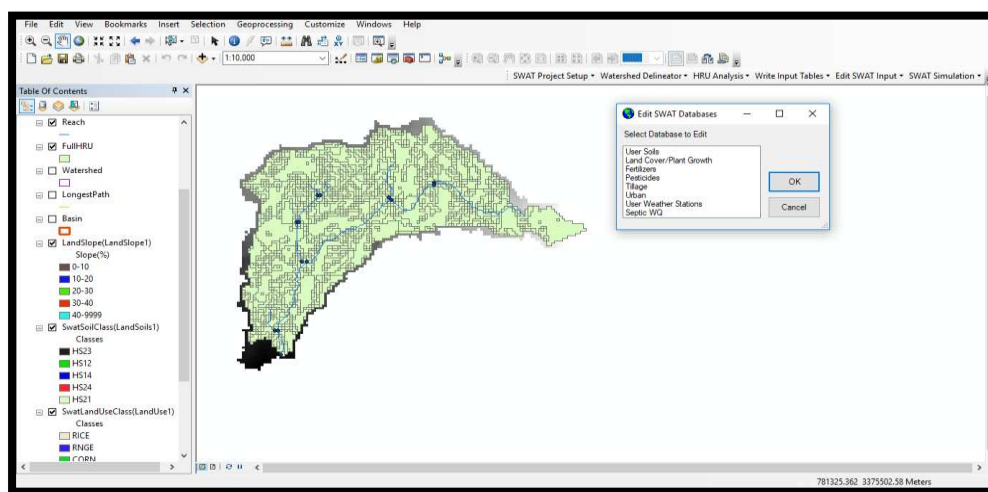
Figure 23. Database of the model

Rest of the important data such as subbasin (.sub), HRU (.Hru), Routing (.Rte), Management (.Mgt), and Operations (.Ops) were edited in the sub basin data file.
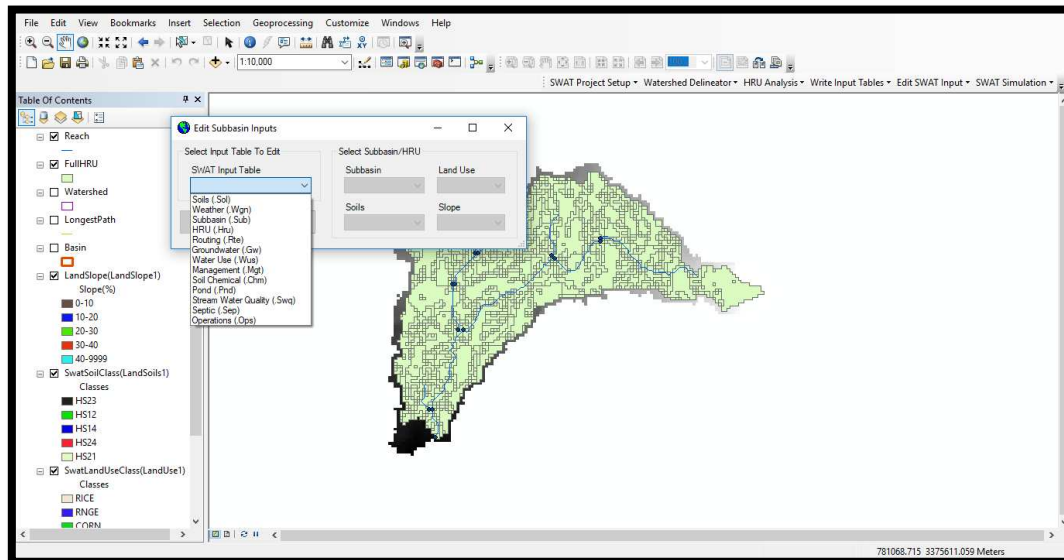
Figure 24. Edit subbasin input option

Editing the management file (.Mgt) of the model was important for sensitivity analysis and calibration. Mainly the crop calendar was incorporated for better simulation.
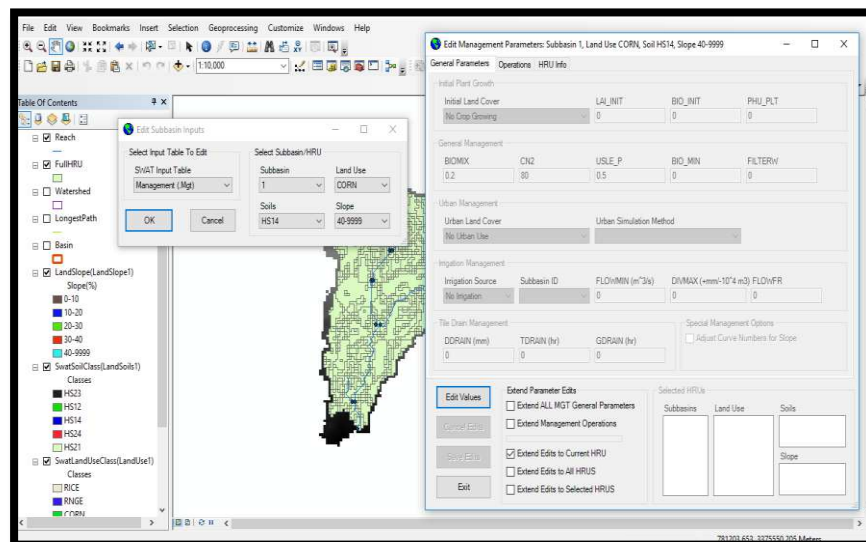
Figure 25. General management parameters

The default setting which assumes crop growth at the beginning of simulation was changed for croplands (for maize and paddy) and sowing and harvesting dates were

added. For scrub and forest default settings were kept unaltered since they have attained their maturity in reality.
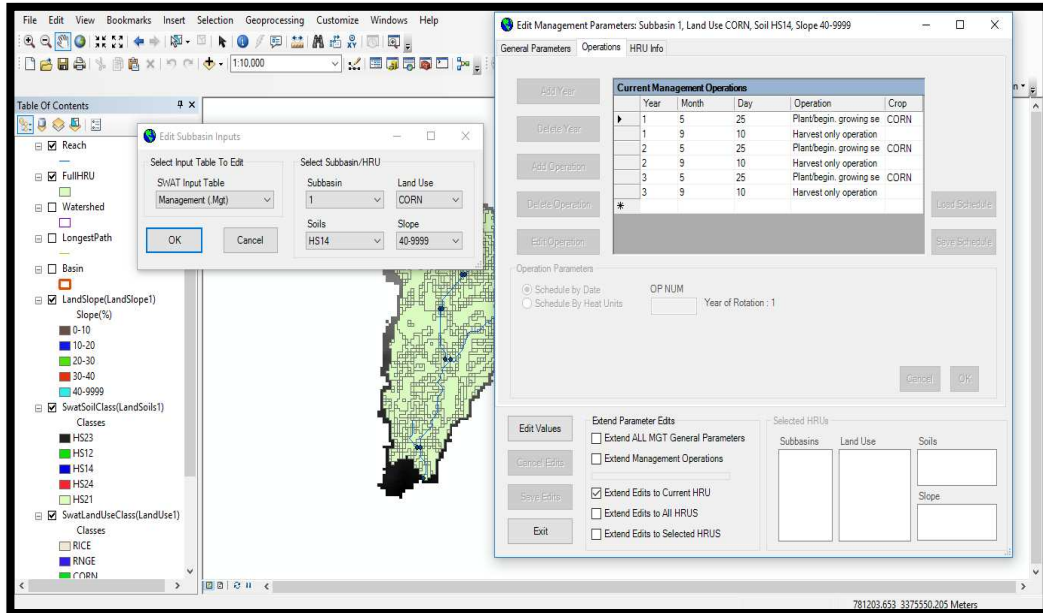
Figure 26. Operation scheduling option

After input incorporation and editing of the database, SWAT was run on a daily basis. Model outputs stored in different folders such as .hru, and .rch, were compared with observed runoff and sediment yield and adjusted the values through calibration.
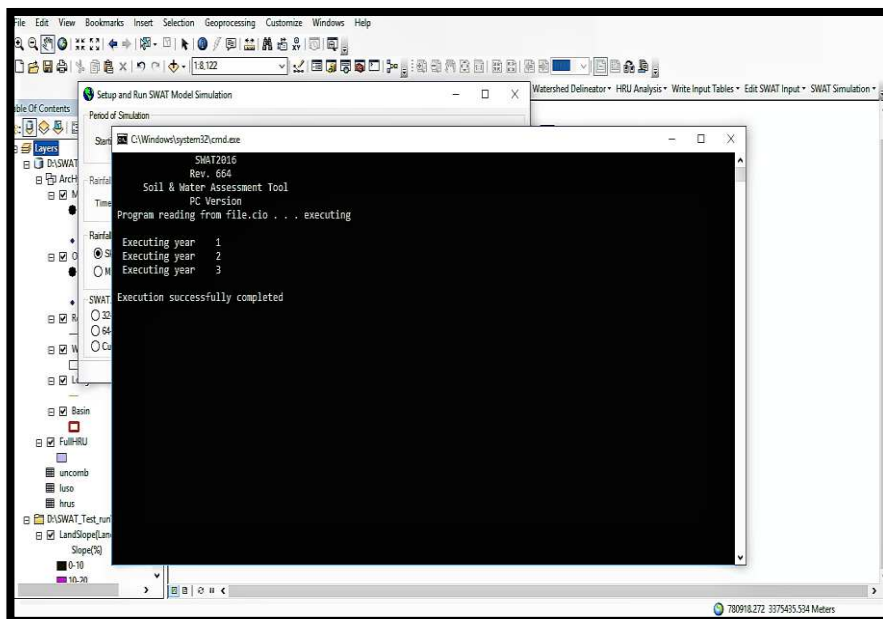
Figure 27. Model execution

3.9 SENSITIVITY ANALYSIS

Sensitivity analysis was performed to understand the effect of various model parameters on the output based on literature. Parameters like CN, AWC, USLE_P, and USLE_C were altered for their influence on runoff and sediment yield.

3.10 MODEL CALIBRATION AND VALIDATION

SWAT was calibrated and validated for daily runoff and sediment yield at the watershed outlet. Data for a total of 28 rainy days was collected for runoff. 16 samples were used to calibrate the model and 12 used for validation. Data for 22 rainy days were available for sediment analysis.12 used for the calibration and the rest used for validation.

3.11 FUTURE CLIMATE DATA AND CLIMATE CHANGE IMPACT ASSESSMENT

To study the future climate change impacts on soil erosion in the study area, climate change scenario developed by the Intergovernmental Panel on Climate Change was selected. The first set of climate change scenario IS92 by IPCC was published in 1992. Later in 2000 the Special Report on Emissions Scenarios (SRES) which is the second generation of projection was released and used for Third Assessment Report (TAR) and Fourth Assessment Report (AR4). But in 2007 IPCC improved the SRES and developed a new set of scenarios called Representative Concentration Pathways (RCPs). These latest scenarios were used in the IPCC's fifth assessment report (AR5) in preference to SRES (Wayne, 2013). RCPs (Table 3) were developed in a way of representing total literature available on emissions and concentrations. These scenarios harmonized the land use and emission data to a 0.5 × 0.5 grid and also harmonized with the data on historical periods. They allow the exploration of possible future climate in a wide range than ever before. It is expected that these scenarios can be used as an input for climate modeling, input into mitigation analysis, input into impact assessment, and to form an analytical thread. This advanced set includes four scenarios which are named based on their projected radiative forcing level for 2100. The RCP 2.6 is the lowest forcing level

and mitigation scenario, among the four scenarios, and also been referred to as RCP3PD (PD- Peak Decline). RCP 4.5 and RCP 6 are the medium stabilization scenarios. The RCP 8.5 is the very high baseline emission scenario. Two representative concentration pathways (RCPs) 4.5 (medium stabilization scenario) and 8.5 (high emission scenario) emission scenarios were selected to predict the future climate impact on soil erosion in the watershed.

Table 3. RCP emission scenarios

Scenarios	Description
RCP 2.6	• Its radiative forcing level first reaches a value of around 3.1 W/m^2 by mid-century and returns to 2.6 W/ by 2100.
RCP 4.5	• a stabilization scenario in which total radiative forcing is stabilized soon after 2100, without exceeding the long-run radiative forcing target level (Clarke *et al.* 2007; Smith and Wigley 2006; Wise *et al.* 2009).
RCP 6	• Total radiative forcing is expected to stabilize soon after 2100, without overshoot, because of the application of technologies and strategies for decreasing greenhouse gas emissions (Fujino *et al.* 2006; Hijioka *et al.* 2008).
RCP 8.5	• This RCP is characterized by increasing greenhouse gas emissions over time, representative of scenarios in the literature that lead to high greenhouse gas concentration levels (Riahi *et al.* 2007).

3.11.1 Marksim weather generator.

Marksim weather generator (Fig. 28) is an online web application which can provide the downscaled data of weather parameters such as rainfall, temperature,

solar radiation etc. Marksim is a daily rainfall generator which calculates the probability of a wet day using a third-order Markov process.
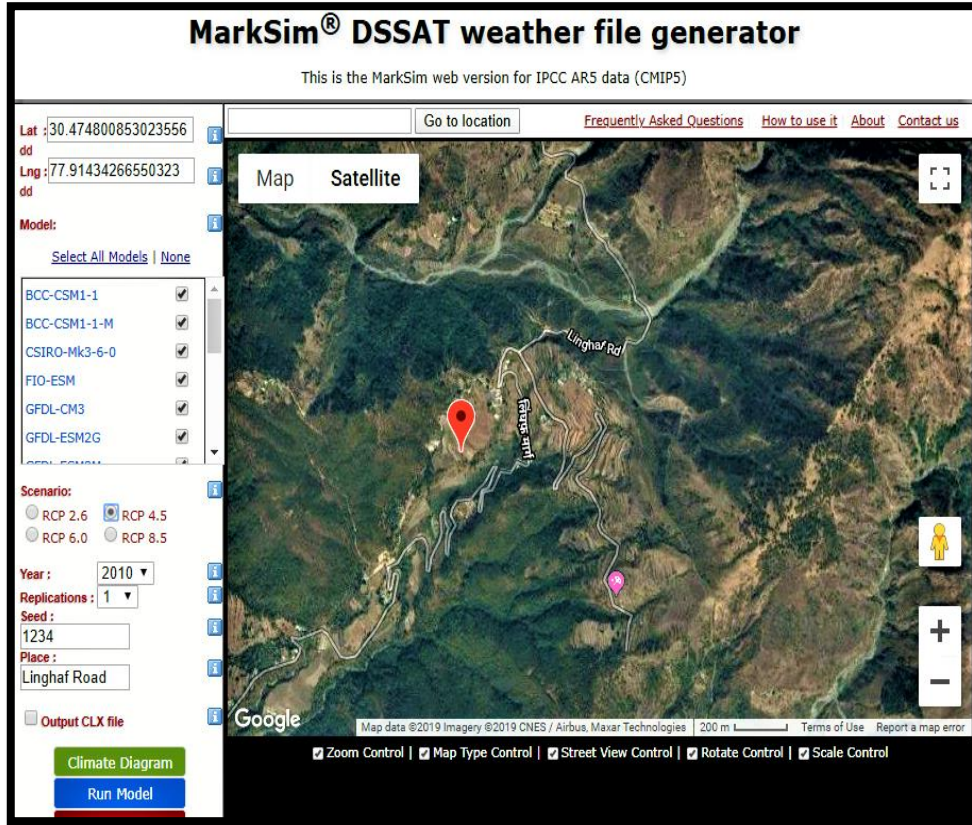
Figure 28. Marksim DSSAT weather file generator interface

Daily values of maximum and minimum temperatures are generated based on routines of Richardson (1985) and Geng *et al*. (1988). Model of Donatelli and Campbell (1997) is used for generating the monthly values of solar radiation from the temperature normal. Downscaled data of daily rainfall and temperature for RCP 4.5 and RCP 8.5 were generated from MarkSim weather generator for 2010 – 2095 by giving latitude and longitude of the study area as inputs. It has 17 Atmosphere-Ocean General Circulation Models (GCMs) and IPCC recommends an average of several models for any impact studies (Wilby *et. al*., 2004) so an average of all these models was downloaded for this study for 100 years. A brief description of the 17 atmospheric models are given below.

3.12.1.1 BCC-CSM 1.1

 BCC-CSM 1.1 is a fully coupled global climate carbon model with a spatial resolution of 2.81×2.81 developed by Beijing climate centre (BCC), China meteorological administration (CMA) (Wu *et al*., 2012).

3.12 .1.2 BCC-CSM 1.1 (m)

This model is also developed by Beijing climate centre (BCC), China meteorological administration (CMA) and also fully coupled with the inclusion of global carbon cycle like BCC-CSM 1.1. BCC-CSM 1.1 (m) has a moderate resolution in their atmospheric component and has a spatial resolution of 2.81°×2.81°.

3.12.1.3. CSIRO-Mk3.6.0

Developed by commonwealth scientific and industrial research organisation and Queensland of climate change centre of excellence. It is an improved version of CSIRO-Mk3.5 GCM (Gordon *et al*., 2010). In Mk3.6 an interactive aerosol treatment and an updated radiation scheme were newly included.

3.12.1.4. FIO- ESM

A coupled climate model named FIO- ESM was developed by The First institute of oceanography, SOA, China (Song *et al*., 2012) and this is the first model that includes surface waves. It has a spatial resolution of 2.81°×2.81°.

3.12.1.5. GFDL CM3

It was developed by the laboratory for Geophysical Fluid Dynamics. The popular complete model of GFDL, CM2.1 (Delworth *et al*., 2006) was used as the starting point to build the CM3 Coupled model of the next generation. The atmospheric aspect was the subject of the main development effort for CM3. It has a 2.0°x 2.5°spatial resolution.

3.12.1.6 GFDL ESM2G, and GFDL ESM2M

These two models were developed by Geophysical fluid dynamics laboratory with a spatial resolution of $2.0º{\times}2.5º$. The models differ mainly in the physical component. In ESM2M vertical coordinate based on depth is used and in ESM2G vertical coordinate is based on density. These two models utilize a more advanced land model.

3.12.1.7 GIS E2- R

This uses the atmospheric code of the ModelIE on a lat-lon grid, a 0.1 mb model with 40 vertical layers, which is coupled to the Russell ocean model. There are three variations of this model that differ in how it treats aerosols and atmospheric chemistry. This model was created by the NASA Godard Space Studies Institute. It has a $2.0ºx2.5º$ spatial resolution.

3.12.1.8 GIS E2- R

It uses the same model ModelIE atmospheric code as GIS E2- R but it is coupled with HYCOM ocean model and have 3 physics version. It has a spatial resolution of $2.0º{\times}2.5º$. This model was developed by NASA Godard institute of space studies.

3.12.1 .9 HadGEM2- ES

The model was developed by the Met Office Hardly centre. It has a spatial resolution of $1.24º{\times}1.87º$. This model is designed to run the major scenarios for IPCC AR5. This is an earth system model which is coupled to AOGCM.

3.12.1.10 IPSL- CM5A-LR and 12. IPSL- CM5A-MR

These models were developed by Institute Pierre-Simon Laplace. It has a spatial resolution of $1.9º{\times}3.8º$. This is the low-resolution version of the IPSL- CM5A earth system model. The IPSL- CM5A-MR is the medium resolution version of IPSL-CM5A earth system model with a resolution of $1.26º{\times}2.5º$.

3.12.1.11 MIROC- ESM

The Institute of Atmosphere and Ocean Research (University of Tokyo), the National Institute for Environmental Studies, and the Japan Agency for Marine Earth Science and Technology have jointly created it. It has spatial resolution of $2.82^{\circ} \times 2.82^{\circ}$. MIROC-AGCM 2010, SPRINTARS 5.00, COCO 3.4, and MATSIRO are interactively coupled in MIROC.

3.12.1.12 MIROC ESM –CHEM

Simulation of atmospheric chemistry in MIROC ESM CHEM is based on the chemistry model CHASER. (Sudo *et al.*, 2002). They consider the detailed photochemistry in the troposphere and stratosphere. It has a spatial resolution of $2.82^{\circ} \times 2.82^{\circ}$.

3.12.1.13 MIROC 5

It has a spatial resolution of $1.4^{\circ} \times 1.4^{\circ}$. It is known as model for interdisciplinary research on climate. A century-long control experiment was performed using the new version with the standard resolution of the T85 atmosphere and 1° ocean models.

3.12.1.14 MRI- CGCM3

Atmospheric component MRI AGCM 3 is interactively coupled with the aerosol model to represent direct and indirect effects of aerosol with a new cloud microphysics scheme. It has a spatial resolution of $1.125^{\circ} \times 1.125^{\circ}$.

3.12.1.15 NorESM1-M

NorESM is the Norwegian earth system model developed by Norwegian Climate Centre. The model is based on the community climate system model version 4 (CCSM 4). NorESM1-M is the first version of the NorESM model with intermediate resolution. It has a spatial resolution of $1.875^{\circ} \times 2.5^{\circ}$.

3.12 PREDICTING FUTURE SOIL EROSION

After calibration and validation, the model was run for RCP 4.5 and 8.5 for three periods namely 2020s (2010 – 2039), 2050s (2040 – 2069), and 2080s (2070 – 2095). Only daily precipitation and temperature data obtained from the Marksim weather generator and WGN file prepared with this data were entered in the model. Rest of the parameters kept unaltered for future prediction.

IV. RESULTS AND DISCUSSION

The results obtained after the land use /land cover observations, analysis of soil properties, present and future weather data calculations, SWAT model calibration, validation and future soil erosion scenarios predicted using the downscaled future climate under RCP 4.5 and RCP 8.5 are discussed in this section.

4.1 TERRAIN CHARACTERIZATION

Terrain analysis was carried out with Cartosat DEM of 10 m resolution. It helped to understand the range of elevation, slope, aspect, drainage, stream power, etc. From the analysis of DEM, elevation was observed as ranging from 835 to 1286 m above mean sea level.

4.2. THEMATIC MAP GENERATION

4.2.1 Slope map

The slope (Fig. 29) of the study area is classified (Table 4) as gentle (0-10), moderate (11-20), moderately steep (21-30), steep (31-40), and very steep (>41). 43.70 % of the study area comes under very steep slope class.
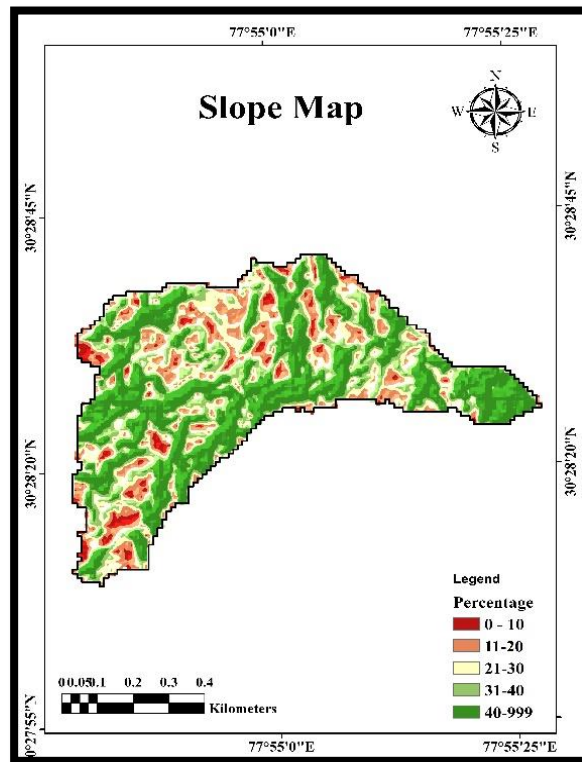
Figure 29. Slope map of the watershed

Followed by moderately steep (19.42%) and steep slopes covered by 18.16%. Moderately sloping area contributes 13.91% and gentle slopes cover 4.81%. A total of 62% of area is covered under steep to very steep slopes. Scrub land in the study area belongs to the very steep (>41) slope category. This higher slope is a major reason for soil erosion and landslips in this region.

Table 4. The area under different Slope class

Sl. No.	Percentage Slope	Description	Area(ha)	Area (%)
1	0-10	Gentle	2.70	4.81
2	11-20	Moderate	7.82	13.91
3	21-30	Moderately Steep	10.92	19.42
4	31-40	Steep	10.21	18.16
5	>41	Very Steep	24.56	43.70

4.2.2 Aspect map

Cartosat DEM was also used to prepare Aspect map (Figure 30) of the watershed. Aspect map gives the idea about the direction that a slope face. When the terrain is flat, there is no slope. From the aspect map, it was clear that most of the slopes face west and southwest direction, which indicates that water flow is in this direction. According to this, it was observed that the mainstream in the study area flows in the same direction, and ground observation was carried out to validate this. Table 5 gives different aspects and percentage of area covered under each aspect. Among this 22.93 % of the area is west facing, 18.01% southwest facing, 15.96% southeast facing, 14.46% south facing, 7.54% east-facing, 4.37% north-facing, 2.43% north east facing, 0.12% of the area with no slope is flat. Aspect of the major land uses

such as scrub land, maize and forest at the lower part of the watershed are facing towards west, southwest and northwest directions. Aspects of paddy and the forest land at the upper part of the watershed are directed towards the east, southeast and south.
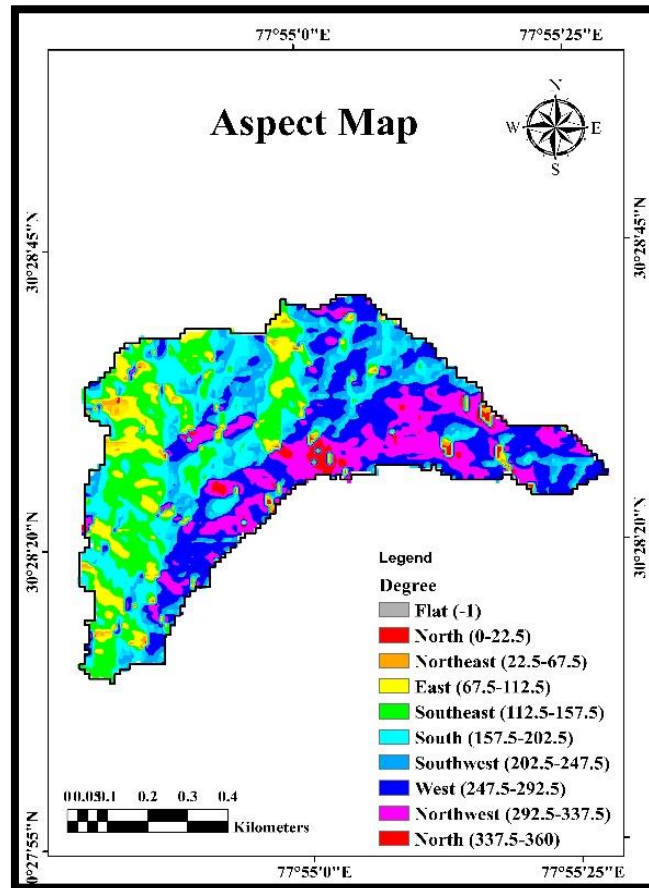
Figure 30. Aspect map of the watershed

The gauging station is built in the third order stream of the study area. Based on Strahler, (1953) stream ordering method (Fig. 31), six first order streams, two second order streams, and one third order stream were identified. Apart from stream ordering, drainage density (Fig. 32) of the watershed was also analysed. A minimum of drainage density of 0.52 to maximum 5.15 was observed per unit area. Higher drainage density indicates higher soil erosion.

Table 5. The area under different aspect class

Sl. No.	Aspect Angle(º)	Aspect Class	Area(ha)	Area (%)
1	-1	Flat	0.07	0.12
2	0-22.5	North	0.80	1.42
3	22.5-67.5	Northeast	1.37	2.43
4	67.5-112.5	East	4.24	7.54
5	112.5-157.5	Southeast	8.97	15.96
6	157.5-202.5	South	8.13	14.46
7	202.5-247.5	Southwest	10.12	18.01
8	247.5-292.5	West	12.89	22.93
9	292.5-337.5	Northwest	7.97	14.17
10	337.5-360	North	1.66	2.95
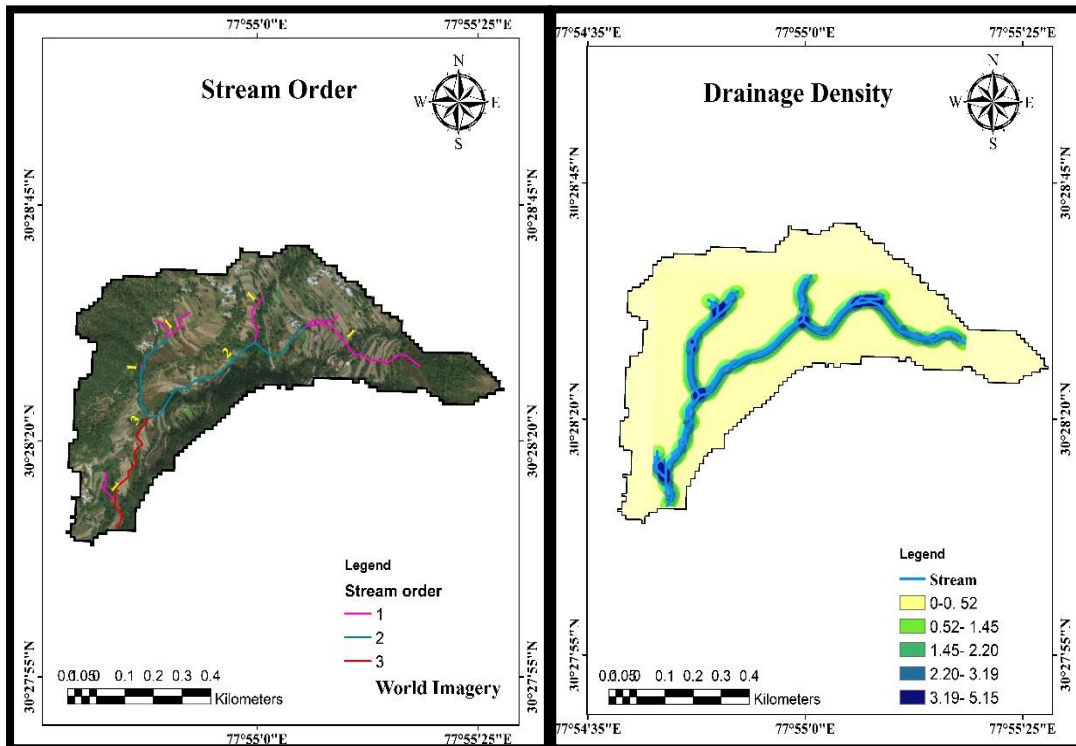
Figure 31. Stream ordering   Figure 32. Drainage density

4.3 LAND USE/ LAND COVER

LU/LC map (Fig. 33) was prepared with the help of LISS IV and Google Earth
image. Paddy, maize, dense forest, scrubland, and settlements were classified as
land use in the watershed. 62.8% of the watershed is under cultivation (maize and
paddy). In this (Table 6) 38.4% area is under maize cultivation and 24.4% is under
paddy fields. Only 2.3% area is occupied by settlements. 14.6% of the study area is
under moderately dense forest and 5% of area is under scrubland. The scrubland is
located in the uppermost part of the watershed, paddy field located in the lower part
of the watershed and maize located upper hillsides of the watershed. The land use/
land cover map prepared was also used as the model input for the runoff and
sediment yield simulation.
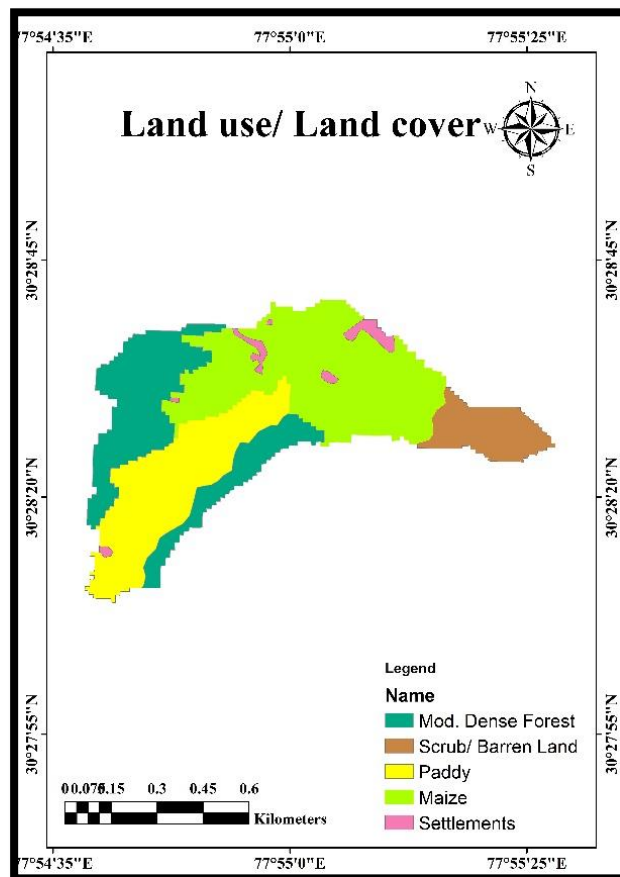
Figure 33. Land Use/Land cover map of the watershed

Table 6. Area of different land uses in the watershed

Land use	Area (ha)	Area (%)
Scrubland	5.0	8.9
Maize	21.6	38.4
Paddy	13.7	24.4
Moderately dense forest	14.6	26.0
Settlements	1.3	2.3

4.4 SOIL PHYSIOGRAPHIC UNITS

Physiographic soil units (Fig. 34) were created based on the geomorphology, topography, and major land use land cover. Five major classes were classified according to slope, position, and land use/ land cover. The major physical and chemical properties are grouped into tables (Table 7-10). During the analysis it was seen that sandy loam is the major soil textural class.
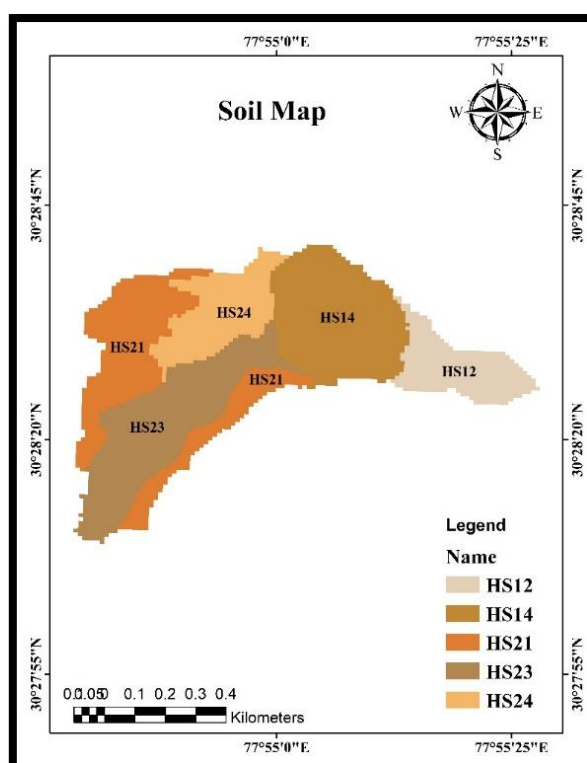
Figure 34. Soil physiographic units of the watershed

Table 7. Soil physiographic unit classification

Geomorphology	Topography	Major land use/ land cover	Legend
Sub- Himalayan Hill side slope (HS)	Very steep	Scrub/ Barren	HS12
		Crop land (Maize)	HS14
	Steep to very steep	Moderately dense forest	HS21
	Moderately steep	Crop land (Paddy)	HS23
		Crop land (Maize)	HS24

The topography of the study area is divided into three such as very steep, steep to very steep, and moderately steep. Very steep area contributes scrub land and maize cropping. Steep to very steep contribute moderately dense forest and moderate topography contributes maize and paddy. This topography comes under Sub-Himalayan hillside slope.

Higher sand content was observed in all physiographic units. Sandy loam is the major soil type in the watershed. This is mainly due to massive erosion of clay and loam particles. In higher elevation, due to slope the major textural class is sandy loam, i.e. erosion is more. But in moderately steep areas loam is the major soil texture. Soil samples collected from the watershed were analysed for various physico-chemical properties of soil such as bulk density, texture, pH, EC, organic matter, organic carbon and aggregate stability.

Table 8. Soil physiographic units of the watershed

Sl. No.	Legend	Area (ha)	Area (%)	Soil Texture
1	HS12	6.48	11.55	Sandy Loam
2	HS14	13.71	24.45	Sandy Loam
3	HS21	14.22	25.36	Sandy Loam
4	HS23	14.13	25.20	Loam
5	HS24	7.54	13.45	Loam

4.4.1 Physical properties of soil in the watershed

Sandy loam was observed as the major soil texture in the watershed. Greater sand content in all land uses indicates high soil erosion. Coarse fragment in the scrub land was high followed by cropland in the steeper slopes. Coarse fragment factor is high in higher elevation and less was observed in the less slope areas (HS21, HS23, and HS24). Higher bulk density was observed in scrub land of 1.56 g/cm^3 followed by upper hill slope maize field of 1.42 g/cm^3. A lower bulk density was observed in forest of 1.12 g/cm^3 followed by paddy of 1.26 g/cm^3. Higher bulk density soils have lower organic carbon content and vice versa. Soil texture and organic matter have important role in USLE K.

Table 9. Soil physical properties of the watershed

Sl. No.	Legend	Sand (%)	Silt (%)	Clay (%)	Texture	Coarse fragment (%)	Bulk Density (g/cm³)
1	HS12	59	24	17	Sandy Loam	28	1.56
		64	22	14	Sandy Loam	26	
2	HS14	52	34	14	Sandy Loam	18	1.42
		59	26	15	Sandy Loam	15	
3	HS21	55	32	13	Sandy Loam	12	1.12
		55	31	14	Sandy Loam	10	
4	HS23	51	35	14	Loam	7.5	1.26
		54	33	13	Sandy Loam	22	
5	HS24	49	34	17	Loam	10	1.36
		51	32	17	Loam	20	

4.4.2 Chemical properties of soil in the watershed.

The soil in the watershed was observed as acidic in nature. The pH value ranges from 3.6 to 5.9. Forest soil was found highly acidic. Also low electrical conductivity was found in forest and more in scrub land. Less organic carbon content can be found in all physiographical units. Less salinity was detected in forest and scrub. Since the farmers use only farmyard manure for crops, less EC can be observed in croplands also. A higher amount of 2.44% organic carbon was found in agricultural field followed by dense forest (2.24%) and low amount of organic carbon was

observed in scrub land (0.67%). Fertilizer and manure applications is the reason for higher organic carbon in soil. Similar pattern was observed in organic matter amount.

Table 10. Soil chemical properties in the watershed

Sl. No.	Legend	pH	EC (dS/m)	Organic carbon (%)	Organic Matter (%)
1	HS12 Scrub Land	5.16	0.22	0.67	1.15
		5.3	0.18	0.62	1.07
2	HS14 Maize	5.9	0.14	2.44	4.20
		4.55	0.13	2.21	3.80
3	HS21 Forest	3.69	0.03	2.24	3.85
		3.66	0.03	1.76	3.03
4	HS23 Rice	4.27	0.04	1.23	2.12
		4.66	0.04	1.01	1.74
5	HS24 Maize	4.85	0.11	0.96	1.65
		5.02	0.14	0.81	1.39

4.5 SOIL HYDROLOGICAL PROPERTIES IN THE WATERSHED

Direct measurement of infiltration rate was conducted using minidisc infiltrometer. A higher (Table 11) infiltration, unsaturated and saturated hydraulic conductivity, and available water content were observed in HS 23 physiographic unit which is paddy field. Lower infiltration rate and unsaturated hydraulic conductivity was found in scrub land. Higher saturated hydraulic conductivity of 44.2 mm/ hr is observed in paddy field and lower was observed in upper maize field. Available water content (AWC) and hydraulic properties were calculated with the help of Soil Plant Atmospheric Water (SPAW) software by giving organic matter, soil texture and EC as inputs. Ksat of agriculture land on the side slope of the hill were higher

when compared to forest. Due to land preparation practices, like ploughing prior to cropping, the surface become less compact and more permeable. The moderately dense forest in the watershed is under the threat of severe erosion processes like rills and gullies. This resulted in low Ksat.

Table 11. Soil hydrological properties in the watershed

Sl. No.	Legend	Soil depth (mm)	Unsaturated Hydraulic Conductivity (mm/hr)	Saturated Hydraulic Conductivity(Ksat) (mm/hr)*	Available water content (cm/cm) **
1	HS12	200	2.7	42.4	0.091
2	HS14	350	6.2	40.6	0.089
3	HS21	800	8.2	40.9	0.090
4	HS23	350	11.4	44.2	0.093
5	HS24	1100	8.4	42.9	0.092

* SPAW Model derived variables

4.6 WEATHER DATA ANALYSIS

Thirty year of rainfall data from 1976 to 2015 of the study area were collected from India Meteorological Department (IMD) and was analysed to find the average rainfall and temperature and compared with future rainfall and temperature under the RCP scenarios. The amount and intensity of rainfall in watershed are more during the monsoon months (July, August and September). Data collected for 2016, 2017and 2018 (Table 12) were analysed to understand the distribution of rainfall for this period.

August month is getting more rainfall, during the summer monsoon, followed by July. The number of rainy days is also more in these months. In September, monsoon rain comes to an end and so the amount and rainy days are less. Analysis of rainfall data also revealed that the average rainfall for 2016-2018 is 2100mm. In addition to that, the average rainfall of the baseline period (30-year) was 2245.1mm.

Table 12. Rainfall data of monsoon months in the study area (July-September)

Year	July		August		September	
	Rainfall (mm)	Rainy days	Rainfall (mm)	Rainy days	Rainfall (mm)	Rainy days
2016	905.51	24	679.20	26	193.83	13
2017	577.34	20	917.70	26	258.57	15
2018	860.55	29	731.26	27	65.28	14

4.8 Modeling runoff and sediment yield with the SWAT model

SWAT is a complex model since it requires a vast amount of daily data. Model parameters which affect the surface runoff were derived from various literature and user manuals. Watershed delineation was done with the help of DEM and Hydrological Response Units (HRUs) were generated based on dominant land use, soil and slope. Prior to this, land use, soil and slope of the watershed were selected and reclassified.

4.9 Sensitivity analysis

Prior to calibration, sensitivity analysis was done to find the sensitive parameters of runoff and sediment yield. Sensitivity analysis revealed that runoff is sensitive

to curve number (CN), available water content and soil evaporation compensation factor (ESCO) and sediment yield is sensitive to USLE crop management factor (USLE_P) and crop practice factor (USLE_C). The results in the Table 13 shows that the surface runoff is more sensitive to the variations in the curve number. The percentage change in parameter value assigned from a previous study using SWAT model at Sitla Rao watershed (Singh, 2009) and considerable change in surface runoff and sediment yield were observed while adding and subtracting the parameters by the assigned values. Negligible change was observed for lesser values. Change in curve number by 4 and resulted in a variation of 57 and -32.8 percent in surface runoff.

Table 13. Sensitivity analysis

Sl.no	Parameters	Change	Surface runoff (%)	Sediment yield
1	Curve number (CN)	-4	-32.8	-30.76
		+4	57	54.7
2	Available Water Content (AWC)	-0.05	-8.2	-2.4
		+0.05	-1.9	-5.6
3	USLE-C	-25	1.10	-10.73
		+25	1.09	11.4
4	USLE-P	-5	-45.1	-98
		+5	45.4	81
5	Slope	-25	-1.13	-35.85
		+25	1.12	40.9
6	BIOMIX	-50	-45	-57.9
		+50	45.2	0.9

The second major sensitive parameter is Available Water Content. Sediment yield is sensitive to USLE-C, USLE-P and BIOMIX. In these, USLE-P is the most sensitive parameter. +5 and -5 variation in USLE-P factor resulted in 81 and -98

percent change in sediment yield. BIOMIX was observed as the second major sensitive parameter.

4.10 CALIBRATION AND VALIDATION

4.10.1 Surface runoff calibration

The model was calibrated manually for surface runoff and sediment yield. After repeated alteration of sensitive parameters most appropriate values for surface runoff prediction were found. Since the CN values and AWC are the most sensitive parameters for runoff, changes were made in those values. The model predicted quiet well for low to medium rainfall events during calibration. The model calibration (Table 14) was assessed (Fig. 35) using correlation coefficient (r) of 0.94, coefficient of determination (r^2) of 0.89, and root mean square error (RMSE) of 4.67 mm/day, which means 89 % of variation can be explained by the calibrated model. The Box and Whisker plot (Fig. 36) gives distribution of each value. According to this, the model is slightly over predicting the surface runoff.

Figure 35. Scatter plot of observed and predicted runoff
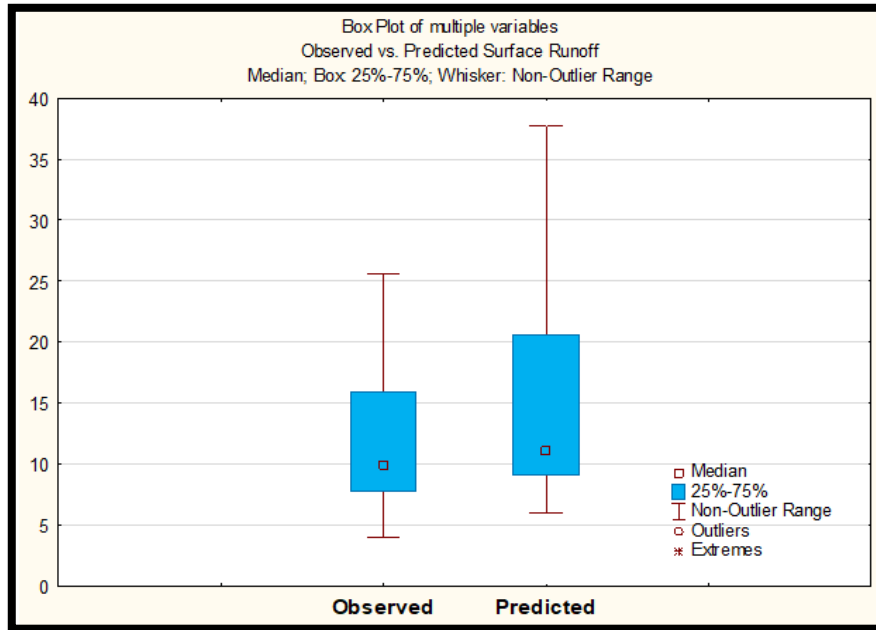
Figure 36. Box and Whisker plot of observed and predicted runoff

Table 14. Scatter plot statistics of observed and predicted runoff

Statistical Parameter	Surface Runoff	
	Observed	**Predicted**
Total number (N)	16	16
Mean	11.978	14.996
Standard deviation	6.805	9.410
Maximum	25.64	37.72
Minimum	4.00	6.04
Root mean square error (RMSE)	4.673	
Correlation coefficient (r)	0.947	
Coefficient of determination (r^2)	0.89	
Nash-Sutcliffe model efficiency (NSE)	0.81	

Table 15. The parameters fixed during surface runoff calibration

Sl.no	Calibrated parameter	Value used	Prescribed range
1	CN	Agriculture-80 Forest-72 Scrub-84	35-98
2	AWC	0.089-0.093	0-1
3	Slope	Based on DEM	-

4.10.2 Sediment yield calibration

Adjustment of USLE_P and USLE_C factors were done for satisfactory result in sediment yield. Significant changes in sediment yield were observed during the calibration process. The model predicted quiet well for low to medium rainfall events during calibration. The model calibration (Table 16) was assessed (Fig. 37) using correlation coefficient (r) of 0.94, coefficient of determination (r^2) of 0.89, and root mean square error (RMSE) of 0.55 t/ha/day, which means 89 % of variation can be explained by the calibrated model. The Box and Whisker plot (Fig. 38) gives distribution of each value. According to this the model is slightly under predicting the sediment yield. This may be due to landslips that occurred in the watershed, which could not be accounted by the model.
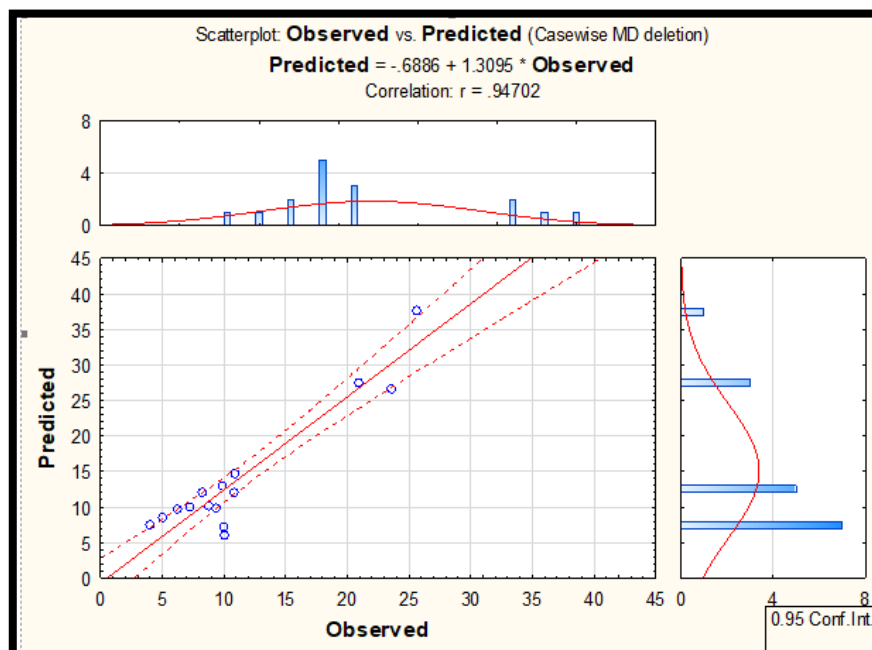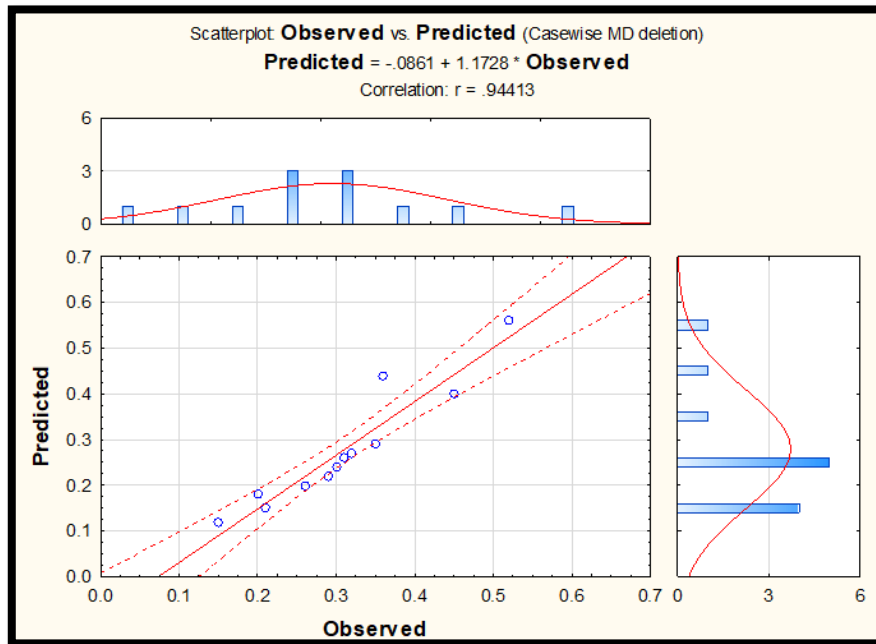
Figure 37. Scatter plot and box plot of observed and sediment loss
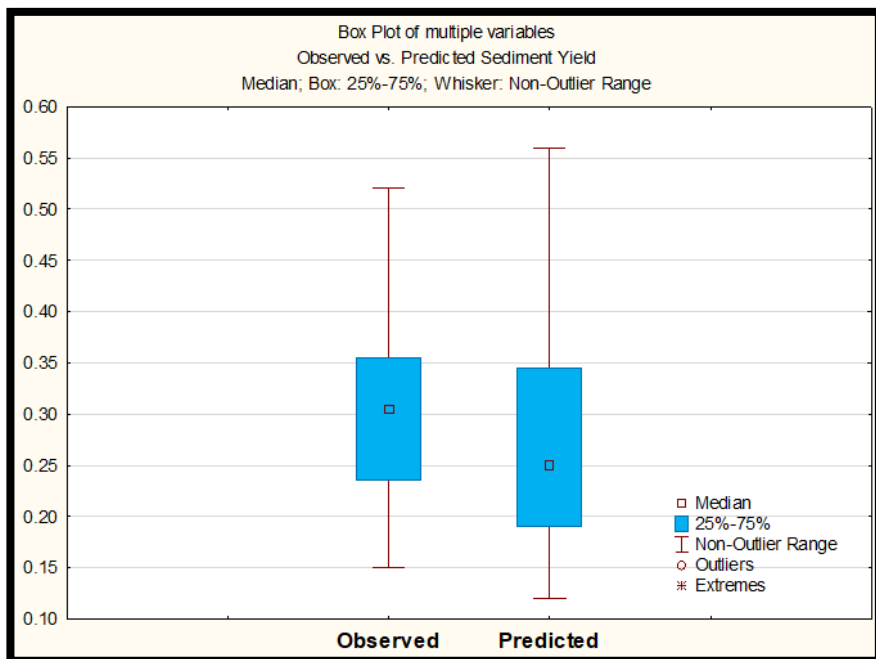
Figure 38. Scatter plot statistics of observed and predicted runoff

Table 16. Scatter plot statistics of sediment yield calibration

Statistical Parameter	Sediment yield (t/ha/day)	
	Observed	**Predicted**
Total number (N)	12	12
Mean	0.310	0.277
Standard deviation	0.103	0.128
Maximum	0.520	0.580
Minimum	0.150	0.120
Root mean square error (RMSE)	0.055	
Correlation Coefficient (r)	0.944	
Coefficient of determination (r^2)	0.89	

Table 17. The parameters fixed during calibration

Sl.no	Calibrated parameter	Value used	Prescribed range
1	USLE-P	0.3-0.9	0-1
2	USLE-C	0.001-0.2	0.001-1
3	Slope	Based on DEM	Based on the area
4	USLE-K	0.08, 0.09	0-0.65

4.10.3 Validation of the model

The model was validated for both runoff and soil loss. From 28 daily runoff data, 12 were used for validation. The model predicted quiet well for low to medium rainfall events during validation.
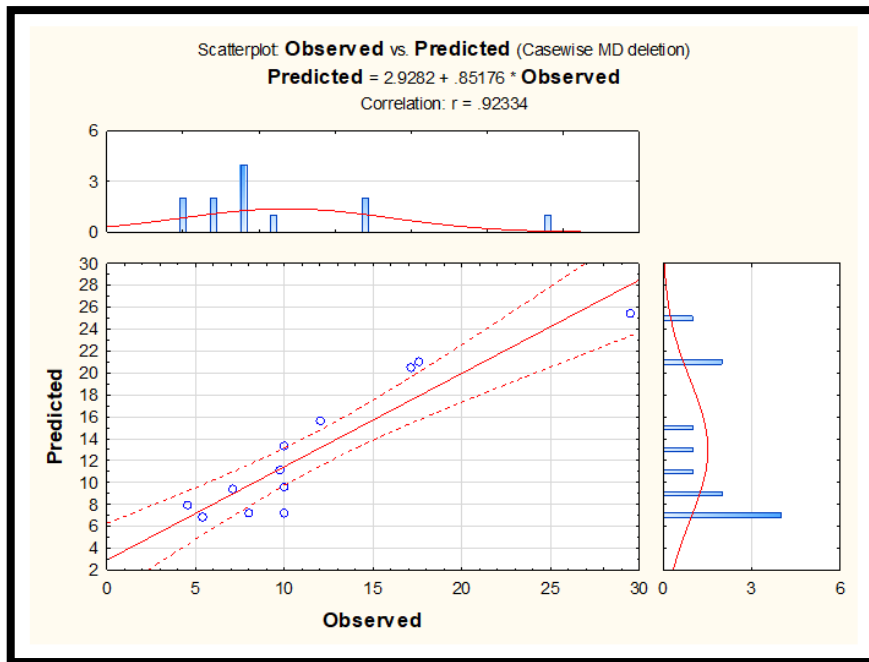
Figure 39. Scatter plot of observed and predicted runoff
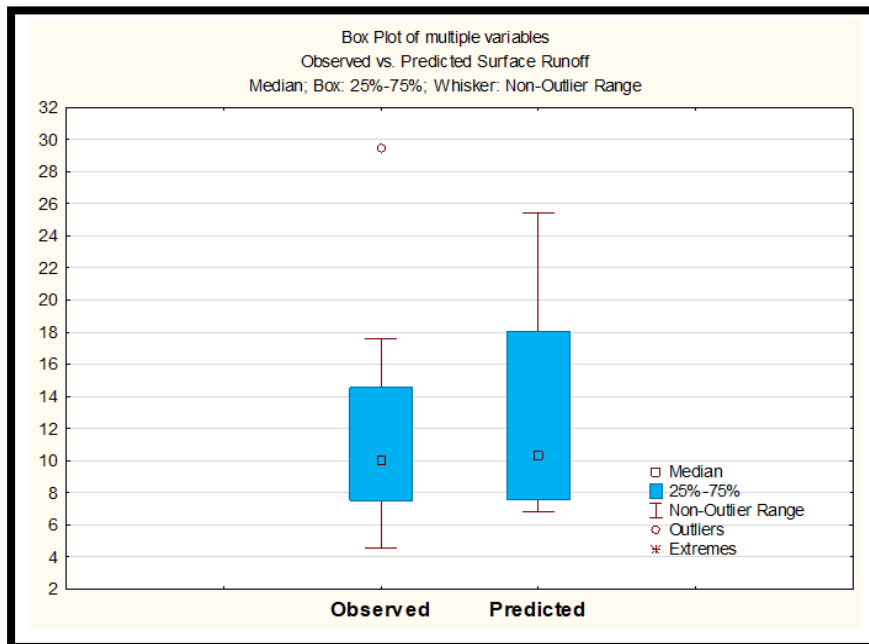
Figure 40. Box and Whisker plot of observed and predicted runoff

For runoff the model validation was assessed (Fig. 39) using correlation coefficient (r) of 0.92, coefficient of determination (r^2) of 0.85, and root mean square error (RMSE) of 2.79 mm/ day, which means 85 % of variation can be explained by the calibrated model. The Box and Whisker plot (Fig. 40) gives distribution of each value. According to the Box and Whisker plot, the model is also slightly over predicting the surface runoff.

22 rainy day data was available for sediment yield. Out of this 10 were used for the validation. The model performance was well for low to medium rainfall events during validation. The model validation (Table 18) was assessed (Fig. 41) using correlation coefficient (r) of 0.93, coefficient of determination (r^2) of 0.86, and root mean square error (RMSE) of 0.048 t/ha/day, which means 86 % of variation can explained by the calibrated model. The Box and Whisker plot gives distribution of each value. According to the Box and Whisker plot (Fig. 42) the model is also slightly over predicting.
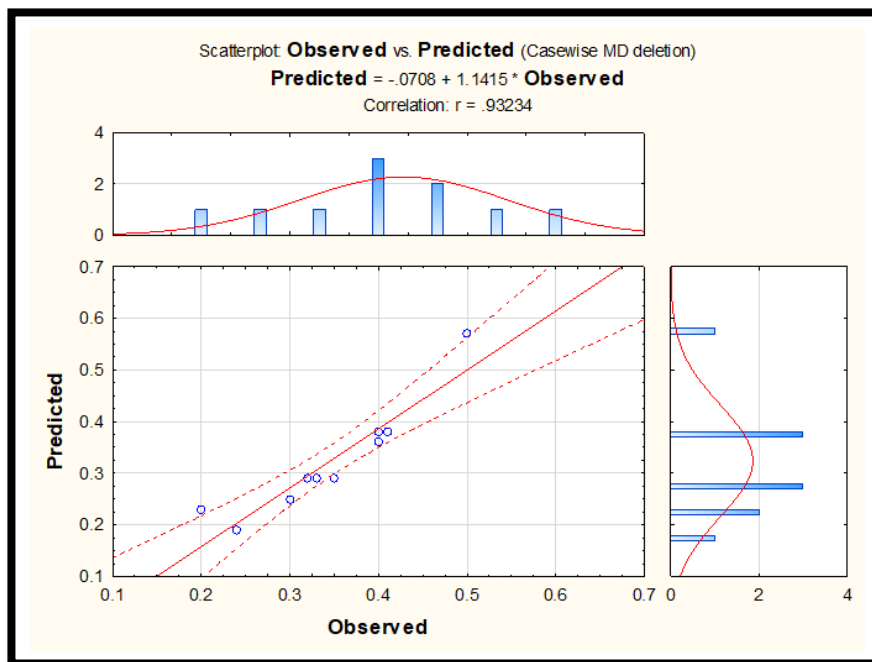
Figure 41. Scatter plot and box plot of observed and sediment loss

After calibration and validation the model performance was assessed with the help of Nash-Sutcliffe model efficiency.
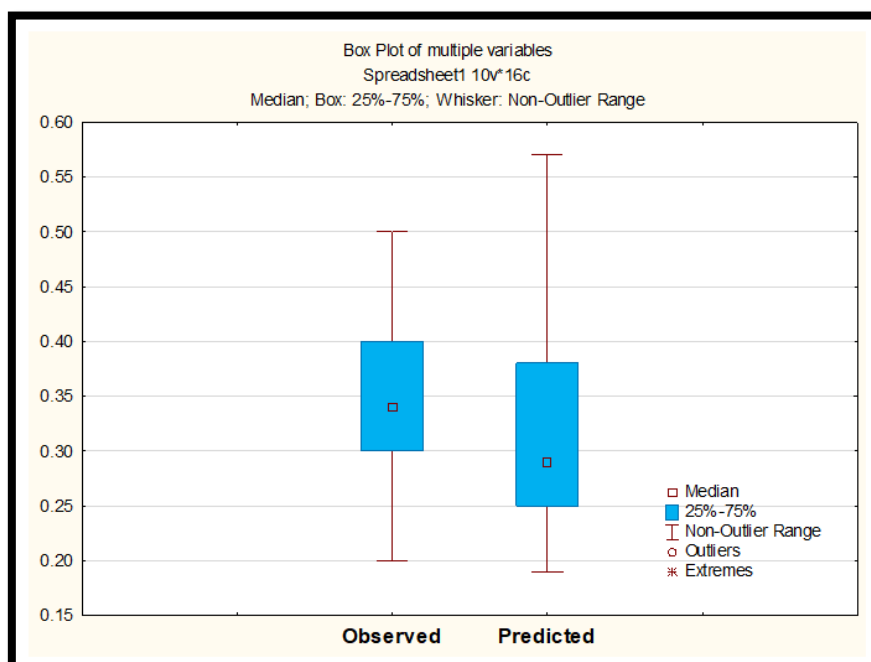
Figure 42. Box plot of observed and sediment loss

Table 18. Model validation and performance

Parameters	Correlation coefficient (r)	Coefficient of determination (r^2)	Root mean square error (RMSE)	Nash-Sutcliffe model efficiency (NSE)
Surface runoff	0.923	0.85	2.79	0.81
Sediment yield	0.932	0.86	0.048	0.70

The model performed quiet well for low to medium rainfall during calibration and validation. But for high rainfall model overestimated the surface runoff and under predicted sediment loss. Overestimated runoff may be due to the high surface coarse fragment and stoniness which can contribute higher surface runoff (Singh and

Kumar, 2012). In addition to that, the cropland has conservation practices like stone bunds and terraces to reduce runoff. Under prediction of sediment loss can happen due to road construction and landslips. The minimum vegetation cover (fallow period) of the paddy field during monsoon (Singh, 2009) can also contribute to a higher sediment yield at the watershed outlet.

4.10.4 Surface runoff and sediment yield prediction

After the calibration and validation model was run to predict surface runoff and sediment yield from each HRU on yearly scale. 13 HRUs were created based on the dominant land use, soil and slope by the model.

Table 19. Average seasonal surface runoff from various land uses

Land Use	Average surface runoff (mm/ season)
Maize	709.2
Moderately dense forest	678.3
Scrub land	930.53
Paddy	720.87

Average surface runoff from various land uses shows that runoff from scrubland is higher due to less cover and lack of conservation practises. Paddy and maize fields have conservation practices but breakage of bunds and terraces is common in the watershed during high intensity rain. Since the moderately dense forest has more canopy and rainfall interception, low runoff was observed. Similarly predicted soil loss was also high in scrubland and low in moderately dense forest. Soil loss from paddy fields was observed as low and runoff as high when compared to the maize fields because of the overflow of standing water from the field.

Figure 43. Land slips occurred in the study area

Table 20. Average soil loss from various land uses

Land use	Soil loss (ton/ ha/yr)
Maize	30.23
Moderately dense forest	20.14
Scrub land	42.78
Paddy	24.06

Table 21. Soil loss from various HRUs

Hydrological response unit (HRU)	Land use	Soil loss (t/ha/ yr)
1	Maize	33.29
2	Moderately dense forest	21.39
3	Maize	29.53
4	Maize	31.36
5	Maize	25.88
6	Scrub land	42.78
7	Moderately dense forest	19.49
8	Maize	31.07
9	Moderately dense forest	19.54
10	Paddy	24.00
11	Paddy	29.09
12	Paddy	24.19
13	Paddy	18.96

Highest soil loss (Fig. 44) (Table 21) was observed from the HRU number 6 which is mainly occupied by scrub land (42.78 tons $ha^{-1}yr^{-1}$). This can happen due to the higher slope, less cover and higher erodibility. HRU number 1 which is a maize field at the upper part of the watershed has a soil loss of 33.29 tons ha^{-1} yr^{-1}followed by HRU 4, HRU 8 (maize).

Soil loss from HRU 13 observed as lowest (18.9 tons $ha^{-1}yr^{-1}$) among all. This is mainly because of the conservation measures practiced in the paddy field. Since the forest in the watershed is moderately dense and under the threat of severe erosion.

19.49 tons ha^{-1}yr^{-1}from HRU 7, 19.59 tons ha^{-1}yr^{-1}from HRU 9 and 21.39 tons ha^{-1} yr^{-1}from HRU 2 were observed.
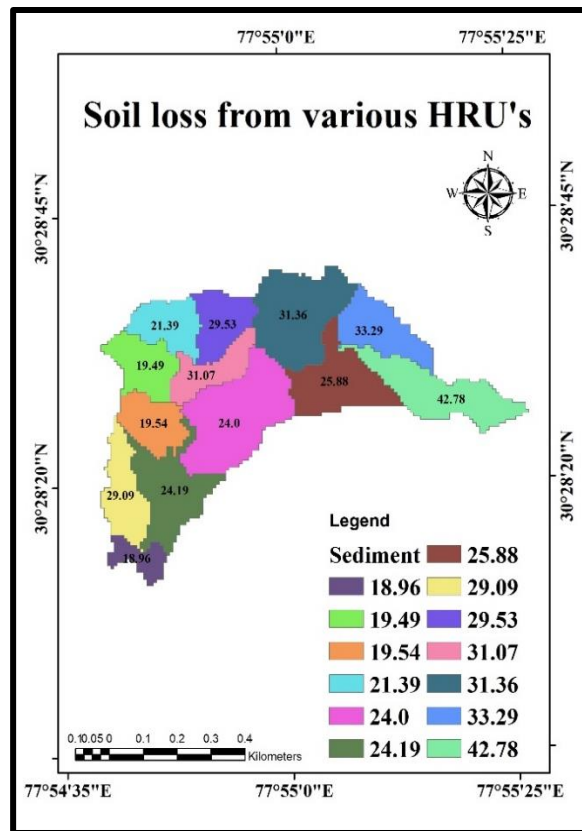
Figure 44. Spatial distribution of soil loss (tons ha^{-1} yr^{-1}) from various HRUs

Among different land uses very less average sediment loss of 20.14 ton ha^{-1} yr^{-1} is observed in moderately dense forest followed by the paddy, of 24.06 ton ha^{-1} yr^{-1}, Higher rates observed in Scrub land (42.78 ton ha^{-1} yr^{-1}). A previous study carried out by Singh, (2012) at the same watershed Sitla Rao shows a soil erosion of 24.66 t/ ha/ yr. But average soil erosion rate increased in the current study of 29.30 t/ ha/ yr. If a soil loss of up to 25 tonnes/ha/yr is considered tolerable in mountainous areas where the natural rate of soil loss is high (Morgan, *et al*., 1986). In this study it is quite higher than tolerable limit. Majority of the subarea soil erosion is above 25 t/ ha/ yr. A study carried out at Pathri Rao sub-watershed in the Himalayan Shivalik area, Kumar and Kushwaha (2013) predicted an average annual soil erosion rate of 35.47 t / ha / yr using RUSLE 3D and GIS techniques. According to Mandal *et al*, (2010) in north-western Himalayas the default soil loss tolerance limit

(SLTL) is ranging from 2.5 -12.5 t/ha/yr is followed for planning soil conservation activities. It is very evident from the report that the all the subarea has soil erosion levels above 10 t / ha / yr, which is a matter of serious concern from the point of view of conservation of natural resources and agricultural production. The lower erosion rate in moderately dense forest is mainly due to the forest cover interception, which reduces the rainfall impact directly to the soil. Also less cover and higher slope in scrub land leads to higher soil erosion rate in scrub land. In the paddy field farmers are adopting conservation practices like bench terraces, stone bunds etc and it helps to reduce soil erosion from paddy field.

Figure 45. Standing water in the paddy fields during monsoon

Figure 46. Breaking of terraces during monsoon

4.11 Analysis of future climate Data

Downscaled future climatic scenarios from Marksim weather generator of RCP 8.5 and RCP 4.5 were analysed to understand the changes in rainfall and temperature (maximum and minimum) under both the RCPs from 2010 to 2095. The values are compared with respect to the baseline period (1986-2015) to find future changes in temperature and rainfall for the years 2020s, 2050s, and 2080s, for the watershed. It was observed that the average annual maximum temperature of base period was 28.1°C and it may increase by 0.2ºC (28.3°C) in the 2020s, 0.4ºC (28.5°C) in 2050s, and 0.9ºC (29°C) the 2080s for RCP 4.5 emission scenario (Fig. 47&48).
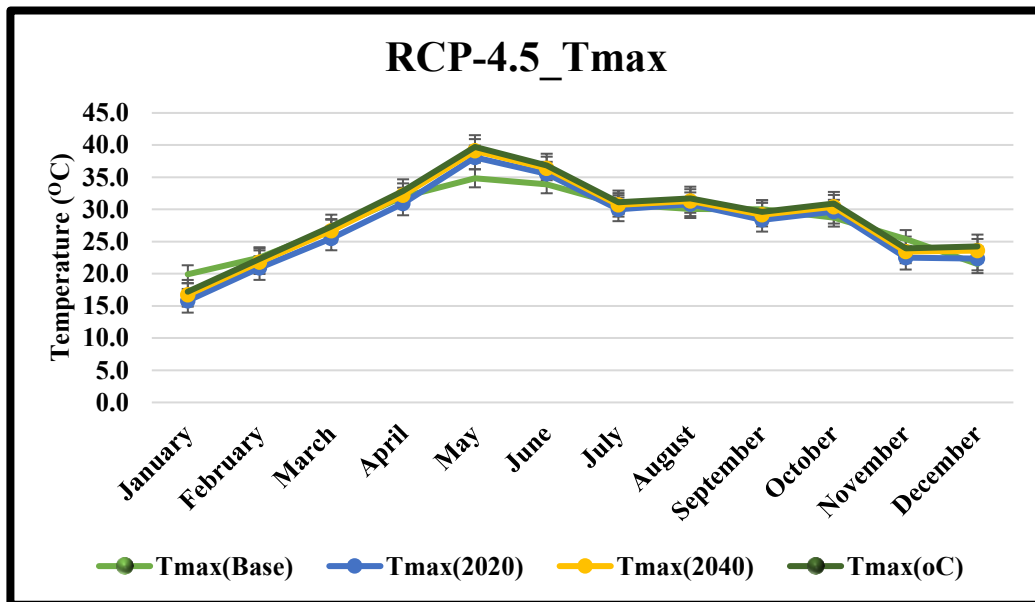
Figure 47. Change in maximum temperature from baseline under RCP 4.5 scenario

It was also observed that the average annual minimum temperature of base period was 15.6°C and it may increase by 0.8 ºC (16.4°C), 1.8 ºC (17.4°C), and 2.4 ºC (18°C) for RCP 4.5 emission scenario in the 2020s, 2050s, and the 2080s respectively. Almost similar pattern was observed in both maximum and minimum temperature. It also shows that the warmest month becomes warmer than the previous years.

It is observed that the average annual total rainfall (Fig. 49&50) of the study area is increasing under the RCP 4.5 scenario.
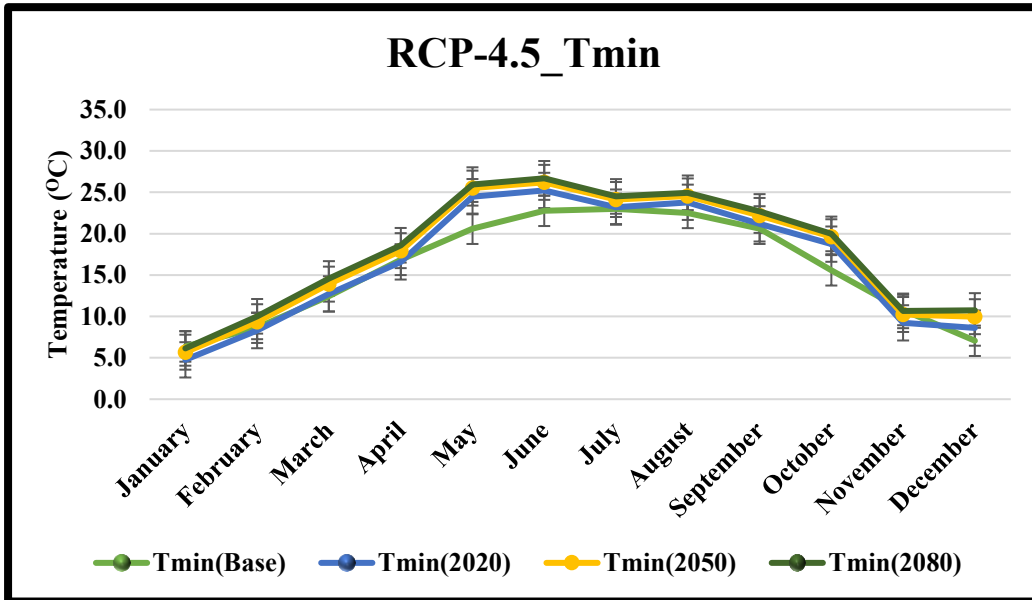
Figure 48. Change in Tmin from baseline under RCP 4.5 scenario
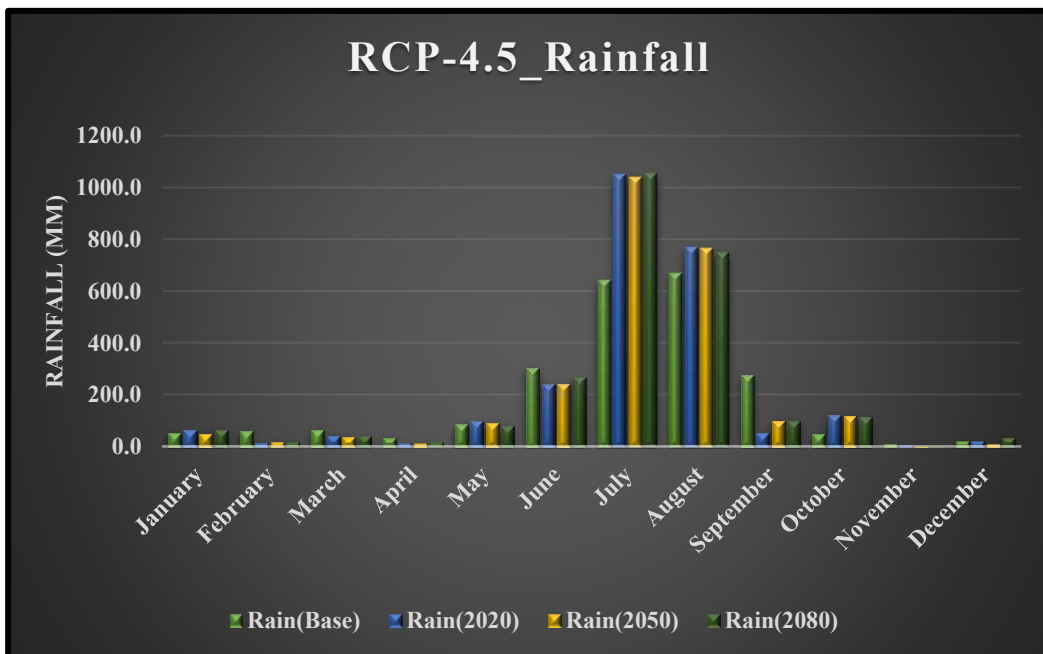
Figure 49. Change in monthly average rainfall from baseline under RCP 4.5 scenario

The value of average annual rainfall in the base period (1976-2015) was 2245.10mm, while 2481.0mm, 2469.4mm, and 2521.8mm were estimated for 2020s (2010-2039), 2050s (2040-2069), and 2080s (2070-2095) respectively (Fig. 50).

The mean temperature shows an increasing trend in both scenarios over Doon valley. (Akarsh, 2013 and Gupta and Kumar, 2017). Bhutiyani *et al*. (2009) conducted a study over north-western Himalayan (NWH) Region using long-term precipitation data for 140 years (1866–2006) and temperature data. In the winter precipitation in the NWH, temperature shows a growing but statistically insignificant trend (at 95 percent confidence level) and statistically significant (95 percent confidence level) decreasing monsoon trend and total annual precipitation during the study period. In the post-monsoon rainfall of Dehradun, Pithoragarh and other western Himalayan stations, Pant *et al*. (1999) found a growing trend, compared with a decrease in winter. Kumar *et al*. (2014) conducted a study over six locations (5 locations of Himachal Pradesh and one from Uttarakhand) which are the part of the Himalayan region.
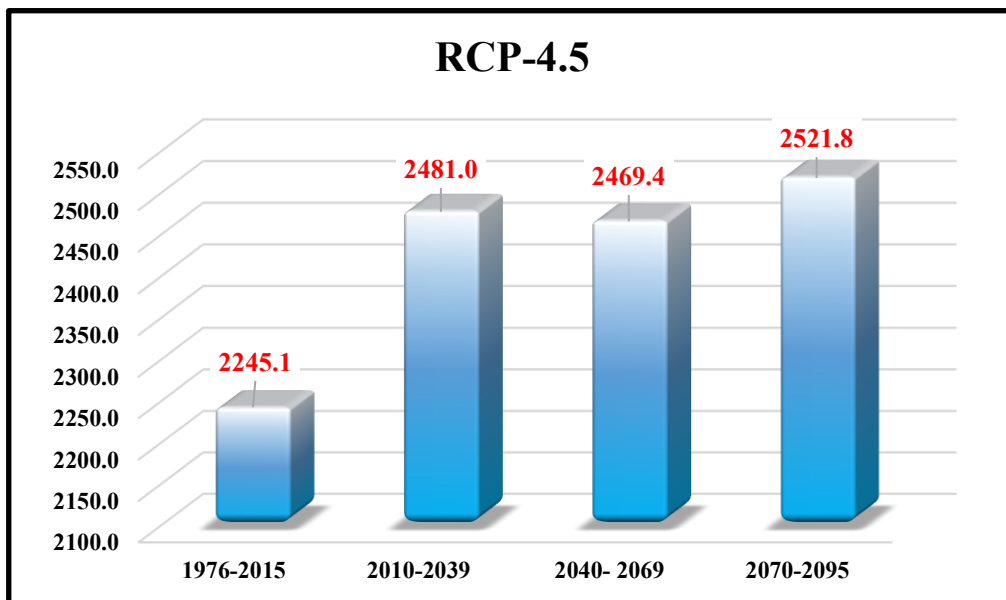
Figure 50. Comparison of estimated average annual rainfall under RCP 4.5 with the base period

The findings indicate a highly significant positive trend (0.5 to 1.1° C / decade) at the annual maximum temperature and a substantial negative trend (-0.4° C / decade) at the annual minimum temperature, and a highly significant rise in Shimla's precipitation trend (22 mm / year).

It is observed that the average annual maximum temperature shows an increase from the base by 0.4ºC (28.5 ºC), 1.2 ºC (29.3 ºC), and 3.2 ºC (31.3 ºC) for RCP 8.5 emission scenario in the 2020s, 2050s, and the 2080s respectively (Figure 51). The RCP 8.5 scenario predicts an increase in the average annual minimum temperature by 0.9 ºC (16.5 ºC) in the 2020s, 2.7 ºC (18.3 ºC) in the 2050s, and 4.7 ºC (20.3 ºC) in the 2080s (Figure 52). Gupta and Kumar, (2017) conducted a study at mid-Himalayas also reported that the average annual maximum temperature may increase by 0.83º C to 3.00 º C for H3A2 and 0.91 º C to 2.2º C for H3B2 emission scenario during 2011-2099.
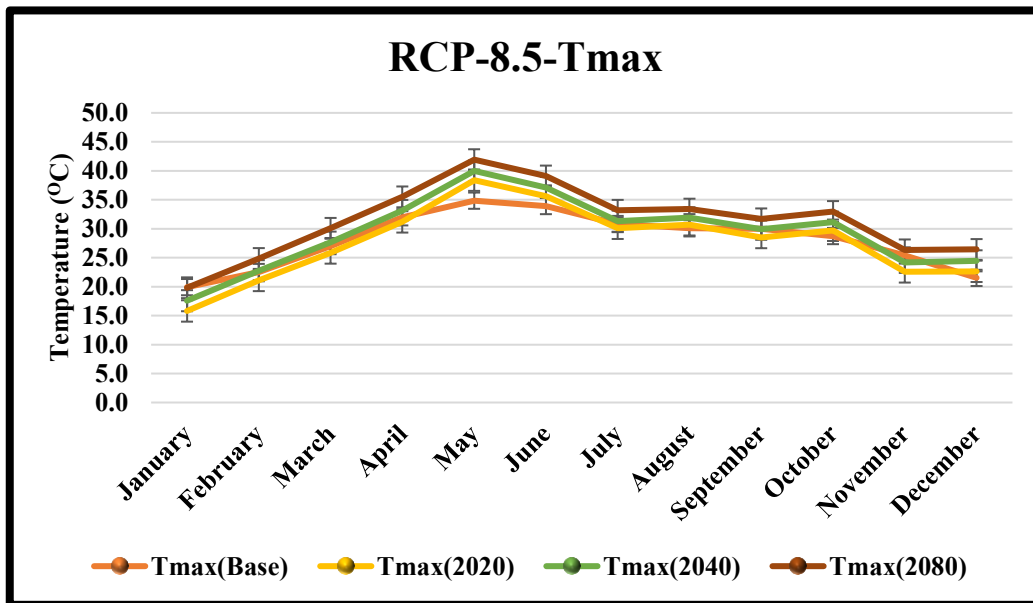
Figure 51. Change in maximum temperature from baseline under RCP 4.5 scenario

Under RCP 8.5, average annual total rainfall (Figure 49) shows an increase within the study area. The change in rainfall under this scenario is relatively higher than that of under the RCP 4.5 scenario. Average annual rainfall in the base period was

2245.1mm, while an increase upto 2240.4mm, was observed in the 2020s, 2564.3mm in the 2050s, and 2472.3mm in the 2080s (Figure 53).

Rainfall data under both scenarios shows July month getting more rainfall and November getting the least. Under RCP 4.5 July month in the period of 2080 has the highest amount of rainfall (1053.4mm). While under RCP 8.5 scenario July month of the 2050 has the highest rainfall (1140.7mm). Akarsh, (2013) also reports that in Doon valley under A2a scenario there could be an increase in rainfall of about 25 to 70% during 2011-2099. Gupta and Kumar, (2017) carried out a study at mid-Himalayas revealed that average annual precipitation may increase by 23.79% to 33.3%for H3A2 and 27.87% to 31.67% for H3B2 scenario during 2011-2099.
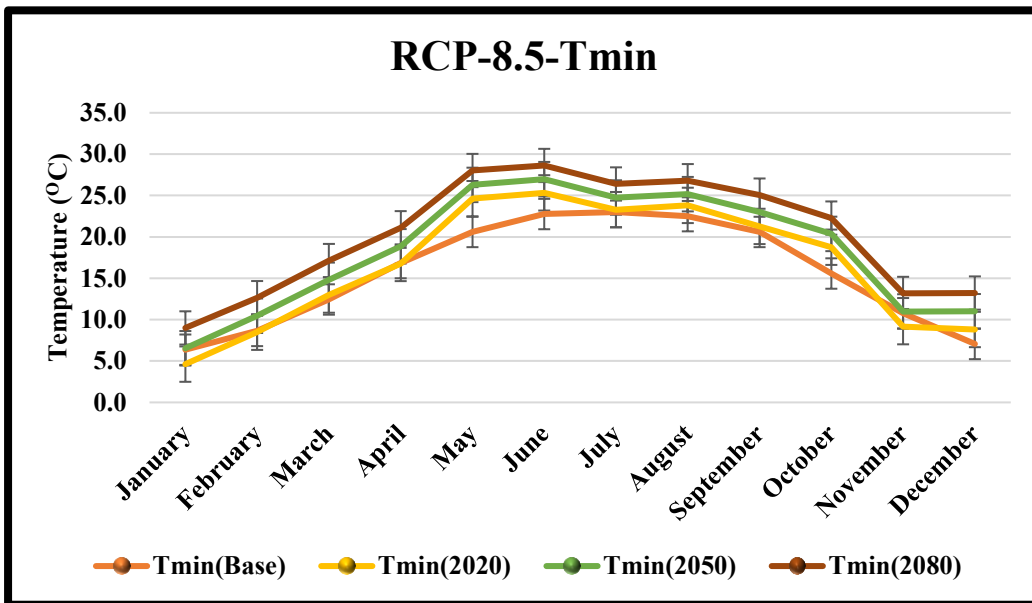
Figure 52. Change in minimum temperature from baseline under RCP 4.5 scenario

The rainfall under RCP 4.5 scenario (Table 21), from the base period, increases by 10.5%, 9.9%, and 12.3% in the years (Figure 51& 52) the 2020s, 2050s, and 2080s respectively.
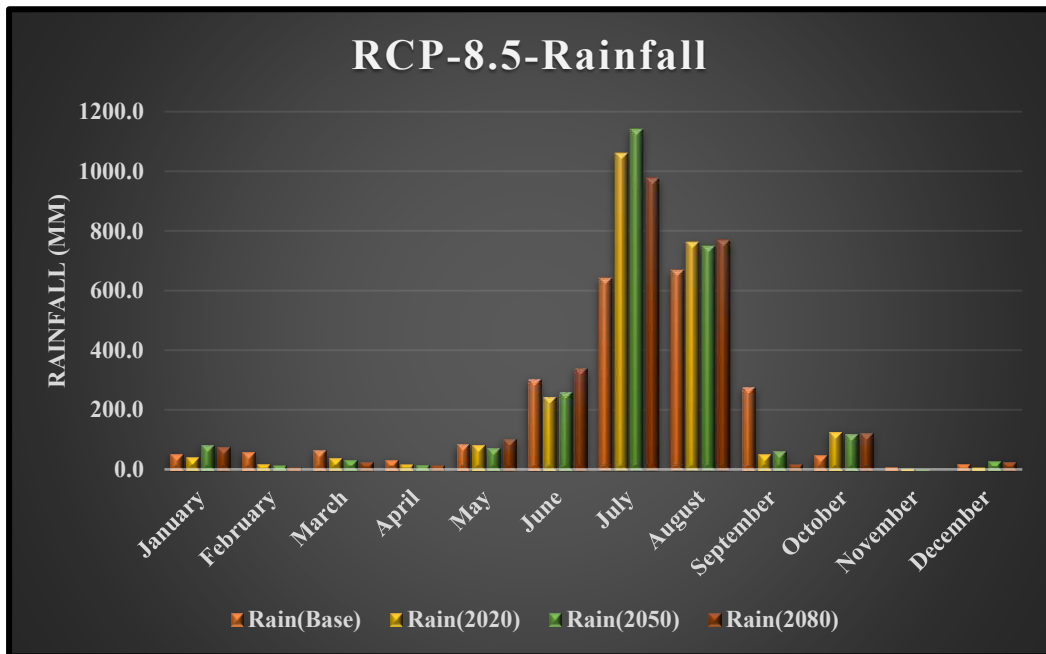
Figure 53. Change in monthly average rainfall from baseline under RCP 8.5 scenario
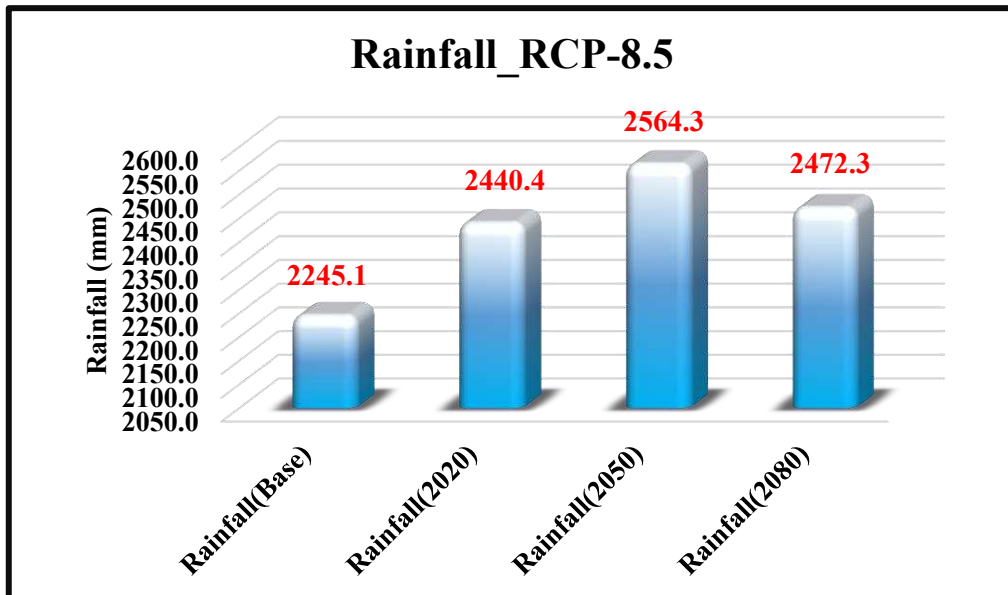
Figure 54. Comparison of estimated average annual rainfall under RCP 8.5 with the base period

By 2050s, rainfall will be decreasing slightly and then will be increasing by 12.3%. The rainfall under the RCP 8.5 scenario from the base period shows an increase by 8.7%, 14.2%, and 10.1% in the years the 2020s, 2050s, and 2080s respectively. The rainfall amount is increasing up to 14.2% under RCP 8.5 scenario.

Table 22. Projected average rainfall under RCP 4.5 and RCP 8.5

Period	RCP 4.5	RCP 8.5
2020s (2010 – 2039)	2481.0	2440.4
2050s (2040 – 2069)	2469.4	2564.3
2080s (2070 – 2095)	2521.8	2472.3

The mean of 30 years of projected precipitation and temperature indicates higher variations (years 2010 – 2039, 2040 – 2069, and 2070 – 2095) for both RCP 4.5 and RCP 8.5.
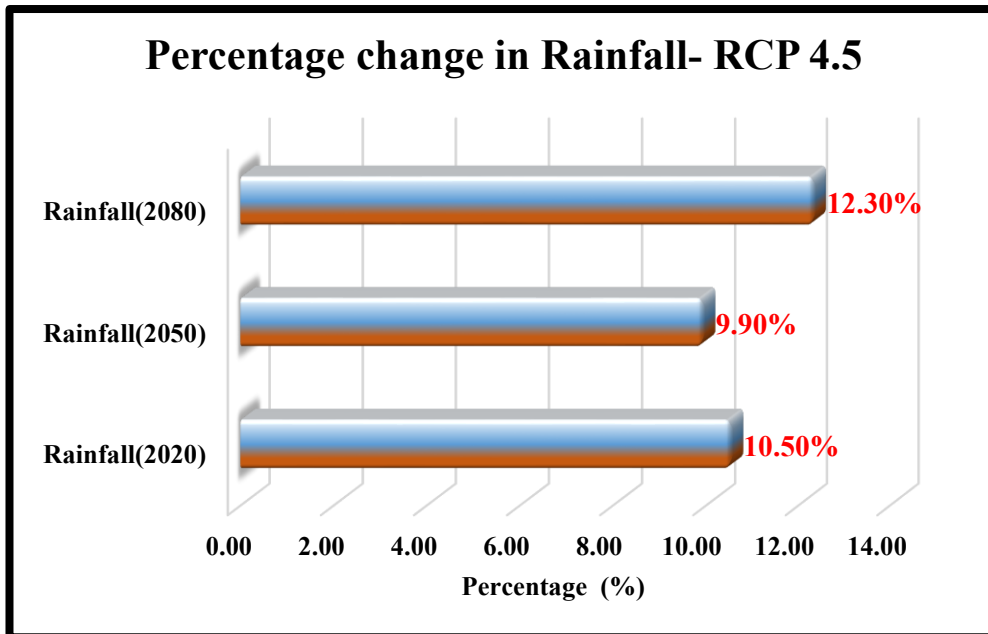
Figure 55. Percentage change rainfall under RCP 4.5
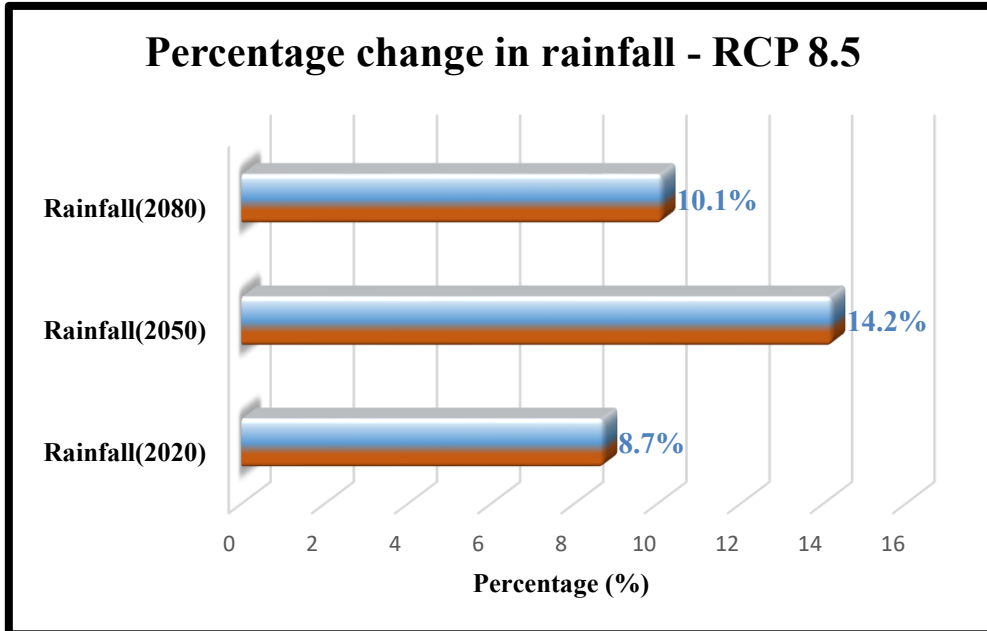
Figure 56. Percentage change rainfall under RCP 8.5

Table 23. Change in Rainfall and temperature under RCP 4.5 and RCP 8.5 scenario from the baseline

Parameter	Scenarios	Base year to 2020s	Base year to 2050s	Base year to 2080s
Rainfall	**RCP 4.5**	10.5 %	9.9 %	12.3 %
	RCP 8.5	8.7 %	14.2 %	10.1 %
Tmax	**RCP 4.5**	0.2°C	0.4°C	0.9°C
	RCP 8.5	0.4°C	1.2°C	3.2°C
Tmin	**RCP 4.5**	0.8°C	1.8°C	2.4°C
	RCP 8.5	0.9°C	2.7°C	4.7°C

The highest and lowest change in rainfall was observed in the 2080s (14.2%) and 2020s (8.7%) respectively under the RCP 8.5 scenario. Highest change in temperature (4.7°C) was also observed under this scenario for the 2080s. In all the very low change states in the western part of the country and the highest change in the north-eastern and southern region of the country under RCP 8.5, precipitation is expected to increase. Most of the cooler northern states currently in India, such as Jammu and Kashmir , Himachal Pradesh and Uttaranchal (2.0° C to 2.2° C at 1.5° C and 2.5° C to 2.8° C at 2.0° C), are likely to witness the most drastic temperature variations in the two RCPs. Under RCP 8.5, the total rainfall in the state of Arunachal Pradesh rose from a maximum of 44.00 mm (-188 to 416 mm) and 107.09 mm (-175 to 400 mm) to a minimum of 7.6 mm (-81 to 124 mm) and 20.01 mm (-69 mm to 91 mm) in Haryana, respectively, for a global temperature rise of 1.5 ° C and 2.0 ° C (Yaduvanshi, 2019). In all seasons, Jammu and Kashmir , Himachal Pradesh and Uttaranchal are anticipated to have higher temperature variations. With a rise of 2.5 ° C-4.5 ° C by the end of the century, several studies have shown comparable results in these areas (Panday *et al*., 2015), the highest temperature change recorded in the western Himalayas (Joshi *et al*., 2018). The need for changes in farm management practises, such as early land preparation and sowing operations, is indicated by increased pre-monsoon rainfall forecasts.

4.12 Future scenario of soil loss

Similar to future precipitation, soil loss shows an increasing pattern under both RCP scenarios. The average soil loss from different land uses was estimated under both RCPs for the 2020s, 2050s and 2080s. Percentage change of soil loss with respect to the baseline period was also calculated for better understanding.

4.12.1 Soil loss prediction under RCP 4.5

Future climate scenario analysis shows that for the periods of 2020s, 2050s and 2080s, rainfall is expected to increase 10.5%, 9.9% and 12.3% respectively from the baseline under RCP 4.5. The average soil loss under RCP 4.5 scenario increased up to 18.1 % from the baseline during 2080, 15.5% during 2020, and 14.6% during

2050s. Less erosion rate was observed in moderately dense forest due to cover factor and higher observed in scrubland due to absence of cover and management practices. From this result, it is clear that the highest expected change in rainfall in the 2080s (12.3%) has the highest soil loss.

Table 24. Average annual soil loss (t/ ha/ yr) and the change in percentile from different land use under 4.5 scenarios.

Land Use	Average soil loss (t/ ha/ yr)				Change		
	Present	2020s	2050s	2080s	2020s (%)	2050s (%)	2080s (%)
Maize	30.23	35.25	34.94	36.07	16.61	15.57	19.33
Mod. Dense forest	20.14	22.10	21.99	22.43	9.73	9.18	11.39
Scrubland	42.78	51.67	51.15	53.20	20.77	19.56	24.36
Paddy	24.06	27.61	27.41	28.22	14.75	13.91	17.28
Average	29.3	34.2	33.9	35.0	15.5	14.6	18.1

Zheng *et al*. (2007) estimated that a 4–18% increase in precipitation can cause a 49–112% increase in runoff and a 31–167% increase in soil loss. Akarsh, 2013 conducted a study shows that the soil erosion increases 37.97% to 221.99% under A2a scenario during 2020 to 2080 period from the base period over Doon valley.

4.12.2 Soil loss prediction under RCP 8.5

Under this scenario expected rainfall for the period of 2020s, 2050s and 2080s have an increase of 8.7%, 14.2% and 10.1% respectively from the baseline. The RCP 8.5 represents higher emission scenario and represents higher change in temperature and rainfall resulting in higher rate of average soil erosion during the 2050s of 20.9% and also less soil erosion was observed during the 2020s (12.8%). Gupta and Kumar, (2017) carried out a study at mid-Himalayan landscape unveiled that the average annual soil erosion rate may increase by 28.38%, 25.64% and 20.33% under H3A2 emission scenario during 2020s, 2050s and 2080s. The erosive ability to detach and carry soil particles increases due to changes in the strength and amount of rainfall due to climate change, and the future average global soil erosion for 2090 is expected to rise by 9 percent due to climate change (Yang *et al*., 2003).

The rate of soil erosion has risen steadily from the 2020s to the 2080s. The soil loss is increased by SVM downscaled data up to 4.75 t / ha / year from years 2020 to 2080s and by SDSM model up to 6.10 t/ ha / year from years 2020 to 2080s (Mondal *et al*., 2015).

The soil erosion analysis shows that there is a significant need for soil conservation measures in the catchment, where the region is situated under critical erosion conditions with high and very high soil erosion, using remote sensing and GIS techniques to estimate spatial soil erosion losses. The study indicates that climate change in the future will be mainly responsible for soil erosion.

RCP 8.5 scenario predicts relatively higher amount of rainfall than RCP 4.5, so erosion will be less in RCP 4.5 scenario. Soil erosion was analysed in various land use/ land cover and similarly the highest erosion rate was found to be in scrublands (42.78 to 54.90 t ha^{-1} yr^{-1}) and followed by agricultural fields (Maize) (30.23 to 35.03t ha^{-1} yr^{-1}), followed by paddy (24.06 to 27.48 t ha^{-1} yr^{-1}). However, similarly in RCP 4.5 scenario dense forest was found to have less erosion risk (20.14 to 22.03 t ha^{-1} yr^{-1}). Under the RCP 8.5 scenario soil erosion increases 12.8% and further

increase to 21% and further reduced to 15% during the 2020s, 2050s, and 2080s respectively.

Table 25. Average annual soil loss and the change in percentile from different land use under 8.5 scenarios.

Land Use	Average soil loss (t/ ha/ yr)				Change		
	Present	2020s	2050s	2080s	2020s (%)	2050s (%)	2080 (%)
Maize	30.23	34.37	36.98	35.03	13.69	22.32	15.88
Mod. Dense forest	20.14	21.77	22.79	22.03	8.07	13.14	9.36
Scrubland	42.78	50.15	54.90	51.43	17.23	28.33	20.21
Paddy	24.06	26.99	28.86	27.48	12.20	19.94	14.19
Average	29.3	33.3	35.9	34.0	12.8	20.9	14.9

Using the possible rainfall data, future soil erosion was estimated. In the analysis, only rainfall was considered, which demonstrates that soil erosion would increase with increasing rainfall. In the future, however, other parameters (soil type, land use, DEM) will be known as constants. Therefore, using remote sensing and GIS techniques, the calculation of spatial soil erosion loss can be achieved. Increased precipitation has resulted in potential changes or rises in soil erosion. There is a

substantial rise in the future relative to the present or observed time. The percentage change of soil loss under RCP 4.5 in the 2080s and 2020s are higher than the 2050s. While under RCP 8.5 highest soil loss was observed in 2050s and 2080s.

V. SUMMARY AND CONCLUSION

The present study on the climate change impact on soil erosion using the SWAT model was conducted at the Pasta micro watershed which belongs to the lesser Himalayas. The model was run to predict future soil loss under RCP 4.5 and RCP 8.5 scenarios. Major findings of the study are the following.

- The major land uses found in the watershed are scrubland, moderately dense forest, paddy, maize and settlements. Most of the area is under cultivation.
- Sandy loam is the major soil texture in the study area and the soils are acidic in nature.
- Infiltration rate and Ksat were high in croplands when compared to the moderately dense forest due to ploughing. Also the forest area is under the threat of severe erosion processes like rills and gullies.
- In the years of 2016, 2017 and 2018 August got more rainfall among the monsoon months of July, August and September.
- The average rainfall of the baseline period (1976-2015) was estimated as 2245.1 mm.
- SWAT was calibrated and validated for surface runoff and sediment yield. The model performed quite well for low to medium rainfall but overestimated surface runoff and under predicted the sediment yield for high rainfall. Overestimation of runoff can be due to the high surface coarse fragment and stoniness and also because of not considering the conservation practices. Under prediction in sediment yield can happen due to the landslides which are not accounted for by the model.
- r^2 and Root Mean Square Error (RMSE) of runoff calibration were 0.89, and 4.67, respectively. For sediment calibration, r^2 was 0.89, and RMSE was 0.055. r^2 and RMSE of runoff validation were 0.85 and 2.79 respectively. For sediment yield validation r^2 was 0.86 and RMSE was 0.048. Also, the Nash – Sutcliffe coefficient of efficiency for the surface runoff was 0.81 and sediment yield was 0.70.

- While predicting the runoff from different land uses high average runoff was generated from scrubland (930.53mm/year) followed by paddy (720.87mm/year), and then by maize (709.2mm/year). Less runoff was predicted from the moderately dense forest (678.3mm/year).

- Soil loss predicted from different Hydrological Response Units which are created by the model shows that highest soil loss occurred from scrubland (42.78 tons ha-1 yr-1), which belongs to the high slope areas, followed by maize (30.23) and paddy (24.06). Less soil loss was predicted from the moderately dense forest (20.14)

- Analysis of rainfall and temperature under RCP 4.5 and RCP 8.5 showed an increasing trend in the future from the baseline period.

- Under the RCP 4.5 scenario, increase in rainfall was 10.5% in the 2020s, 9.9% in 2050 and 12.3% in 2080s.

- Under the RCP 8.5 scenario, expected increase in rainfall in 2020 is 8.7%. In the 2050s and 2080s it is expected to increase up to 14.2% and 10.1% respectively.

- Likewise, in the future maximum temperature (Tmax) under RCP 4.5 is expected to increase by 0.2°Cin the 2020s 0.4°C in the 2050s and 0.9°C in the 2080s. while future minimum temperature (Tmin) is estimated to increase by 0.8°C in the 2020s, 1.8°C in the 2050s and 2.4°C in the 2080s, from the baseline period.

- Tmax under RCP 8.5 is increasing by 0.4°C in the 2020s, 1.2°C in the 2050s and 3.2°C in 2080s. Tmin is changing by 0.9°C in the 2020s, 2.7°C in the 2050s and 4.7°C in the 2080s from the baseline period.

- At present the average annual soil loss from the watershed is 29.3 tons ha-1 yr-1. Under RCP 4.5 it is expected to increase up to 34.2 tons ha-1 yr-1in the 2020s, 33.9 tons ha-1 yr-1 in the 2050s and 35 tons ha-1 yr-1 in 2080s.

- Under RCP 8.5, soil loss is expected to increase up to 33.3 tons ha-1 yr-1in the 2020s, 35.9 tons ha-1 yr-1 in the 2050s and 34 tons ha-1 yr-1 in 2080s.

In the Sitla Rao watershed of the hilly basin of Uttarakhand, India, a quantitative assessment of the annual loss of soil erosion with respect to climate change was carried out. With the Marksim Weather Generator Tool, which provides downscaled regional climate, the future climate change scenario was used. In the future, model production suggests an rise in temperature and rainfall. To identify the priority erosion prone region in the watershed, the SWAT model is used. Using the potential rainfall data, future soil erosion was estimated. In the analysis, only rainfall was taken into account , which means that soil erosion would increase with increasing rainfall. However, other parameters are assumed to be unchanged in the future, such as slope, soil properties, land usage. This study indicates that the region 's agricultural and scrub lands are more vulnerable to erosion, which is primarily due to various tillage and cropping practises. The report also shows that climate change in the future would pose a significant challenge to soil erosion. This research also shows a rise in soil erosion compared to previous studies conducted by Singh (2013) in the Sitla Rao watershed. This study shows that soil protection measures in the watershed are necessary everywhere the region is observed in a hazardous erosion condition with moderate and very moderate soil erosion.

Suggestions

As additional increases in soil erosion are anticipated in catchments, vegetative and structural control measures are urgently required to mitigate the threat of soil erosion.

- ✓ In a mildly sloping area (1-6%) contour farming is helpful to reduce energy of runoff water
- ✓ Tillage makes soil surface more permeable to infiltration of rainwater. This practice also reduces runoff, soil and nutrient losses and enhance crop yield.
- ✓ Mechanical measures like contour bunds can be used for soil conservation.
- ✓ To reduce the slope and slope length bench terrace can be used.
- ✓ Maintenance and strengthening of terraces and stone bunds in the cropland by growing grass along the bund and terraces can reduce the chances of breakage of these and overflow of runoff water during monsoon season.

- ✓ For suitable natural drainage grassed waterways are essential on agricultural land.
- ✓ Since the watershed belongs to the Doon valley it is suitable to use different grasses like *Panicum repens, Brachiaria mutica* and *Cynodon plectostachyus*.
- ✓ For forest and scrubland trenching is helpful to reduce runoff.

Future line of work

- ✓ Downscale the rainfall and temperature according to A2 and B2 scenario.
- ✓ Change the other parameter such as slope, land use, erodibility and practice factor and predict soil loss.
- ✓ Validation of predicted rainfall and temperature.

REFERENCES

Akarsh, A., 2013. Surface runoff, Soil erosion and Water Quality estimation using APEX model integrated with GIS -A case study in Himalayan Watershed, M.Tech (RS& GIS) thesis, Andra University, Andra Pradesh, 80p.

Anders, A.M., Roe, G.H., Hallet, B., Montgomery, D.R., Finnegan, N.J. and Putkonen, J., 2006. Spatial patterns of precipitation and topography in the Himalaya. *Special Papers-Geological Society of America*, *398*: 39.

Ansari, Z.R., Rao, L.A.K. and Saran, S., 2013. Comparative study of morphometric parameters derived from topographic maps and ASTER DEM. *Int J Sci Eng Res*, *4*(8): 508-528.

Arnalds, O., Borarinsdottir, E.F., Metusalemsson, S., Jonsson, A., Arnason, G.o.A, 2001. Soil erosion in Iceland. The Soil Conservation Service and the Agricultural Research Institute, Reykjavík, 121p.

Arnold, J.G. and Williams, J.R., 1995. SWRRB-A watershed scale model for soil and water resources management. Water Resources Publications, 847-908.

Arnold, J.G., Williams, J.R. and Maidment, D.R., 1995. Continuous-time water and sediment-routing model for large basins. *Journal of Hydraulic engineering*, *121*(2): 171-183.

ASD [Agriculture & Soils Division], 2001. IIRS P.G. Diploma Course pilot project report on Land Evaluation for Landuse Planning by integrated use of Remote Sensing and GIS – a case study of Bhogabati Watershed in Kolhapur district.

Azari, M., Moradi, H.R., Saghafian, B., Faramarzi, M., 2016. Climate change impacts on stream flow and sediment yield in the north of Iran. Hydrol. Sci. J. 61 (1): 123–133.

Barros, A.P., Chiao, S., Lang, T.J., Burbank, D. and Putkonen, J., 2006. From weather to climate-seasonal and interannual variability of storms and implications

for erosion processes in the Himalaya. *Special Papers-Geological Society of America*, *398*: 17.

Bhatt, B.C. and Nakamura, K., 2005. Characteristics of monsoon rainfall around the Himalayas revealed by TRMM precipitation radar. *Monthly Weather Review*, *133*(1): 149-165.

Bhutiyani, M.R., Kale, V.S. and Pawar, N.J., 2009. Climate change and the precipitation variations in the northwestern Himalaya: 1866–2006. *International Journal of Climatology: A Journal of the Royal Meteorological Society*, *30*(4): 535-548.

Blanco-Canqui, H. and Lal, R., 2008. No-tillage and soil-profile carbon sequestration: An on-farm assessment. *Soil Science Society of America Journal*, *72*(3): 693-701.

Bookhagen, B. and Burbank, D.W., 2006. Topography, relief, and TRMM-derived rainfall variations along the Himalaya. *Geophysical Research Letters*, *33*(2006): 1-8.

Bookhagen, B., 2010. Appearance of extreme monsoonal rainfall events and their impact on erosion in the Himalaya. *Geomatics, Natural Hazards and Risk, 1*(1): 37-50.

Bookhagen, B., et al. (2005a), Abnormal monsoon years and their control on erosion and sediment flux in the high, arid northwest Himalaya, *Earth Planet. Sci. Lett.*, 231: 131– 146.

Borah, D., G. Yagow, A. Saleh, P. Barnes, W. Rosenthal, E. Krug and L. Hauck. 2006. Sediment and nutrient modeling for TMDL development and implementation. Trans. ASAE 49:967-986.

Bryant RB, Gburek WJ, Veith TL, Hively WD. 2006. Perspectives on the potential for hydropedology to improve watershed modeling of phosphorus loss. Geoderma 131: 299–307. DOI: 10.1016/j. geoderma.2005.03.011.

Centre for Science and Environment (CSE) Report (2014) Society of Environmental Communication. Centre for Science and Environment (CSE) Report, New Delhi.

Chang, M., 2006. Forest hydrology, an introduction to water and forest. 2nd ed. Ames: Iowa State University, 556p.

Clarke L, Edmonds J, Jacoby H, Pitcher H, Reilly J, Richels R, 2007. CCSP synthesis and assessment product 2.1, Part A: scenarios of greenhouse gas emissions and atmospheric concentrations. U.S. Government Printing Office, Washington, DC, 122p.

CSWCRTI [Central Soil Water Conservation Research and Training Institute] 2010. Central Soil Water Conservation Research and Training Institute, Dehradun, 118p.

Delworth, T. L., and Coauthors, 2006. GFDL's CM2 coupled climate models. Part I: Formulation and simulation characteristics. *J. Climate*, 19: 643–674.

Dimri, A.P., 2006. Surface and upper air fields during extreme winter precipitation over the western Himalayas. *Pure and Applied Geophysics*, *163*(8), pp.1679-1698.

Donatelli, M., and G.S. Campbell. 1997. A simple model to estimate global solar radiation. PANDA Project, Subproject 1, Series 1, Paper 26. ISCI, Bologna, Italy.

Duan, K. and Yao, T., 2003. Monsoon variability in the Himalayas under the condition of global warming. *Journal of the Meteorological Society of Japan. Ser. II*, *81*(2): 251-257.

Edwards, W.M. and Owens, L.B., 1991. Large storm effects on total soil erosion. *Journal of Soil and Water Conservation*, *46*(1): 75-78.

El-Swaify, S.A., Moldenhauer, W.C. and Lo, A., 1985. Soil Erosion and Conservation. Soil Conservation Society of America. *Ankeny, Iowa, USA*, 794p.

Favis-Mortlock, D.T., Guerra, A.J.T., 1999. The implications of general circulation model estimates of rainfall for future erosion, a case study from Brazil. Catena 37: 329–354.

Favis-Mortlock, D.T., Savabi, M.R., 1996. In: Anderson, M.G., Brooks, S.M. (Eds.), Shifts in rates and spatial distributions of soil erosion and deposition under climate change. Advances in Hillslope Processes, vol. 1. Wiley, Chichester.

Fernandez, H.M., Martins, F.M., Isidoro, J.M., Zavala, L. and Jordán, A., 2016. Soil erosion, Serra de Grândola (Portugal). *Journal of Maps*, *12*(5): 1138-1142.

Fowler, H.J., Blenkinsop, S., Tebaldi, C., 2007. Linking climate change modelling to impacts studies: recent advances in downscaling techniques for hydrological modelling. Int. J. Climatol. 27 (12): 1547–1578.

Francipane, A., Fatichi, S., Ivanov, V.Y., Noto, L.V., 2015. Stochastic assessment of climate impacts on hydrology and geomorphology of semiarid headwater basins using a physically based model. J. Geophys. Res. Earth Surf. 120 (3): 507–533.

Fujino, J., Nair, R., Kainuma, M., Masui, T., Matsuoka, Y., 2006. Multigas mitigation analysis on stabilization scenarios using aim global model. *The Energy Journal Special issue* #3:343–354.

Garde, R. J. and Kothyari, U. C.: 1987, Sediment yield estimation, Journal Irrigation and Power (India) 44(3): 97–123.

Geng, S., J. Auburn, E. Brandsletter, and B. Li. 1988. A program to simulate meteorological variables: Documentation for SIM- METEO. Agronomy Rep. 204. Crop Extension, Univ. of California, Davis, CA, 204p.

González-Hidalgo, J.C., Peña-Monné, J.L. and de Luis, M., 2007. A review of daily soil erosion in Western Mediterranean areas. *Catena*, *71*(2): 193-199.

Gordon, H.B., O'Farrell, S., Collier, M., Dix, M., Rotstayn, L., Kowalczyk, E., Hirst, T. and Watterson, I., 2010. *The CSIRO Mk3. 5* CSIRO and Bureau of Meteorology. *climate model* 74p.

Haan, C.T., et al., 1994. Design hydrology and sedimentology for small catchments. San Diego, CA: Academic Press, San Diego, 588 p.

Hatwar, H. R., B. P. Yadav, and Y. V. R. Rao (2005), Prediction of Western Disturbances and associated weather over Western Himalayas, Curr. Sci., 88(6): 913–920.

Hijioka, Y., Matsuoka, Y., Nishimoto, H., Masui, T., Kainuma, M., 2008. Global GHG emission scenarios under GHG concentration stabilization targets. *J. Glob. Environ. Eng.* 13: 97–108.

Imeson, A.C., Lavee, H., 1998. Soil erosion and climate change the transect approach and the influence of scale. *Geomorphology 23*(2-4): 219–227.

IPCC [Intergovernmental panel on climate change], 1995. Second assessment Synthesis of Scientific- Technical information relevant to interpreting Article 2 of the UN framework Convention on Climate Change. Geneva, Switzerland. 64 p.

IPCC [Intergovernmental panel on climate change], 2007 Climate Change 2007: the physical science basis. Contribution of Working Group I to the Fourth Assessment Report of the Intergovernmental Panel on Climate Change, Cambridge, UK and New York, USA, 333p.

IPCC [Intergovernmental panel on climate change], 2013: Climate Change 2013: the Physical Science Basis. Contribution of Working Group I to the Fifth Assessment Report of the Intergovernmental Panel on Climate Change. Cambridge University Press, Cambridge, New York, 1538p.

Jones, D.S., Kowalski, D.G. and Shaw, R.B., 1996. Calculating revised universal soil loss equation (RUSLE) estimates on department of defense lands: A review of RUSLE factors and US army land condition-trend analysis (LCTA) data gaps. Center for Ecological Management of Military Lands, Colorado State University.

Joshi, R., Sambhav, K. and Singh, S. P., 2018. Near surface temperature lapse rate for treeline environment in western Himalaya and possible impacts on ecotone vegetation. *Tropical Ecology*. 59: 197–209.

Kalambukattu, J. and Kumar, S., 2017. Modelling soil erosion risk in a mountainous watershed of Mid-Himalaya by integrating RUSLE model with GIS. *Eurasian Journal of Soil Science*, *6*(2): 92-105.

Kinnell, P.I.A., 2005. Why the universal soil loss equation and the revised version of it do not predict event erosion well. Hydrological Processes, 19: 851–854.

Klik, A., Eitzinger, J., 2010. Impact of climate change on soil erosion and the efficiency of soil conservation practices in Austria. J. Agric. Sci. 148 (05): 529–541.

Krishnamurthy, V., 2012. Extreme events and trends in the Indian summer monsoon. In: Surjalal A, Bunde A, Dimri VP, Baker DN (eds) Extreme events and natural hazards: the complexity perspectives. American Geophysical Union, Washington, DC, 380p.

Kulkarni, A., and others (2010). Climate change scenarios 2030s. Indian Institute of Tropical Meteorology, National Workshop. New Delhi, India: Climate Change and India – A 4x4 Assessment.

Kumar, K.K., Kamala, K., Rajagopalan, B., Hoerling, M.P., Eischeid, J.K., Patwardhan, S.K., Srinivasan, G., Goswami, B.N., and Nemani, R. 2011. The once and future pulse of Indian monsoonal climate. *Climate Dynamics*, *36*(11-12): 2159-2170.

Kumar, P.V., Rao, V.U.M., Bhavani, O., Prasad, R., Singh, R.K. and Venkateswarlu, B., 2015. Climatic change and variability in mid-Himalayan region of India. *Climatic change*, *551*: 235-243.

Kumar, S., Kushwaha, S.P.S. 2013. Modelling soil erosion risk based on RUSLE-3D using GIS in a Shivalik sub-watershed. *Journal of Earth System Science* 122 (2): 389–398.

Lal, R. (Ed.), 1999. Soil Quality and Soil Erosion. Soil and Water Conservation Society, Ankeny, IA.

Lal, R. and Stewart, B.A., 1990. Soil degradation: a global threat. *Advances in Soil*.

Lal, R., 2001. Soil degradation by erosion. *Land degradation & development*, *12*(6): 519-539.

Lal, R., 2003. Soil erosion and the global carbon budget. *Environment international*, *29*(4): 437-450.

Lal, R., Ahmadi, M., Bajracharya, R.M., 2000. Erosional impacts on soil properties and corn yield on Alfisols in central Ohio. Land Degrad. Dev. 11 (6): 575–585.

Lang, T. J., and A. P. Barros (2004), winter storms in central Himalayas, J. Meteorol. Soc. Jpn. 82(3): 829–844.

Langdale GW, West LT, Bruce RR, Miller WP, Thomas AW (1992) Restoration of eroded soil with conservation tillage. Soil Technol 5:81–90.

Letey, J., 1985. Irrigation uniformity as related to optimum crop production—additional research is needed. *Irrigation Science*, *6*(4): 253-263.

Letey, J., 1985. Relationship between soil physical properties and crop production. Adv. Soil Sci. 1: 277–294.

Li, Y., Chen, B.M., Wang, Z.G., Peng, S.L., 2011. Effects of temperature change on water discharge, and sediment and nutrient loading in the lower Pearl River basin based on SWAT modelling. Hydrol. Sci. J. 56 (1): 68–83.

Maeda, E.E., Pellikka, P.K.E., Siljander, M., Clark, B.J.F., 2010. Potential impacts of agricultural expansion and climate change on soil erosion in the Eastern Arc Mountains of Kenya. Geomorphology 123 (3-4): 279–289.

Maeda, E.E., Pellikka, P.K.E., Siljander, M., Clark, B.J.F., 2010. Potential impacts of agricultural expansion and climate change on soil erosion in the Eastern Arc Mountains of Kenya. Geomorphology 123 (3–4): 279–289.

Mandal, D. and Sharda, V.N., 2011. Assessment of permissible soil loss in India employing a quantitative bio-physical model. *Current Science (Bangalore)*, *100*(3): 383-390.

Mandal, D., Singh, R., Dhyani, S.K. and Dhyani, B.L., 2010. Landscape and land use effects on soil resources in a Himalayan watershed. *Catena*, *81*(3): 203-208.

Michael, A., Schmidt, J., Enke, W., Deutschlander, T., Malitz, G., 2005. Impact of expected increase in precipitation intensities on soil loss-results of comparative model simulations. Catena 61 (2-3): 155–164.

Milliman JD, Syvitski JPM. Geomorphic/tectonic control of sediment discharge to the ocean: the importance of small mountainous rivers. J Geol 1992: 100:325

Mondal, A., Khare, D. and Kundu, S., 2018. A comparative study of soil erosion modelling by MMF, USLE and RUSLE. *Geocarto international*, *33*(1): 89-103.

Mondal, A., Khare, D., Kundu, S., Meena, P.K., Mishra, P.K. and Shukla, R., 2015. Impact of climate change on future soil erosion in different slope, land use, and soil-type conditions in a part of the Narmada River Basin, India. *Journal of Hydrologic Engineering*, *20*(6): C5014003.

Morgan RPC, Morgan DDV, Finney HJ (1984). A predictive model for the assessment of erosion risk. J. Agric. Eng. Res. 30: 245 – 253.

Morgan, R.P.C. (2001) A simple approach to soil loss prediction: a Revised Morgan-Morgan-Finney model. Catena 44: 305-322.

Morgan, R.P.C., 2005. Soil erosion and conservation, 3nd edn. Blackwell Science Ltd, Oxford.

Morgan, R.P.C., Martin, L., Noble, C.A. 1986. Soil erosion in the United Kingdom: a case study from mid-Bedfordshire. Silsoe College Occasional Paper no. 14. Silsoe College, Cranfield Univ., Silsoe, UK.

Mullan, D., 2013a. Managing soil erosion in Northern Ireland: a review of past and present approaches. Agriculture 3 (4): 684–699.

Nakicenovic, N., Swart, R., 2000. Special Report on Emissions Scenarios: A Special Report of Working Group III of the Intergovernmental Panel on Climate Change.

Nearing, M.A., 2001. Potential changes in rainfall erosivity in the U.S. with climate change during the 21st century. Journal of Soil and Water Conservation 56 (3): 229–232.

Nearing, M.A., Foster, G.R., Lane, L.J., 1989. A process-based soil erosion model for USDA water erosion prediction project. Trans. ASAE 32: 1587–1593.

Nearing, M.A., Jetten, V., Baffaut, C., Cerdan, O., Couturier, A., Hernandez,M., Le Bissonnais, Y., Nichols,M.H., Nunes, J.P., Renschler, C.S., Souchere, V., van Oost, K., 2005. Modeling response of soil erosion and runoff to changes in precipitation and cover. Catena 61 (2-3): 131–154.

Nearing, M.A., Jetten, V., Baffaut, C., Cerdan, O., Couturier, A., Hernandez, M., Le Bissonnais, Y., Nichols, M.H., Nunes, J.P., Renschler, C.S., Souchère, V., van Oost, K., 2005. Modeling response of soil erosion and runoff to changes in precipitation and cover. Catena 61: 131–154.

Nearing, M.A., Jetten, V., Baffaut, C., Cerdan, O., Couturier, A., Hernandez, M., Le Bissonnais, Y., Nichols, M.H., Nunes, J.P., Renschler, C.S. and Souchère, V., 2005. Modeling response of soil erosion and runoff to changes in precipitation and cover. *Catena*, *61*(2-3): 131-154.

Nearing, M.A., Pruski, F.F., O'Neal, M.R., 2004. Expected climate change impacts on soil erosion rates: a review. J. Soil Water Conserv. 59 (1): 43–50.

Neitsch, S.L., Arnold, J.G., Kiniry, J.R. and Williams, J.R., 2011. *Soil and water assessment tool theoretical documentation version 2009*. Texas Water Resources Institute.

Neitsch, S.L., Arnold, J.G., Kiniry, J.R., Williams, J.R. and King, K.W., 2005. Soil and Water Assessment Tool Theoretical Documentation Grassland, Soil and Water Research Laboratory, Temple ,Texas,506p.

Nunes, J.P., Seixas, J. and Keizer, J.J., 2013. Modeling the response of within-storm runoff and erosion dynamics to climate change in two Mediterranean watersheds:

A multi-model, multi-scale approach to scenario design and analysis. *Catena*, *102*: 27-39.

Oldeman LR. The global extent of soil degradation. In: Greenland DJ, Szabolcs I, editors. Soil resilience and sustainable land use. Wallingford: CAB International; 1994: 99– 118.

Panday P K, Thibeault J and Frey K E 2015 Changing temperature and precipitation extremes in the Hindu Kush-Himalayan region: an analysis of CMIP3 and CMIP5 simulations and projections. *Int. J. Climatol*. 35: 3058–77.

Pande, L.M., Prasad, J., Saha, S.K. and Subramanyam, C. 1992. Review of Remote Sensing applications to soils and agriculture. Proc. Silver Jubilee Seminar, IIRS, Dehra Dun, 423p.

Pant, G.B., Rupa, Kumar, R.R., Borgaonkar, H.P., 1999. Climate and its long-term variability over the western Himalaya during the past two centuries. In S.K., Dash, & J., Bahadur, (Eds). The Himalayan Environment (pp. 171- 184), New Age International (P) Ltd., Publishers: New Delhi, India.

Parajuli, P.B., Jayakody, P., Sassenrath, G.F. and Ouyang, Y., 2016. Assessing the impacts of climate change and tillage practices on stream flow, crop and sediment yields from the Mississippi River Basin. *Agricultural Water Management*, *168*: 112-124.

Pimentel D, Harvey C, Resosudarmo P, Sinclair K, Kurz D, McNair M, 1995 Environmental and economic costs of soil erosion and conservation benefits. *Science,* 267(5201) :1117– 23.

Pimentel, D. and Burgess, M., 2013. Soil erosion threatens food production. *Agriculture*, *3*(3): 443-463.

Pimentel, D., 2006. Soil erosion: a food and environmental threat. Environ. Dev. Sustain. 8 (1): 119–137.

Plangoen, P., Babel, M., Clemente, R., Shrestha, S., Tripathi, N., 2013. Simulating the impact of future land use and climate change on soil erosion and deposition in the Mae Nam Nan sub-catchment, Thailand. Sustainability 5 (8): 3244–3274.

Pruski, F.F. and Nearing, M.A., 2002a. Climate-induced changes in erosion during the 21st century for eight US locations. *Water Resources Research*, *38*(12): 34-1.

Pruski, F.F., Nearing, M.A., 2002b. Runoff and soil-loss responses to changes in precipitation: a computer simulation study. *J. Soil Water Conserv.* 57 (1): 7–16.

Renard, K.G., Foster, G., Weesies, G., McCool, D., Yoder, D., 1997. Predicting Soil Erosion by Water: A Guide to Conservation Planning with the Revised Universal Soil Loss Equation (RUSLE), 703. United States Department of Agriculture Washington, DC, 407p.

Riahi, K., Grübler, A., Nakicenovic, N., 2007. Scenarios of long-term socio-economic and environmental development under climate stabilization. *Technol. Forecast. Soc. Chang.* 74:887–935.

Richardson C.W. 1985. Weather simulation for crop management models. Trans. ASAE 28:1602–1606.

Rivington, M., Miller, D., Matthews, K.B., Russell, G., Bellocchi, G., Buchan, K., 2008. Evaluating regional climate model estimates against site-specific observed data in the UK. Clim. Chang. 88 (2): 157–185.

Routschek A, Schmidt J, Kreienkamp F (2014) Impact of climate change on soil erosion - a high-resolution projection on catchment scale until 2100 in Saxony/Germany. CATENA 121:99–109, ISSN 0341-8162.

Rupakumar, K, Kumar, K, Prasanna, V, Kamala, K, Desphnade, NR, Patwardhan, SK & Pant, GB 2003, 'Future climate scenario, In: Climate Change and Indian Vulnerability Assessment and Adaptation', Universities Press (India) Pvt Ltd, Hyderabad, 69–127.

Rupesh, J. P., Shailesh, K. S., Sanjay, T., Aribam, P. M. S., 2017. Use of remote sensing, GIS and C++ for soil erosion assessment in the Shakkar River basin, India, *Hydrological Sciences Journal*, 62:2, 217-231, DOI: 10.1080/02626667.2016.1217413.

Sadeghi, S.H.R. and Mahdavi, M., 2004. Applicability of SEDIMOT II model in flood and sediment yield estimation. Journal of Agricultural Sciences and Technology, 6: 147–154.

Sadeghi, S.H.R., 2004. Comparison of some methods to estimate rainfall erosivity. Journal of Agricultural Sciences and Industries, 19 (1), 45–52. (In Persian.)

Sadeghi, S.H.R., et al., 2007a. Conformity of MUSLE estimates and erosion plot data for storm-wise sediment yield estimation. Terrestrial, Atmospheric and Oceanic Sciences, 18 (1): 117–128.

Salazar, S., Francés, F., Komma, J., Blume, T., Francke, T., Bronstert, A., Blöschl, G., 2012. A comparative analysis of the effectiveness of flood management measures based on the concept of "retaining water in the landscape" in different European hydro climatic regions. Nat. Hazards Earth Syst. Sci. 12 (11): 3287–3306.

Samaras, A.G., Koutitas, C.G., 2014. Modeling the impact of climate change on sediment transport and morphology in coupled watershed-coast systems: a case study using an integrated approach. Int. J. Sediment Res. 29 (3): 304–315.

Scherr SJ, Yadav S., 1996. Land degradation in the developing world: implications for food, agriculture and the environment to 2020. IFPRI, Food, Agric. and the Environment Discussion Paper 14, Washington, DC, 36 p.

Sharma, K.D. and Singh, S., 1995. Satellite remote sensing for soil erosion modelling using the ANSWERS model. *Hydrological sciences journal*, *40*(2): 259-272.

Shrestha, A. B., C. P. Wake, J. E. Dibb, and P. A. Mayewski, 2000: Precipitation fluctuations in the Nepal Himalaya and its vicinity and relationship with some large scale climatological parameters. *Int. J. Climatol.,* 20: 317–327.

Shrestha, D.P. (1997) Assessment of soil erosion in the Nepalese Himalaya: A case study of Likhu Khola Valley, Middle Mountain Region. Land Husbandry, 2(1): 59-80.

Singh, A., 2009. Characterizing Runoff Generation Mechanism for Modelling Runoff and Soil Erosion in Small Watershed of Himalayan Region. M.Tech. thesis, International Institute For Geo-Information Science And Earth Observation Enschede, The Netherlands, 86p.

Singh, G., Chandra, S, and Babu, R.: 1981, Soil loss and prediction research in India, Central Soil and Water Conservation Research Training Institute, *Bulletin No. T-12/D9*.

Singh, Pratap, Ramasastri, K. S., and Kumar, N. (1995) Topographical intluences on precipitation distribution, in different ranges of western Himalayas, Nordic Hydrology, Vol. 26, (415): 260-286.

Singh, R.P. 2012. Surface runoff, Soil erosion and Water Quality estimation using APEX model integrated with GIS -A case study in Himalayan Watershed. M. Tech. (RS & GIS) thesis, Andhra University, Visakhapatnam, 98.

Smith, S.J. and Wigley, T.M.L.,2006. Multi-gas forcing stabilization with the *MiniCAM. Energ J* SI3:373–391.

Song, Z., Qiao, F., Song, Y., 2012. Response of the equatorial basin-wide SST to wave mixing in a climate model: An amendment to tropical bias, *J. Geophys. Res.,* 117, C00J26.

Strahler, A., 1964. Quantitative geomorphology of drainage basins and channel networks, in Handbook of Applied Hydrology, edited by V. T. Chow, pp. 4-39-4-76, McGraw-Hill, New York, 29p.

Sudo, K., Takahashi, M. and Akimoto, H., 2002. CHASER: A global chemical model of the troposphere 2. Model results and evaluation. *Journal of Geophysical Research: Atmospheres, 107*(D21), pp.ACH-9.

SWCS [Soil Water Conservation Society], 2003. A report from the soil and water conservation society. Conservation implications of climate change: soil erosion and runoff from cropland. *Soil and Water Conservation Society, with financial support from the US Department of Agriculture's Natural Resources Conservation Service, Cooperative Agreement No*. 68-3A75-2-98.

Tamene, L., 2005. Reservoir siltation in the drylands of northern Ethiopia: causes, source areas and management options, Ph. D. Thesis, Ecology and Development Series 30, Center for Development Research, University of Bonn, 207p.

Tiwari, P., 2008. Land use changes in Himalaya and their impacts on environment, society and economy: A study of the Lake Region in Kumaon Himalaya, India. *Advances in Atmospheric Sciences*, *25*(6): 1029.

Troeh, F.R., Hobbs, J.A., Donahues, R.L., 1991. Soil and Water Conservation. Prentice-Hall, Englewood, 135p.

UNEP [United Nations Environmental Programme], 1986. Sands of change: why land becomes desert and what can be done about it. UNEP Brief #2, United Nations Environment Programme, Nairobi, Kenya, 8 p.

USDA-SCS [U.S. Department of Agriculture-Soil Conservation Service], 1972. SCS National Engineering Handbook, Section 4, Hydrology. Chapter 10, Estimation of Direct Runoff from Storm Rainfall. U.S. Department of Agriculture, Soil Conservation Service, Washington, D.C., 10.1-10.24.

Walkely, A. and Black, I.A. 1934. An examination of the defy are method for determination of chronic acid method. *Soil Sci, 37*: 29-38.

Walling DE, Webb BW. Erosion and sediment yield: a global overview. Erosion and sediment yield: global and regional perspectives. Proc. Exeter Symp, July 1996. IAHS Publ, vol. 236. 1996. p. 3– 19.44.

Wardle DA, Bardgett RD, Klironomos JN, Seta¨la¨ H, van der Putten WH, Wall DH (2004) Ecological linkages between aboveground and belowground biota. Science 304:1634–1637.

Wayne, G.P., 2014. The Beginner's Guide to Representative Concentration Pathways, Skeptical Science, 25p.

Wen, D., 1993. Soil erosion and conservation in China. *World soil erosion and conservation*, 63-85.

Wilby, R.L., Charles, S.P., Zorita, E., Timbal, B., Whetton, P. and Mearns, L.O., 2004. Guidelines for use of climate scenarios developed from statistical downscaling methods. *Supporting material of the Intergovernmental Panel on Climate Change, available from the DDC of IPCC TGCIA, 27.*

Williams, J., Nearing, M.A., Nicks, A., Skidmore, E., Valentine, C., King, K., Savabi, R., 1996. Using soil erosion models for global change studies. Journal of Soil and Water Conservation 51 (5): 381–385.

Wischmeier, W.H. 1962. Storms and soil conservation. *J. Soil Water Consv*. 17 (2): 55-59.

Wischmeier, W.H., Johnson, C.B. and Cross, B.V., 1971. Soil erodibility nomograph for farmland and construction sites. *Journal of soil and water conservation*, 26: 189-193.

Wischmeier, W.H., Smith, D.D., 1978. Predicting rainfall erosion losses. A guide to conservation planning. United States Department of Agriculture, Agricultural Handbook #537. 67p.

Wise, M., Calvin, K., Thomson, A., Clarke, L., Sands, R., Smith, S.J., Janetos, A., Edmonds, J., 2009. The implications of limiting CO2 concentrations for agriculture, land-use change emissions, and bioenergy. technical report. [PNNL-17943].

Wu, T., Li, W., Ji, J. and Xin, X., 2012. The 20th century global carbon cycle from the Beijing Climate Center Climate System Model (BCC CSM). *J Clim* 12: 1573-1600.

Yaduvanshi, A., Zaroug, M., Bendapudi, R. and New, M., 2019. Impacts of 1.5 C and 2 C global warming on regional rainfall and temperature change across India. *Environmental Research Communications*, *1*(12): 125002.

Yang, D., Kanae, S., Oki, T., Koike, T. and Musiake, K., 2003. Global potential soil erosion with reference to land use and climate changes. *Hydrological processes*, *17*(14): 2913-2928.

Yang, D., Kanae, S., Oki, T., Koike, T. and Musiake, K., 2003. Global potential soil erosion with reference to land use and climate changes. *Hydrological processes*, *17*(14): 2913-2928.

Yuksel, A., Gundogan, R. and Akay, A., 2008. Using the remote sensing and GIS technology for erosion risk mapping of Kartalkaya dam watershed in Kahramanmaras, Turkey. *Sensors*, *8*(8): 4851-4865.

Zabaleta, A., Meaurio, M., Ruiz, E., Antigüedad, I., 2014. Simulation climate change impact on runoff and sediment yield in a small watershed in the Basque Country, northern Spain. J. Environ. Qual. 43 (1): 235–245.

Zhang, X.C., 2007. A comparison of explicit and implicit spatial downscaling of GCM output for soil erosion and crop production assessments. Clim. Chang. 84 (3): 337–363.

Zhang, X.C., 2012. Cropping and tillage systems effects on soil erosion under climate change in Oklahoma. Soil Sci. Soc. Am. J. 76 (5): 1789–1797.

Zhang, X.C., Nearing, M.A., 2005. Impact of climate change on soil erosion, runoff, and wheat productivity in central Oklahoma. Catena 61 (2-3): 185–195.

Zhang, X.C., Nearing, M.A., Garbrecht, J.D., Steiner, J.L., 2004. Downscaling monthly forecasts to simulate impacts of climate change on soil erosion and wheat production. Soil Sci. Soc. Am. J. 68 (4): 1376–1385.

Zhang, Y.G., Nearing, M.A., Zhang, X.C., Xie, Y., Wei, H., 2010. Projected rainfall erosivity changes under climate change from multimodel and multiscenario projections in Northeast China. J. Hydrol. 384 (1-2): 97–106.

Zheng, J.J., Xiu-Bin, H.E., Walling, D., Zhang, X.B., Flanagan, D. and Yong-Qing, Q.I., 2007. Assessing soil erosion rates on manually-tilled hillslopes in the Sichuan Hilly Basin using 137Cs and 210Pbex measurements. *Pedosphere*, *17*(3): 273-283.

Ziadat, F.M. and Taimeh, A.Y., 2013. Effect of rainfall intensity, slope, land use and antecedent soil moisture on soil erosion in an arid environment. *Land Degradation & Development*, *24*(6): 582-590.

POTENTIAL IMPACT OF CLIMATE CHANGE ON SURFACE RUNOFF AND SEDIMENT YIELD IN A WATERSHED OF LESSER HIMALAYAS

By

SOORYAMOL K. R.

2014-20-115

ABSTRACT

Submitted in partial fulfilment of the

requirements for the degree of

B.Sc. - M.Sc. (Integrated) Climate Change Adaptation

Faculty of Agriculture

Kerala Agricultural University, Thrissur

ACADEMY OF CLIMATE CHANGE EDUCATION AND RESEARCH

VELLANIKKARA, THRISSUR – 680 656

KERALA, INDIA

2020

ABSTRACT

The young and fragile North-Western Himalayan Mountain region witnessing high rates of soil erosion in the country because of the rugged terrain characteristics, immature soil, poor water holding capacity and ongoing tectonic activities. In addition to that, intensive agricultural practices, road constructions and clearing forest land etc. leads to instability in soil properties which can make the land vulnerable to erosion processes. Soil erosion is getting more attention in the context of climate change because of changing rainfall amount, distribution and intensity over time. In this situation, a study was conducted in the Sitlarao watershed of the Lesser Himalayan landscape to simulate the surface runoff and sediment yield using Soil and Water Assessment Tool (SWAT) model and the future climate scenario was predicted for the 2020s (2010-2039), 2050s (2040-2069), and 2080s (2070-2095). Model inputs like land use /land cover were obtained from Resourcesat-1 LISS-IV satellite data. Various physical and chemical properties of soil were collected by analysing soil samples from the watershed. The model calibration and validation for surface runoff and sediment yield were done on daily basis with respect to the measured data from the gauging station located at the outlet of watershed for 2016-2018 and the model predicted well. The correlation coefficient (r^2) and Root Mean Square Error (RMSE) of runoff calibration were estimated of 0.89 and 4.67, respectively. For sediment calibration, correlation coefficient (r^2) obtained of 0.89, and RMSE was 0.055. The correlation coefficient (r^2) and RMSE of runoff validation were 0.85 and 2.79, respectively. For sediment yield validation r^2 was 0.86 and RMSE was 0.048. Also, the Nash – Sutcliffe of coefficient of efficiency for surface runoff was 0.81 and sediment yield was 0.70. To study the impact of future climate on soil erosion downscaled data of rainfall and temperature of RCP 4.5 and RCP 8.5 were obtained for the study area from the MarkSim weather generator and identified the changes in rainfall with respect to the baseline period. Both RCP 4.5 and 8.5 scenarios showed an increase in rainfall from the baseline period. Under RCP 4.5 scenario change in rainfall calculated was 10.5% in the 2020s, 9.9% in 2050 and 12.3% in 2080s. Highest change in rainfall which is 14.2% and lowest change which is 8.7% from baseline were observed under RCP

8.5 in the 2050s and 2080s respectively. In the 2020s, the change observed was 10.1%. SWAT model predicted soil loss from study area on the basis of hydrological response units (HRUs). Highest average soil loss was observed from scrub land (42.78%) and the lowest was predicted from moderately dense forest (20.14%). From cropland maize and paddy 30.23% and 24.06% predicted respectively. For highest (14.2%) and lowest (8.7%) rainfall change which is under RCP 8.5, highest and lowest soil loss was observed respectively. The study concluded that due to climate change, increasing rainfall under both RCPs will result in increase of soil erosion in the future in Lesser Himalayan region.

Keywords: Soil erosion and runoff modelling, SWAT model, Lesser Himalayas, RCP